2010

Computational Hurricane Hazard Analysis A Performance Based Engineering View

Christopher Michael Vanek
University of Central Florida

COMPUTATIONAL HURRICANE HAZARD ANALYSIS- A PERFORMANCE BASED ENGINEERING VIEW

by

CHRISTOPHER MICHAEL VANEK
B.S.C.E University Of Central Florida, 2009

A thesis is submitted in partial fulfillment of the requirements
for the degree of Master of Science
in the Department of Civil, Environmental and Construction Engineering
in the College of Engineering and Computer Science
at the University of Central Florida
Orlando, Fl

Fall Term

2010

ABSTRACT

Widespread structural damage to critical facilities such as levees, buildings, dams and bridges during hurricanes has exemplified the need to consider multiple hazards associated with hurricanes as well as the potential for unacceptable levels of performance even if failure is not observed. These inadequate standards warrant the use of more accurate methods to describe the anticipated structural response, and damage for extreme events often termed performance based engineering (PBE). Therefore PBE was extended into the field of hurricane engineering in this study.

Application of performance-based principles involves collection of the numerous hazards data from sources such as historical records, laboratory experiments or stochastic simulations. However, the hazards associated with a hurricane typically include spatial and temporal variation therefore, more detailed collection of data from each hazard of this loading spectrum is required. At the same time, computational power and computer-aided design have advanced and potentially allows for collection of the structure-specific hazard data. This novel technique, known as computational fluid dynamics (CFD), was applied to the wind and wave hazards associated with hurricanes to accurately quantify the spectrum of dynamic loads in this study.

Numerical simulation results are presented on verification of this technique with laboratory experimental studies and further application to a typical Florida building and bridge prototype. Both the time and frequency domain content of random process signals were analyzed and compared through basic properties including the spectral density, autocorrelation, and mean. Following quantification of the dynamic loads on each structure, a detailed structural

FEM was constructed of each structure and response curves were created for various levels of hurricane categories.

Results show that both the time and frequency content of the dynamic signal could be accurately captured through CFD simulations in a much more cost effective manner than laboratory experimentation. Structural FEM models showed the poor performance of two coastal structures designed using deterministic principles, as serviceability and strength limit states were exceeded. Additionally, the response curves created for the prototype structure could be further developed for multiple wind directions and wave periods. Thus CFD is a viable option to wind and wave laboratory studies and a key tool for the development of PBE in the field of hurricane engineering.

ACKNOWLEDGEMENTS

Special thanks to Dr. Kevin Mackie for all of his support and guidance throughout this thesis project. I would also like to thank Dr. Necati Catbas and Dr. Manoj Chopra for serving on my committee and providing great feedback for improving the thesis manuscript. I would also like to thank my family for their support during my thesis preparation.

TABLE OF CONTENTS

LIST OF FIGURES

LIST OF TABLES

LIST OF ABBREVIATIONS

ΔPmax Central pressure difference

ρ Density of water,

A Tributary area.

ACI American Concrete Institute

ADCIRC ADvanced CIRculation model for oceanic, coastal and estuarine waters

ASCE American Society of Civil Engineers

BLWT Boundary Layer Wind Tunnel

CAARC Commonwealth Advisory Aeronautical Research Council

Cp Pressure coefficient

CFD Computational Fluid Dynamics

CDF Cumulative Distribution Function

CTE Computational Tsunami Engineering

CWE Computational Wind Engineering

d Water depth or surge level

DAD Data Assisted Design

DL Dead Load

FEM Finite Element Model

FEMA Federal Emergency Management Agency

FFT Fast Fourier Transformation

FSI Fluid-Structure Interaction

g Acceleration due to gravity

H_s Significant Wave height,

HDF Hierarchical Data Format

HURDAT HURricane DATabase

HAZUS HAZard US xvi

IBC International Building Code

LES Large Eddy Simulation

LL Live Load

LRFD Load and Resistance Factor Design

NCSU North Carolina State University

NDBC National Data Buoy Center

NIST National Institute of Standards and Technology

NOAA National Oceanic and Atmospheric Administration

NRL Naval Research Laboratory

NWS National Weather Service

ρ_w Density of water

PBE Performance Based Engineering

PBTE Performance Based Tsunami Engineering

PBWE Performance Based Wind Engineering

PEER Pacific Earthquake Engineering Research

PBEE Performance Based Earthquake Engineering

PD&E Project Development and Environment

PDF Probability Distribution Function

PSD Power Spectral Density

RANS Reynolds Average Navier Stokes

SDOF Single Degree of Freedom

SLOSH Sea, Lake Overland Surges from Hurricane

SWAN Simulation of Waves in Near Shore area

SWH Significant Wave Height

TWB Tsunami Wave Basin

OSU Oregon State University

UF University of Florida

UWO University of Western Ontario

Rmax Maximum hurricane radius

RPG Random Pulse Generation

CHAPTER ONE: INTRODUCTION

Tropical cyclones are intense low pressure storm systems that occur over the tropical ocean, driven by the ocean's latent heat, mainly in late summer and autumn (Holmes, 2001). The most intense and severe class of these cyclones develop in the Caribbean seas and are termed hurricanes. Therefore, structures in coastal communities along the Atlantic and Gulf Coast region are subject to the most severe nature of the numerous hazards that accompany these storms. These hazards are not limited to the large wind gusts that are notorious to the event. Intense storm surge and flooding have been shown to be the most damaging aspect to human life and property.

Despite these hazards the population has grown in many of these communities, driven by the moderate year round climate, theme park attractions and beautiful beaches. Due to the increase in population in these areas, civil infrastructure has been constructed to accommodate the public need. As a result, more structural systems have been exposed to these hazards such as buildings, bridges, floodwalls (levees), dams and other coastal structures. Devastating hurricanes such as Andrew or Katrina have shed light on the poor performance of the existing design methodologies and codes, with numerous coastal infrastructure failures. According to NIST report 1476, collaboration of over 26 experts from over 16 organizations including NIST, FHWA and USACE recommends the establishment of a risk-based design methodology for coastal structures, such as bridges.

A performance based design methodology integrates risk analysis alongside the standard design objectives with a embedded goal of reducing loss to life and property. This shift requires a more realistic prediction of the structural behavior of the system under a more accurate

description of the spectrum of loadings anticipated during the life-cycle. Therefore deterministic based design conventions are to be replaced with a more scientifically oriented design approach similar to the field of earthquake engineering. This approach is termed performance-based hurricane engineering (PBHE).

However a distinct challenge is present in the implementation of such a methodology, because the wind and wave hazards are distinctly different from earthquake hazards. The spatial and temporal variation of the wind and wave loading is very drastic compared to earthquake motion. Site-specific seismic ground motion records are typically applied to a structure's foundation and spatial variation is not considered due to the rapid speed of seismic waves. On the other hand, hurricane hazards, such as wind and waves are drastically different as the structural configuration; orientations, and local site conditions all affect the loading distribution. This phenomenon creates the need for a wealth of simulated pressure/force records from an array of sensors placed all over the structure to take detailed readings during an extreme event. However, each record is site and structure specific and must be performed for a vast array of structures. Obviously, such an implementation is a drastic challenge to applying PBE.

Currently this void in this data has prevented widespread forecasting and damage mitigation efforts (Masters, 2010). Only recently in 2010 with the formation Digital Hurricane Consortium (DHC) has widespread collaboration among field activities have initiated in developing such a database. Distinct challenges are present in instrumentation, regularity of multiple platforms, and field logistics. Additionally three main contributions of uncertainty in characterizing the wind field include: (i) inherent or aleatory uncertainty due to the unpredictable nature of the wind velocity and magnitude, (ii) epistemic uncertainty due to incomplete or

missing data or information, and (iii) modeling uncertainty from estimating wind load effects on structural response (Kiureghan and Ditlevesen, 2009).

The current framework for modeling hurricane hazards can be shown in Figure 1. Hurricane hazards are quantified in a probabilistic sense to determine quantities such as an appropriate distribution. From this point two different design approaches are available, codified hazard quantification and linear structural analysis techniques can be performed or time history pressure/forces readings can be collected for finite element modeling (FEM). A bridge between the two philosophies has been approached through a database assisted design procedure (DAD).

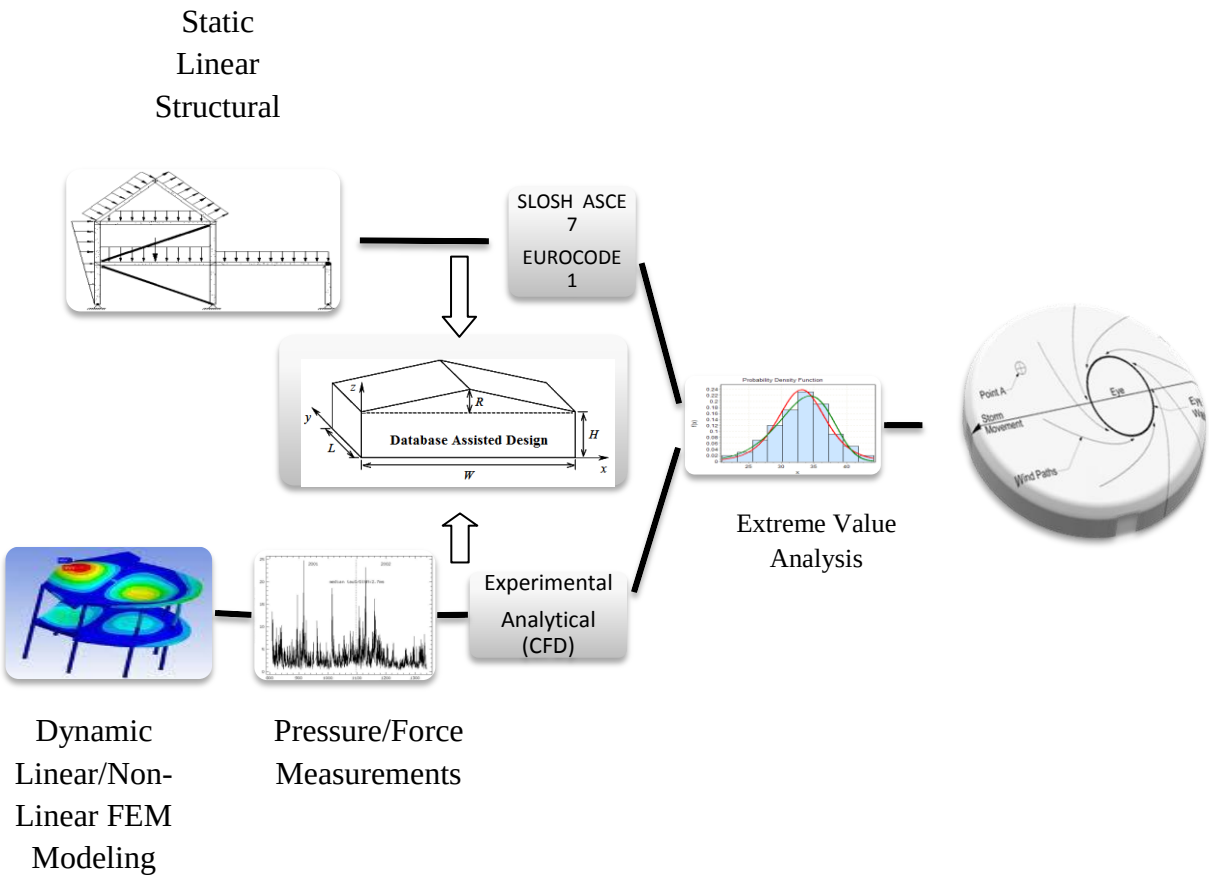

Figure 1: Current Hurricane Hazard Analysis Framework

Therefore, in this study, an analytical method was undertaken to thoroughly investigate the major hazards including wind and waves that accompany a hurricane event for several structures. To quantify these hazards for PBE, a database of recorded data on simulated hurricane hazards is required for structural analysis. However the resources for experimental simulation of these multiple hazards are very limited and currently unavailable at the UCF structures research facility at this time.

At the same time, the recent rise in computational hardware and computing power has formed an efficient field of experimental research. Numerical simulations using computational fluid dynamics (CFD) have risen in both the wind and wave engineering field, allowing more cost effective multiple hazard research. The use of fluid structure interaction (FSI) software has been validated in the aerospace and mechanical engineering fields for airfoils, racecars, and ship design for 20 years. Only recently has the concept been extended in Civil Engineering FSI problems such as wind and wave phenomena.

In this study, CFD simulations were to be carried out on several prototype structures to thoroughly quantify the fluid hazards posed by a hurricane. Dynamic loads were to be generated for comprehensive linear and non-linear structural evaluation. The Tampa Bay region was selected due to the wide range of coastal structures and its susceptibility to Hurricane damage.

Before CFD simulations will be carried out on the prototype structures, verification of the accuracy of the numerical simulation results is vital. Therefore, several records of laboratory wind tunnel and wave tank basin experimental data were collected to verify the accuracy of this tool. These verifications are a significant contribution as thorough comparisons shall continue to

enhance the confidence and warrant the practical use of CFD in structural design. Additionally the widespread application of PBHE requires a versatile tool such as CFD

CHAPTER TWO: LITERATURE REVIEW

Numerous structural hazards are associated with hurricanes that accompany the storm event. Identification and quantification of these extreme hazards are essential to application of a performance based structural design. Performance based engineering design has been historically applied to the field of earthquake engineering to assess hazards such as earthquake intensity or liquefaction. However, the hazards that are associated with a hurricane can range from wind, storm surge, waves and the potential for airborne or waterborne debris. Therefore in this study the concept of PBE was extended in the hurricane engineering field.

Hurricane Hazards

Maximum Wind Speed

The classification of a tropical storm/cyclone into a hurricane is quantified through the maximum wind speed. When the sustained maximum speed of the storm winds reach (33m/s, 74mph), the storm is officially classified as a hurricane according to the Saffir-Simpson scale. These intense warm low pressure systems have an organized structure as shown in Figure 2 (Holmes). The Figure shows the circulation of the flow occurs with radial components toward the "eye" where a region of intense thermal convection causes air currents to spiral upward. Outside the eye of the hurricane, the wind speed at the upper storm levels decays with radial distance from the storm center. The gradient wind equation can therefore be used to determine the wind speed at any radial distance from a storm center. The terms in the equation include the Coriolios parameter (f), the radius from the storm center (r), the density of air (ρ), and the

atmospheric pressure (p). To apply the gradient wind equation a mathematical representation of the pressure gradient such as the one proposed by Holland (1980) leads to Equation 1.

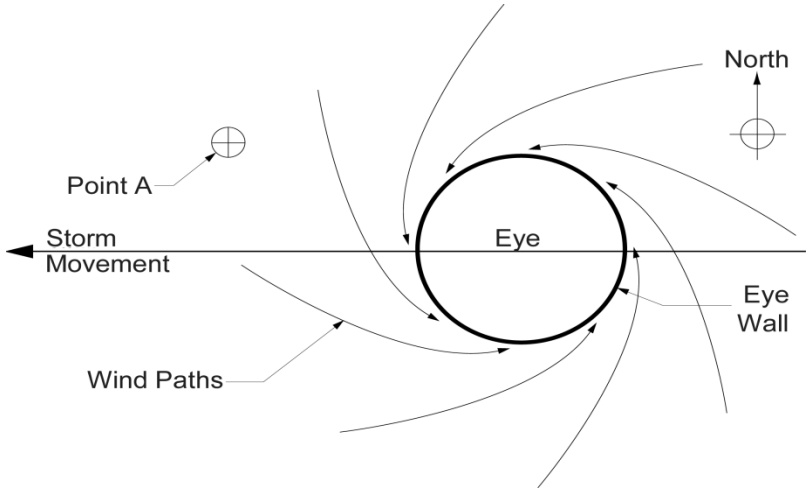

Figure 2: Structure of a Hurricane (Holmes, 2001)

Equation 1 describes the mean velocity field of an hurricane as a function of the radius to storm center (r), the change in pressure across the storm (Δp), the characteristic scaling parameters A and B, and Coriolis parameter (f).

$$U = -\frac{|f|r}{2} + \sqrt{\frac{f^2 r^2}{4} + \frac{\Delta p}{\rho_a}\frac{AB}{r^B}\exp\left(-\frac{A}{r^B}\right)} \qquad (1)$$

To illustrate this effect, an anemometer reading 10m above the ground in a hurricane is plotted in Figure 3. The Figure shows a period of very low recorded wind speeds as the eye of the hurricane passed over this wind station and the wind direction changed nearly 180 degrees.

Also from the figure one can see the physical wind profile of a hurricane as the wind speed decays from the eye of the storm.

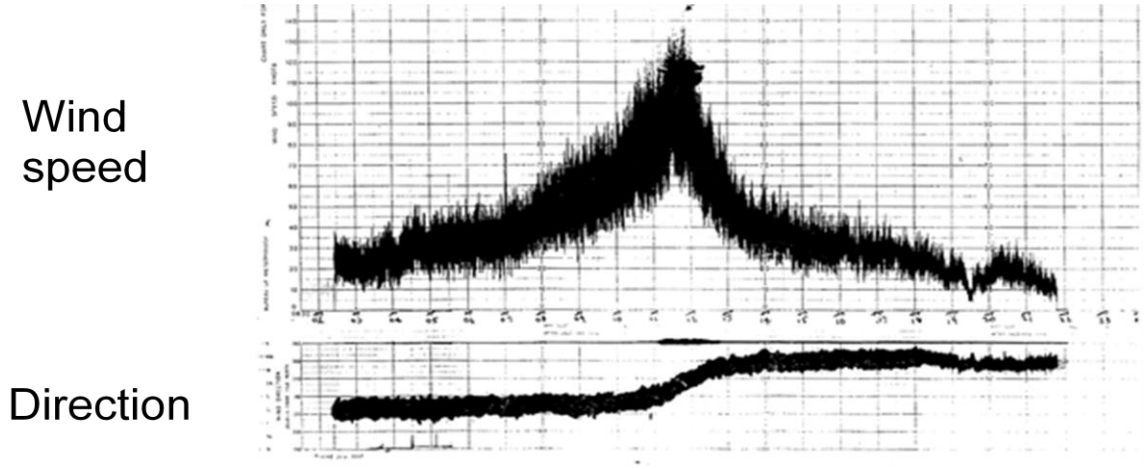

Figure 3: Variation of Wind Speed/Direction at a point in a hurricane (Holmes, 2001)

The modeling and simulations of the natural wind flow phenomena around structures were first studied using wind tunnels. Both aeroelastic and rigid scaled models equipped with numerous transducers are commonly tested for fluctuating pressures induced by blowers or fans. This technique has been validated in studies from surface pressure measurements on several existing structures. One of these studies includes the Silsoe Structures building experiment started in November 1990 by the UK Building Research Establishment. A large steel portal frame building equipped with pressure taps and strain gauges to measure structural response (Robertson, 1988). Results indicated for transverse flow from (0-180°), that accurate pressure coefficients were obtained for both peak and time averaged values. Generally these measurements justified the use of wind tunnel simulations for low-rise buildings.

However distinct challenges are still present in the use of wind tunnels in areas such as similitude scaling. An exact equality of the kinematic, geometric and dynamic similarity including Reynolds number and the Rossby Number for both prototype and model flows cannot be obtained (Cermak, 1975). Conversely Reynolds number independence can be achieved for these flow characteristics in a long wind tunnel composed of numerous roughness elements.

Different modeling techniques are typically employed in wind tunnel modeling such as the high-frequency force balance technique which was first reported by Tschanz et al. (1983). The method involves using a very rigid, high-frequency balance model system where only the exterior surface of the structure is represented. Wind tunnel studies are then carried out on this system and the overall fluctuating pressures are combined with the structural properties to analytically determine the full-scale responses. Conversely, aero-elastc models involve simulating the interaction between the motion of the structure and the aerodynamic forces. Applications of this method typically include lightweight, deformable or lightly damped structural systems where stationary models cannot accurately capture the potential additional motion induced forces such as flutter.

Although structural failure rarely occurs from extreme wind speeds, a vast majority of the structural wind damage occurs primarily to single family residential dwellings (Prevatt, 2009). Wind damage to low rise buildings is primarily attributed to loss of the building envelope and roof damage. Therefore researchers such as Simui et al. (2003) contend that the simplifications of the current ASCE 7-05 analytical procedure can produce vast differences when compared to experimental wind tunnel pressure fluctuation loads.

Storm Surge

Storm surge can be simply defined as the rise of water toward the shore by the force of the wind swirling around an advancing storm (National Oceanic Atmospheric Adminstration-NOAA). The surge created from the winds combines with the mean sea level to create a hurricane storm tide.

Storm surge caused by hurricanes is one of the most devastating natural phenomena as nine out of every ten hurricane related fatalities are attributed to storm surge (FEMA-456). Some of the deadliest natural disasters in United States history occurred from storm surge waves impacting coastal communities. The potential for this hazard is intensified today as much of the Atlantic and Gulf Coast communities are densely populated and lie less than (4.5m, 15ft) above the mean sea level.

Storm surge heights are affected by several variables including the timing of astronomical tides, maximum wind speed and bathymetry of the ocean bottom. For example a steep drop from the shoreline creates a deep pocket of water that reduces the storm surge effect but produces a more powerful wave. Conversely, a long and gently sloping shoreline can produce higher storm surges with small waves. Figure 4 displays this effect as the deep water reduces the energy of the oncoming wave and allows that energy to dissipate.

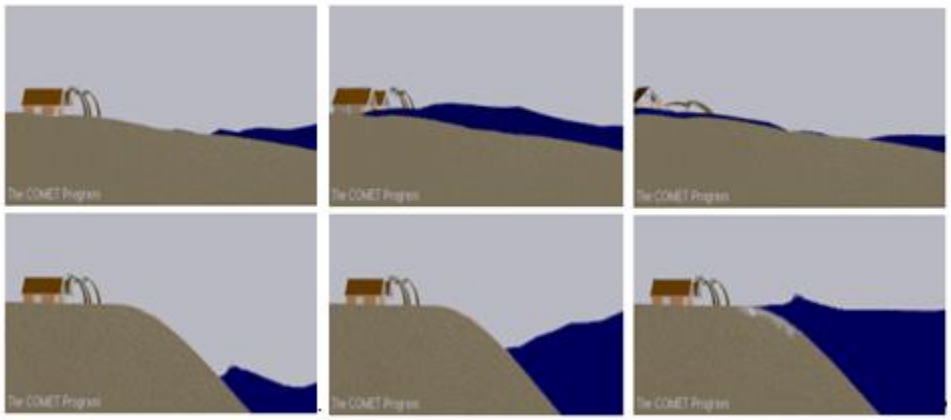

Figure 4: Storm Surge Comparison Top: Shallow Coastal Slope Bottom: Steep Continental Shelf

Waves

Waves are typically generated in the deep water by the wind blowing across the surface. Some of the key characteristics of waves are the height, wave length and wave period. In fluid dynamics, the wave height of a surface wave is the difference between the elevations of a crest and a neighboring trough. The wavelength is a measure of the horizontal distance between the crest and trough, and the wave period is the time it takes for two consecutive crests or troughs to pass a fixed point (Kinsmen, 1984). .

The waves that are generated during a hurricane are composed of a series of random waves with various heights and periods. The height and period of these waves are affected by numerous factors, including wind speeds; wind duration, fetch length and water depth. Illustrations of the effect of some of these variables are shown in Figure 5. The fetch can be seen as the distance over which a wind profile will travel before reaching the structure. From the

Figure, one can see that the increased duration of the wind has significantly increased the wave height over time until they reach a state of a fully developed wave.

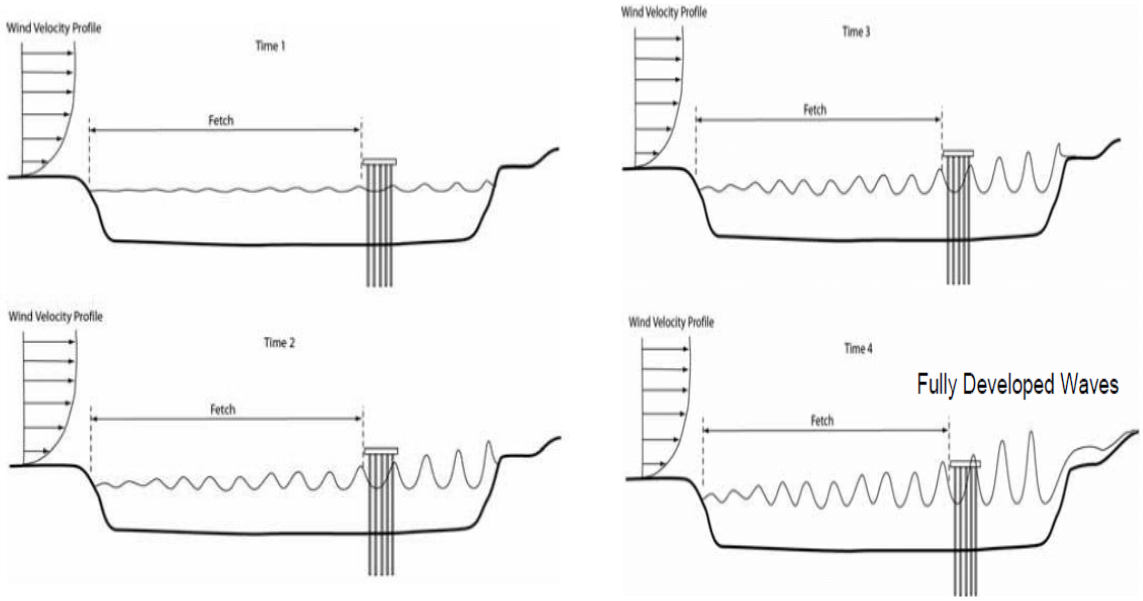

Figure 5: Fetch Length and Wind Duration Effects of Wind-generated waves (Sheppard, 2006)

Wave damage from hurricanes is significant and is most common in the coastal bridge infrastructure. Recent Hurricanes including Hurricanes Ivan and Katrina, heavily damaged most of the existing low-lying Gulf Coast concrete bridges. These bridges were subjected to the wave forces of the hurricane as storm surge levels rose and inundated many of the bridges superstructures.

Bridges are not the only structure affected by hurricanes as coastal buildings are also subjected to wave forces due to the rising storm surge and tidal conditions. During a survey of post-Katrina Hurricane damage, a number of failures of parking garages in flat slab, double-tee

and prestressed concrete floor systems resulted from the hydrodynamic uplift induced by the surge and wave action (Robertson, 2007).

These detrimental effects have initiated numerous studies into the quantification of "wave – in-deck loads" which can be defined as hydraulic loads applied by waves to the deck or other protruding elements (Cuomo, 2007). Laboratory wave tank basin facilities are currently the accepted form of gathering wave-in-deck time dependent loads .

Researchers such as Sheppard et al. (2009) and Cuomo et al. (2007) have concluded that wave-in-deck loads can be classified into two classes, Impact and Quasi-static. A specific frequency or time period is not specified to distinguish the two categories, as the structure properties affect the classification. Typically wave-in-deck loads can be classified as impact loads if the load rise time is less than twice the resonant period for the mode related to the applied load (Cuomo, 2007). Both characteristics are seen in a typical wave loading and thus the time history is idealized as shown in Figure 6.

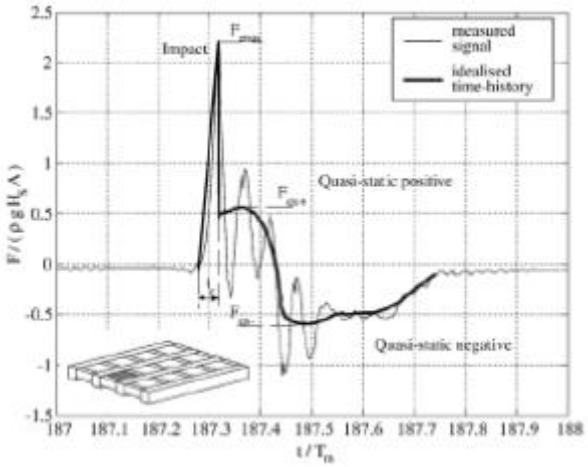

Figure 6: Idealized Wave Time History Superimposed of recorded signal from flume tests at HR Wallingford, UK (Cuomo, 2007)

Scour

A secondary source of structural damage occurs to foundation systems during the recession of a passing hurricane. Receding water flowing around the structure at a high rate may led to erosion of the soils which support the foundation. The rate at which scour occurs depends primarily upon the soil type. In addition to any storm or flood-induced erosion that occurs in the general area, scour is generally limited to small, cone-shaped depressions. Localized scour reduces the resistance of the foundation system by reducing its embedment. This reduction in bearing capacity can readily cause the partial or total collapse of a coastal foundation.

The soil scour phenomena can occur as a shear or liquefaction-induced failure. The liquefaction-induced scour is more ubiquitous during hurricane episodes (Robertson, 2008). The soil matrix undergoes pore pressure change as the periodic wave action induces flow of the soil particles below the foundation. This scour can then be intensified by the rapid drawdown of the water in an inundated area as pore pressure changes are occurring much more rapidly.

Flooding

Flooding can occur during a hurricane event, both inland and along the coastal communities. Inland flooding (typically termed flash flood) occurs from intense rainfall that in a very small region over a relatively small time interval. Coastal flooding is typically created from a combination of storm surge, oceanic tides, and rainfall.

Flooding has a variety of impacts on coastal buildings and their foundations, including hydrostatic forces, hydrodynamic forces, flood borne debris forces, and erosion and scour. These

forces can dislodge buildings from their foundation with poor connections. Flooding is also a major concern to emergency officials as it is the leading cause of fatalities during hurricanes.

Wind and Waterborne Debris

Wind Damage to structures is not limited only to the fluctuating surface pressures on the building envelope but flying debris that are generated in the wind field also. These airborne missiles have the possibility of striking the structure and penetrating the building envelope. The loss of the building enclosure can lead to undesirable consequences like high internal pressures, additional debris and water damage (Holmes, 2001).

Waterborne debris can be produced during flood events and can include a variety of objects. The potential for waterborne debris has been mapped in specific regions as determined by the ASCE. The waterborne debris region is defined as areas within hurricane-prone regions within one mile of the coastal mean-high-water line where the basic wind speed is (49 m/s, 110mph).

Wind and waterborne debris are not as widespread as other hazards that are associated with the hurricane event and are therefore not as thoroughly quantified. One empirical formula is provided by ASCE 7 for impact forces. In Equation 2, the impact force (F) is given by the weight of the object (w), impact velocity (v), acceleration of gravity (g) and the impact duration (Δt) (typically 0.03-0.3 sec).

$$F = \frac{\pi w v}{2 g \Delta t} \tag{2}$$

However, the location and time varying aspect of this loading phenomenon is not fully understood and is rarely accounted for in structural design. Additionally, according to a survey of post-Katrina coastal damage, very few structures were damaged by debris from the storm (Robertson, 2008).

Quantification of Hurricane Hazards

Some effort has been made to quantify the hazards that are associated with hurricane events. The Saffir-Simpson Scale was formulated in 1969 by Herbert Saffir, a consulting engineer, and Dr. Bob Simpson, Director of the National Hurricane Center. The need for the scale was founded on the principle of communicating the gradations of risk that are associated with hurricanes that may allow emergency officials to better manage these disasters. Although the scale is based on physical observations of wind damage and storm surge events seen in hurricanes, the rating of a storm is highly subjective and is not a definitive probabilistic quantity. Due to the non-uniform nature of the hurricane structure, a single category rating for the entire storm will yield inaccurate results. Thus, the application of the Saffir-Simpson scale in PBE is very limited but it is a useful tool in describing the potential hazards associated with the intensity of the storm.

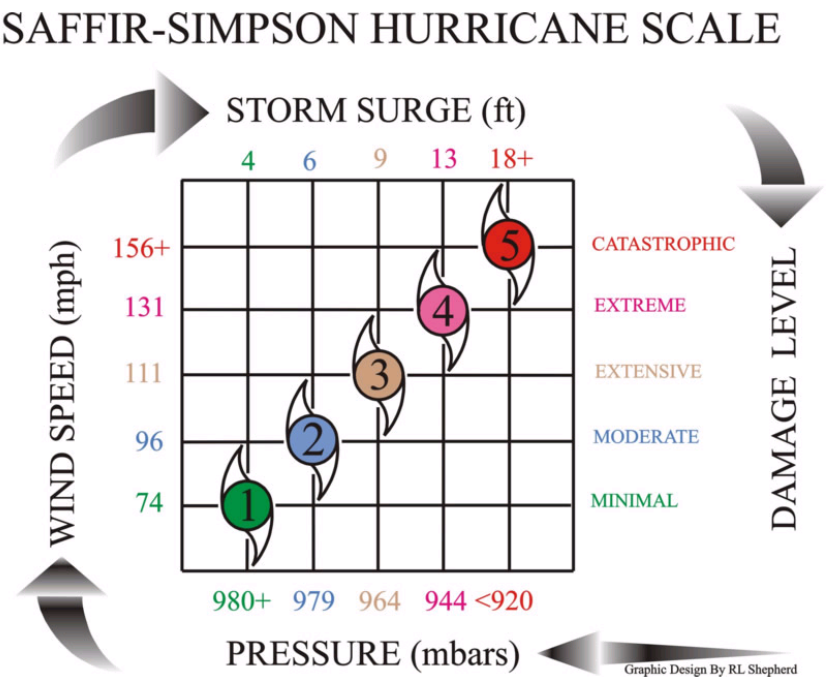

Figure 7: Saffir-Simpson Scale (National Weather Service)

Performance Based Engineering

Performance based structural engineering entails analyzing structures under the extreme hazards identified to achieve better performance or protection. The response of the structure is not only termed in states of failure and safe, as the case with conventional Load and Resistance Factor Design Method (LRFD), but all spectrums of the response are quantified, including states such as safe, partially safe and unsafe. This shift requires a more realistic prediction of the structural behavior of the system under a more accurate description of the spectrum of loadings anticipated during the life-cycle. The need for this change in design methodology arose from the prescriptive nature of current design codes and the desire for more accurate design methodology. These codes contain minimum standards of care (and performance) and no information on how

to achieve better performance or protection against manmade or natural hazards (Whittaker, 2005). The current codes in practice including ASCE 7 and International Building Code (IBC) are only reviewed following a disastrous event and are based on judgments by distinguished design professionals as to whether the losses were acceptable, given the severity of the event. This lack of quantitative evaluation of the performance of the structures gives very inaccurate conclusions on the state of the design community. Therefore it is believed that the development of performance-based engineering tools for extreme loadings on structures will improve out civil infrastructure. PBE was first applied to earthquake engineering but, it has been extended into other extreme hazards both manmade and natural including blast, fire, hurricanes, and tornadoes.

An example framework of the PBE methodology has been outlined by the Pacific Earthquake Engineering Research (PEER). A typical PBE assessment approach is a four step procedure that first involves identifying all potential hazards in a more scientifically oriented procedure called *Hazard Analysis*. Next, the structure is analyzed under the given hazards in *Structural Analysis* to determine demand parameters, such as the story drift. According to the specific building type and arrangement, the structural response can be mapped to the damage potential in *Damage Analysis*. Once the damages of the structure have been determined, the Losses of the structure can be quantified in terms of loss of time, money and life in *Loss Analysis*.

Performance-Based Hurricane Engineering

Performance based hurricane engineering (PBHE) is a relatively active field of research. Currently, most of the work in PBHE has been focused on specific hazards that are associated with the hurricane event, and no current experimental research has been conducted on the combined effects of hurricanes including wind and hydrostatic and hydrodynamic forces. Numerous studies are currently active in investigating these loads through both numerical and experimental measures.

Numerous studies have been conducted on designing structures due to wind loads in a performance based manner. Some of these studies include Sibilio and Ciampoli et al. (2007) in which advanced Monte Carlo simulation was carried out on a footbridge subjected to turbulent wind. Norton et al. (2007) presented an efficient method for analyzing structures under hurricanes loads for tall buildings. Ongoing research at the University of Florida has been focused on both full and 1/3 scale residential structures composed of wood subjected to the UF Hurricane Simulator (Prevatt, 2009).

Another field of PBHE is in the field of wave and storm surge effects to structures termed as Performance Based Tsunami Engineering (PBTE). Waves are generated by both tsunamis and hurricanes, which have been shown to have devastating effects to life and property. Currently engineers have little to no guidance to when designing structures in wave prone areas (Yim, 2009). However numerous studies have been recently conducted on the wave effects on structures.

Some of this research includes work from Cuomo et al. (2007) in which guidance for hydraulic loads for bridge decks were given from wave flume tests at HR Wallingford in the UK. Shepperd et al. (2009) developed a theoretical wave force models from a wide range of wave conditions from 1200 wave basin tests. Ongoing research at the Tsunami Wave Basin (TWB) is being performed to investigate the response of residential structures by subjecting scaled 1/6 models. Wave Induced forces are measured for different building configurations to see the change in the wave- induced loads (Yim, 2009).

Database Assisted Design (DAD)

A Database Assisted Design methodology implements directional time history data of experimental pressure coefficients obtained from wind tunnel testing for use in the design and analysis of structures (Main and Fritz, 2006). The first step in building a DAD program is the collection of a plethora of wind tunnel data for various wind angles and surface terrain conditions.

One such application of the DAD procedure was in the development of a MATLAB program named WINDPRESSURE (Main and Fritz, 2006). The program provides a graphical user interface that develops structural responses such as internal bending moment and deflection that can allow the performance of the structure to be assessed. The DAD program then utilizes an interpolation algorithm to allow for mapping of tested building models to any building dimensions. Therefore once developed any building of similar structural orientation and arrangement may be designed to achieve better performance.

Storm Surge Models

The ability to accurately predict the estimated levels of storm surge and waves anticipated from a given hurricane event is crucial for emergency officials and design engineers. Several computer generated surge and wave prediction models are currently available. Currently two commonly used packages are Sea, Lake Overland Surges from Hurricane (SLOSH) and ADvanced coastal CIRCulation and storm surge modeling (ADCIRC).

ADCIRC is based on solving the time dependent, free surface circulation and transport problems in two and three dimensions. Typical ADCIRC applications have included everything from analysis of hurricane storm surge and flooding to dredging and material disposal studies. One study coupled the ADCIRC (ADvanced CIRCulation) surge model and the SWAN (Simulation of Waves in Near shore areas) wave models. The team simulated the storm surge and wind waves generated by Hurricane Katrina on the Mississippi and Alabama coasts for developing a theoretical wave equation for bridge decks (Douglass, 2006).

A government created surge model commonly used by FEMA officials is named SLOSH, which was created by the National Weather Service (NWS). SLOSH is two-dimensional, numerical and dynamic storm surge modelers that can be used to develop real time estimates of storm surge levels generated from Hurricanes, by taking into account a storm's pressure, size, forward speed, forecast track, wind speeds, and topographical data. SLOSH is not considered a predictive tool as the track of the hurricane at landfall must be known for accurate simulation of the storm surge. The SLOSH program divides the US Atlantic and Gulf Coasts into 41 basins, which are further subdivided into smaller polar coordinate grids that allow for more accurate refinement of each basin. Using these refined grid meshes the individual elements of the

SLOSH grid are the basis for calculating the water surface elevations caused by storm surge in a specific SLOSH basin. The transport equations of motion are used for calculating the storm surge in the SLOSH models (Jelesnianski, 1992).

Computational Fluid Dynamics (CFD)

Computational Fluid Dynamics is a subset of fluid mechanics in which numerical methods and algorithms are utilized to solve and analyze fluid flow problems. The basis of all CFD modeling packages is the use of the Navier-Stokes equations of fluid flow. A system of nonlinear partial differential equations of second order defines the conservations of mass, impulse and energy of a three-dimensional fluid flow. Solution techniques include finite element, finite volume and spectral analysis.

CFD modeling typically has been applied in the field of mechanical and aerospace engineering. Airfoils, spacecraft, racecars and other high rate traveling mechanical machinery have been simulated both in small scale wind tunnels and CFD modeling packages. Numerical simulations reduce the overall cost of conducting real world experiments, making it a very active field of research. More recently, this computational power has been actively researched in the structural engineering field. Extreme structural loads such as wind, waves, blast and impact have been modeled using CFD techniques. Specifically, research in the wind and wave engineering community began in the late 1980's in which simulations of fluid flow interaction with structures is conducted. Today increased computer performance has stimulated this research and a specific field of computational wind and tsunami engineering has been developed.

Computational Wind Engineering (CWE)

The application of CFD in wind engineering is termed computational wind engineering. This field of research is still very limited in its widespread use, but it has seen a recent rise in interest. Hardware and software capabilities have increased tremendously since CWE's inception in the late 1980's. This has led to significant progress toward application of CWE to evaluate wind loads on buildings. Some countries such as Japan have established methods for assessing pedestrian wind levels using Reynolds Averaged Navier Stokes equations (RANS) and Large Eddy Simulation (LES) (Dagnew, 2009).

RANS and LES turbulence modeling approaches are typically performed in any CFD modeling application to reduce computational demand. Direct solution of the Navier-Stokes equations requires very fine grids to accurately capture all turbulence scales in the flows and is not applicable to typical Reynolds numbers encountered in wind engineering (Franke, 2004). LES involves solving the time-dependent fluid equations on a coarse grid which removes the small scale turbulence of the flow. The RANS modeling approach employs turbulence models to the averaged equations to directly yield the steady state solution of the flow variables (Franke, 2004). The RANS modeling approach is the most common approach used in CWE.

As stated by Dr. Dagnew from Florida International University (FIU) that "at this stage in the CWE community, a systematic validation of CWE models through comparison with wind tunnel experiments will enhance the confidence and warrant its use for practical applications." Thus, numerous researchers from around the nation are working on improving this technique and validating its precision. Ganeshan (2009) presented LES simulation coefficient of drag comparisons for stack interface applications. Numerical wind loading pressures developed on a

basic cube were investigated in studies by (Stathopoulous, 2002) and (Lim, 2009). Some of the computational efforts that have devoted to tall buildings include Huang et al (2007) and Braun et al. (2009) in which flow patterns and both mean and RMS pressure coefficients were compared. A thorough comparison of pressure coefficients obtained from both experimental wind tunnel tests and a Commonwealth Advisory Aeronautical Council (CAARC) were presented in Dagnew et al. 2009. Wind tunnel results from 1:400 scale rigid models tested were compared against RANS modeling of the CAARC building model. Figure 8 shows a comparison of the computational dimensions and fluid boundary conditions to the wind tunnel test setup. Results of this study showed good agreement between the CAARC numerical simulation and the wind tunnel mean pressure coefficients. An example of the pressure coefficients at various points on the building are shown in Figure 9. Also included in the plot are other researchers work on the same data collected including Braun (2009) and Huang (2007). Pressure coefficient comparisons deteriorate slightly at the sidewalls but improve at the leeward wall (Dagnew, 2009). The shapes of the plots are very similar to a horseshoe vortex shape contour generated along the windward face that agrees with the wind tunnel simulations.

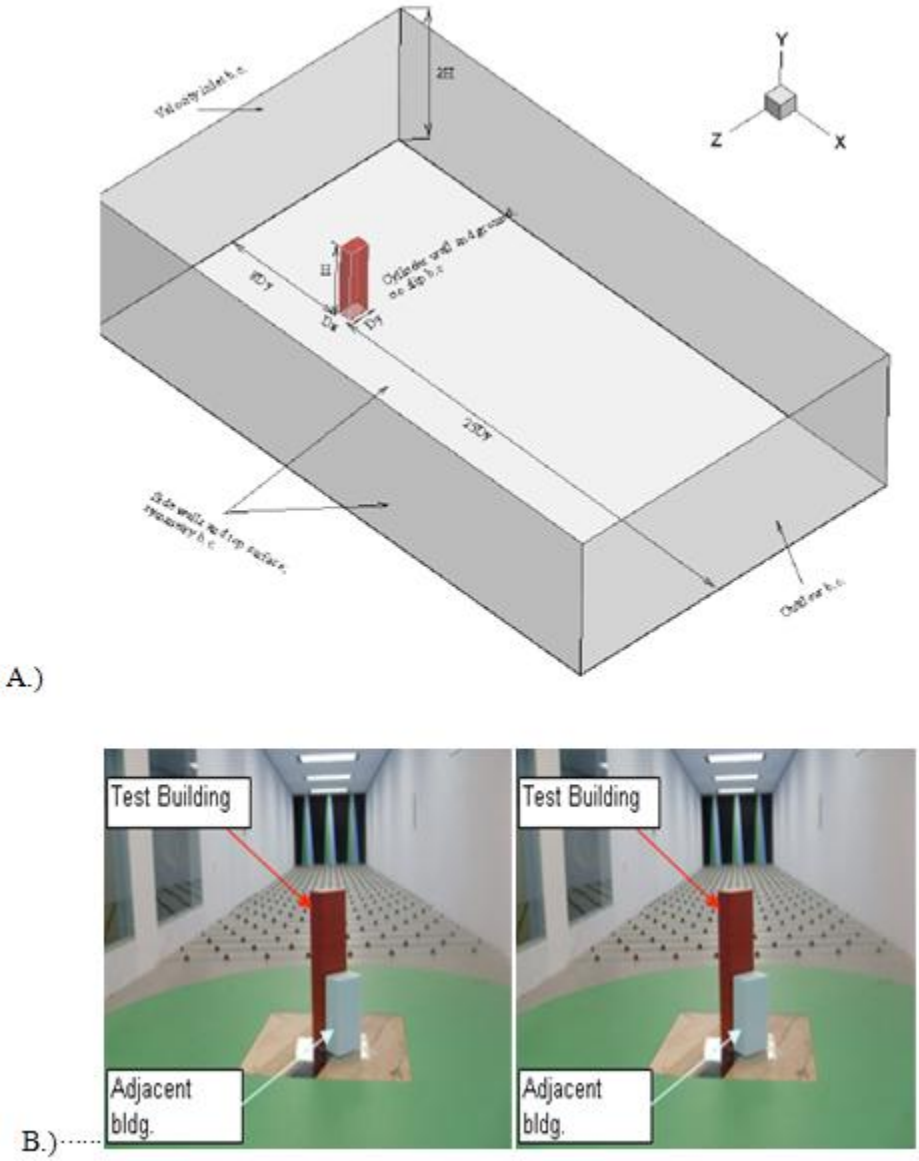

Figure 8: A.)CAARC building computational building domain and boundary conditions B.) Wind Tunnnel Configuration (Dagnew, 2009)

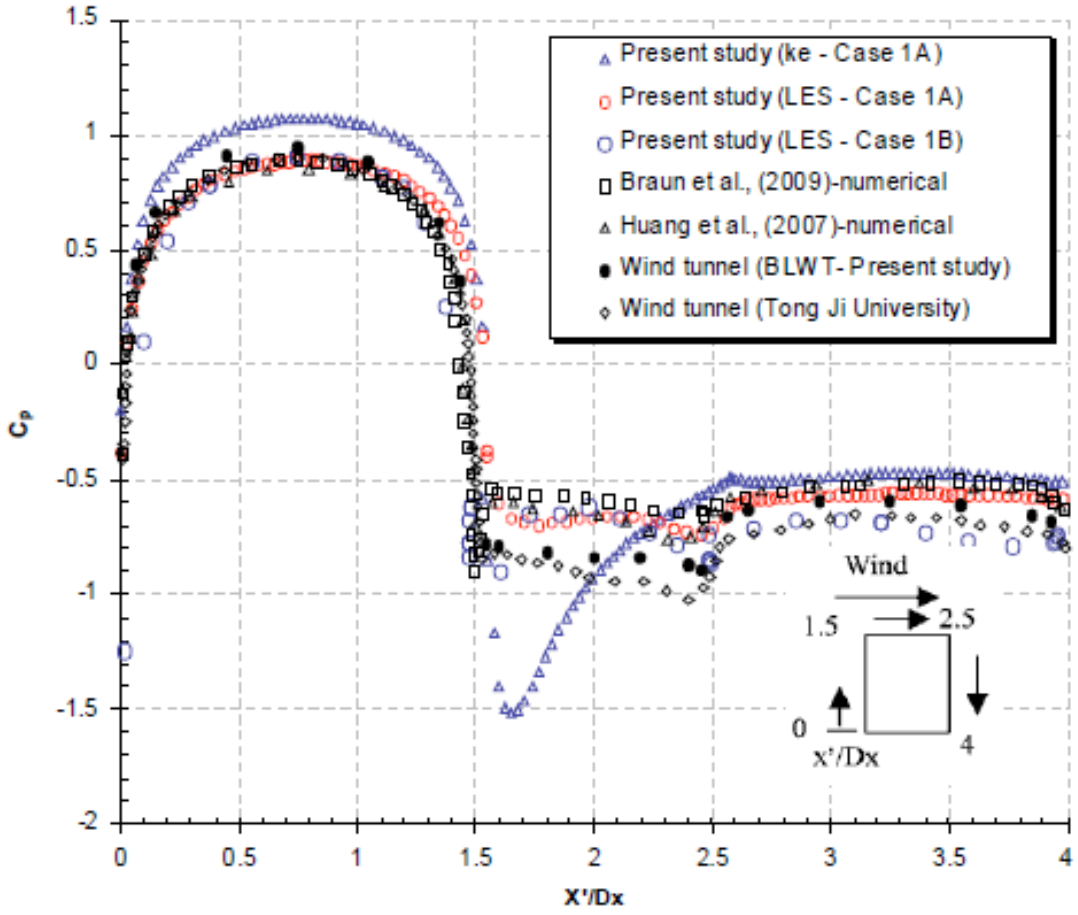

Figure 9: Mean Pressure Coefficient Comparison among numerous researchers along the perimeter of the CAARC test building at two thirds the height. (Dagnew, 2009)

Mean pressure coefficients have shown to be relatively in good agreement with other CWE models as shown by similar researchers such as Palmer et al. (2003), however no current research is known into the time dependent pressure coefficient comparison has been made. This is a vital requirement for use of CFD data in performance based engineering as dynamic response is measured.

Computational Tsunami Engineering (CTE)

The application of CFD techniques are also currently being researched in the field of coastal engineering. The application of CFD to Tsunamis is termed Computational Tsunami Engineering. Similar to CWE research, CTE is a very innovative field and only a select few Universities are conducting such research. As discussed previously, the TWB at OSU was constructed to further understand the dynamic interactions of tsunamis and structures. Also computational efforts are being conducted on the use of CFD modeling for predicting the wave forces generated during tsunamis or hurricanes.

One such study included single setup waves impacting a cylinder in the TWB. Impact forces were compared with CFD numerical model simulations, using the software LS-DYNA (Yim, 2009). This work was performed as a preliminary check to address the validity of the numerical simulation. Comparisons of the two methods are shown in Figure 10. Very good agreement is seen between the CFD models and the TWB experimental data. Additionally, wave surface pressures are also estimated for various depths using the LS-DYNA simulation. This study confirmed that the possibility of CFD modeling of extreme wave forces from tsunamis or hurricane-generated waves is feasible.

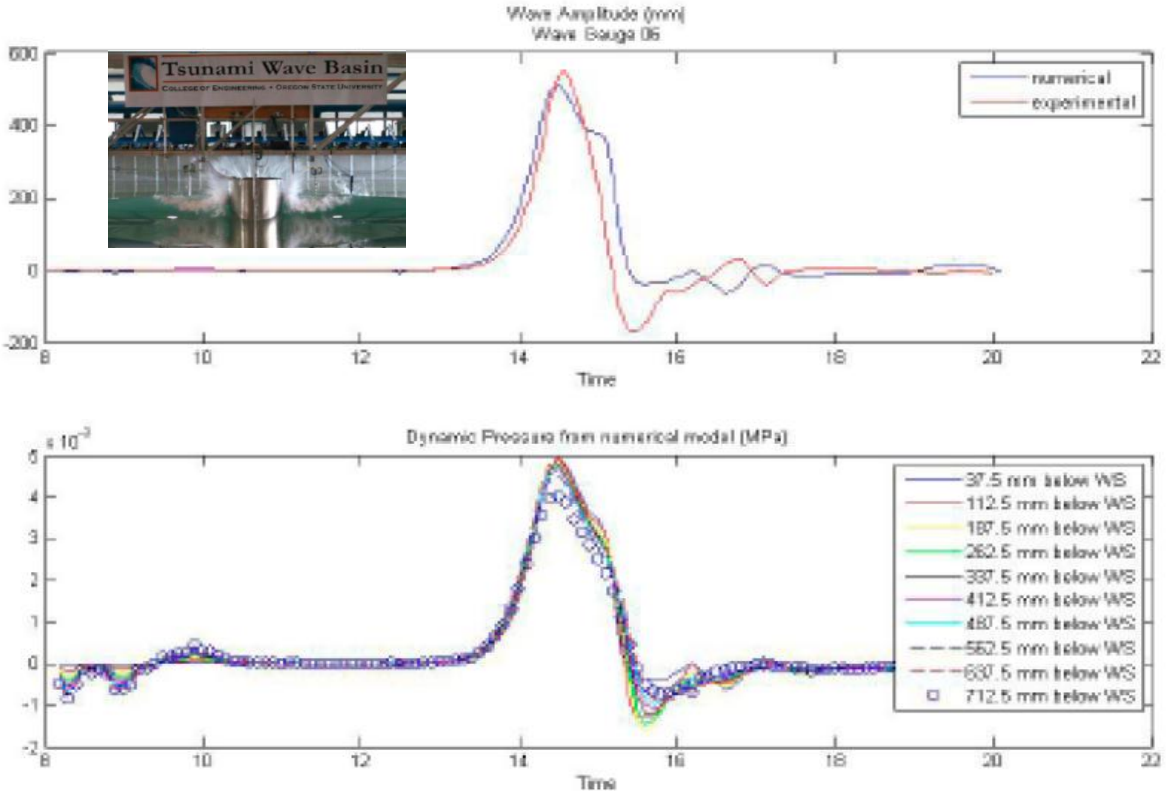

Figure 10: Comparison of numerical and experimental wave amplitude and surface pressure time histories. (Yim, 2009)

MSC DYTRAN

Dytran is an explicit finite element analysis (FEA) software with the ability to solve a variety of highly complex non-linear structural analysis problems (Dytran, 2008). Most FEA programs implement implicit methods to carry out transient solutions using a Newmark iteration technique to integrate forward in time (Dytran, 2008). Explicit methods typically employ a central difference scheme to advance in time (Dytran, 2008). Explicit methods are particularly suitable if the time step required for problem is very small. Some example problems requiring such small iteration steps include very large material nonlinearity, geometric non-linearity such

as friction, or problems containing physics demands such as stress wave formulation (Dytran, 2008). Therefore for models containing a high number of elements and notable material nonlinearity, then explicit methods provide more efficient solution technique as they do not require the costly formulation and decomposition of matrices each time step. Instead the typical sequence of each time step loop is carried out as shown in Figure 11. However other commercially available CFD programs such as FLUENT, employ both implicit and explicit techniques for FSI simulations. Implicit methods are suitable for steady state results as large time steps introduce truncation error of the independent variables.

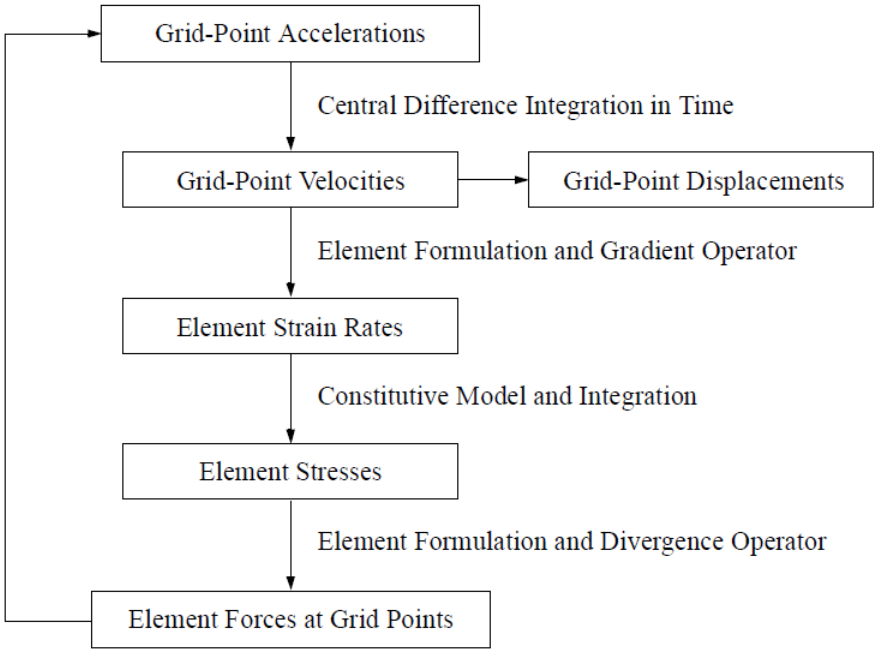

Figure 11: Explicit time stepping method for Dytran (Dytran Users Manual, 2008)

One of the main features of Dytran is the ability to model fluid-structure interaction problems. This feature is accomplished through the use of two separate descriptions of motion.

This step is an important consideration for simulating flow problems using numerical methods as the choice of an appropriate kinematical description of the flow field can affect the accuracy and stability of the results (Donea and Huerta, 2003). The algorithms of continuum mechanics make use of three distinct types of description of motion: the Lagrangian, the Eulerian and the ALE description. Dytran employs both Eulerian and Lagrangian descriptions to model both fluid and structure motion. A short illustrative description of each technique is provided below.

The Lagrangian formulation is utilized in Dytran for the motion of elements with a constant mass such as rigid structural materials. The motion of the material points, relate the material coordinates (X), to the spatial coordinates (x) by mapping φ. Therefore during any time interval the link between X and x can be described by the law of motion. Due to the one to one mapping φ and since material points coincide with the same grid points during motion, the free surfaces and interfaces between materials is tracked easily through the inverse transformation (Donea and Huerta, 2003). Therefore the material is collected into a mesh, and as the body deforms each grid point moves with the material and the element distorts (Dytran, 2008). However, when large deformations occur such as vortices in fluids, Lagragian applications may be unable perform such calculations or even result in large errors (Donea and Huerta, 2003).

Conversely, the Eulerian meshes are in a fixed reference frame in space and the continuum moves and deforms with respect to the computational grid. Conservation equations are formulated for variables and functions having an instantaneous significance in a specific fixed region (Donea and Huerta, 2003). This formulation therefore disassociates the mesh nodes from the material particles and introduces convective terms. This result enables the treatment of complex material motion but, introduces difficulties in tracking the material interfaces and boundaries. Thus the Eulerian Solver is utilized in Dytran for modeling fluids or materials that

undergo large deformations. Under this technique, the material of a body under analysis moves through the Eulerian mesh, as the mass, momentum, and energy of the material are transported from element to element (Dytran, 2008). Additionally, through the use of the dynamic viscosity term in modeling of Eulerian elements, the use of Navier-Stokes Equations is executed for the fluid domain.

The ability of any FSI simulation is made possible through the use of a coupling algorithm where both materials can interact In Dytran, both the Eulerian and Lagrangian meshes can be combined in the same computation through the use of a general coupling surface or Arbitrary Lagrangian-Eulerian (ALE) coupling surface. This surface acts as a boundary to the flow of material in the Eulerian mesh. The stresses in the Eulerian material then exert forces on the surface of the Lagrangian mesh, causing those elements to distort. However, the fluid response is also a function of the structures' surface motion requiring a feedback loop to be executed each time step (Donea and Huerta, 2003). The general coupling surface is used when fluid displacements are small and linear elastic structures are used. Conversely the ALE formulation is recommended to model nonlinear fluid interaction with nonlinear structural elements. A visual representation of the setup of FSI in Dytran is seen in Figure 12.

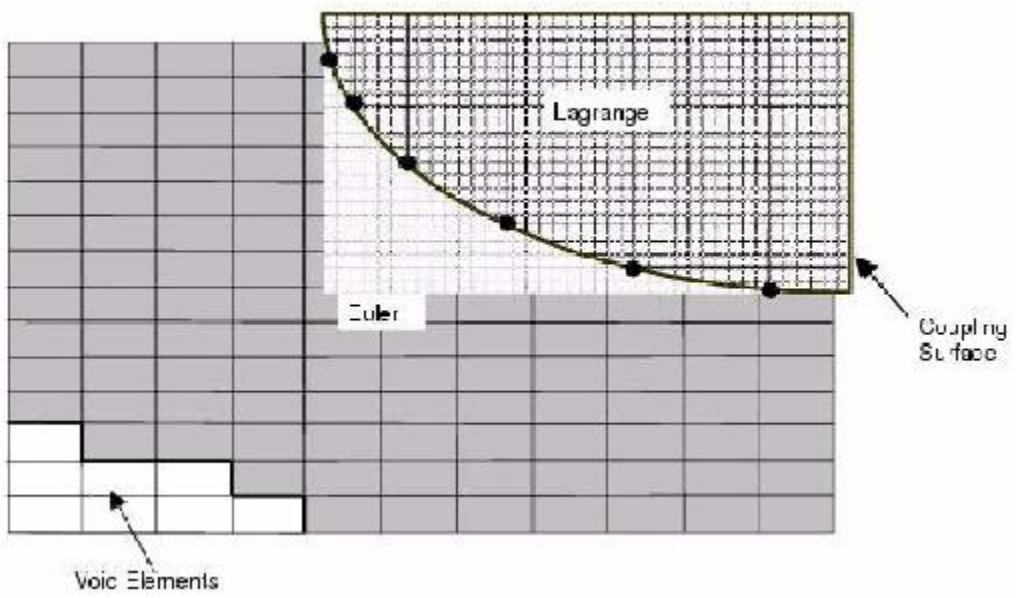

Figure 12: Fluid-Structure interaction in Dytran. (Dytran, 2008)

In this study, Dytran will be used for all CFD modeling applications for both wind and wave loadings. The goal of the study is to have the ability to generate both wind and wave load spectrums from Dytran simulations on two prototype structures. CFD has the ability to create a vast wealth of data on a variety of structural orientations, wind/wave velocities, and surface roughness conditions that a typical experimental setup is unable to reproduce. This computational power is one of the only solutions to full-scale application of PBHE.

CHAPTER THREE: METHODOLGY

In this study, a thorough investigation of hurricane hazards was performed using computational simulations. Numerous hazards associated with a hurricane event were reviewed including primary and secondary effects. However, due to wide scope and range of hurricane hazards, only the most probable effects that a typical structure experiences will be investigated. These hazards typically include extreme wind speeds, storm surge and the hydrodynamic forces from waves.

The first step in applying CFD to modeling hazards such as wind was to verify the accuracy of the results obtained through these simulations. This was performed by collecting existing experimental data from full scale laboratory experiments and comparing the time dependent forces/pressures to those predicted from the CFD analysis. Once the models were verified, prototype simulations were performed on bridge and building structures. Once dynamic time history loads were generated structural FEM models were carried out to demonstrate demand analysis on prototype structures. This process is shown in Figure 13.

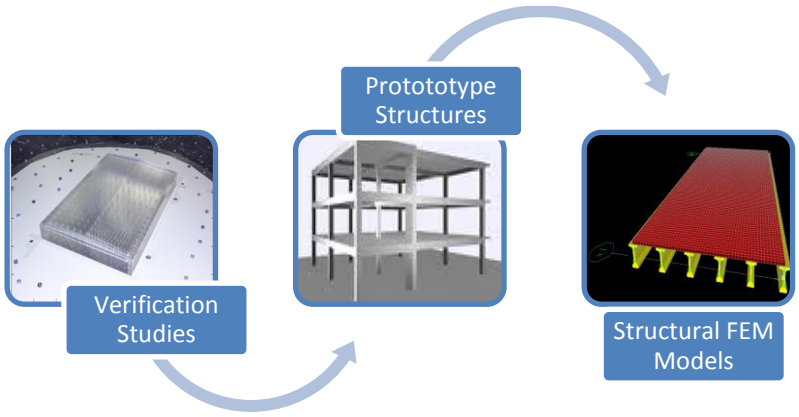

Figure 13: Research Methodology

Verification Studies

To validate the use of Dytran for PBHE, both wind tunnel experiments and wave tank basin experimental data was collected. Information regarding the experiment setup, atmospheric conditions, boundary conditions and data collection devices was recorded to enable the reproduction these experiments numerically. This will enable signal comparisons to be conducted using digital signal processing techniques and structural analysis techniques.

Wind Tunnel Validation

The wind tunnel data utilized in this study was collected at the UWO BLWT. These wind tunnel time histories were presented in Ho et al. (2005) and were utilized in the development of WINDPRESSURE. A total of eight different tests were run on different building configurations for various wind angles. During each test, a series of various pressure taps recorded the wind pressure distribution on the model. Due to time constraints and the scope of this study only one building configuration was used for numerical validation.

The building configuration chosen is a typical gabled structure. The model consisted of a 1:100 scale structure with dimensions (57 X 36.5 X 5.5 X 1.5 m, 187.5 X 120 X 18 X 5 ft (Length X Width X Eave Height X Rise). This building was placed in the UWO short wind tunnel equipped with approximately 4000 pressure taps sampled at 500 Hz for 100 seconds. Pictures of the building and experimental setup are shown in Figure 14.

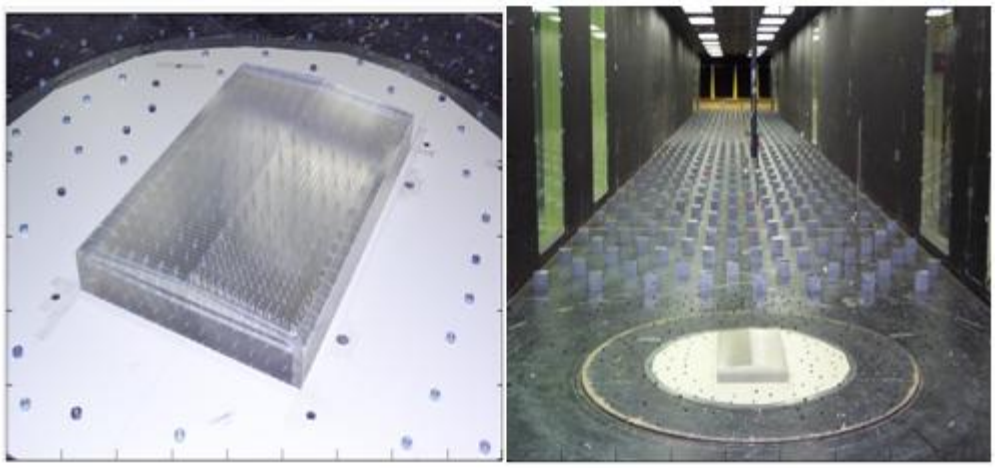

Figure 14: Photos of Building Model in UWO wind tunnel. (WINDPRESSURE, 2005)

Consequently, the exact building was replicated using LES in Dytran. The same 1:100 scale model was made with 424 Lagragian shell elements made of an Elasto-Plastic steel material (DMATEP). However, the model was constructed to be effectively rigid by defining a thick shell for the structure. The boundary layer atmosphere was constructed with over 13,000 Eulerian quadrilateral solid elements (CHEXA). Figure 15 shows both the Eulerian and Lagragian Mesh of the CFD model used for wind tunnel verification. The initial properties of the air that were input in the program are the initial velocity, internal pressure, specific internal energy, dynamic viscosity, and density. Information regarding many of these properties is standardized for room temperature and only the initial velocity state of the material was assumed, and the specific internal energy was set to zero. The initial velocity was set to zero to simulate stagnant conditions in the wind tunnel. The specific internal energy of the air was set to zero to eliminate the gamma gas law. Boundary conditions on the Eulerian mesh were set to simulate the actual wind tunnel test. Air flow was initiated by air entering one side of the

Eulerian mesh and exiting on the opposite boundary. Only a constant wind speed can be input into the DYTRAN simulation and therefore several surface roughness elements were created upstream of the building model to create more turbulence in the numerical simulation. However, due to computational resources and time constraints, extensive use of roughness elements in the CFD models was unfeasible. These elements drastically increase the number of elements in both the Lagragian and Eulerian mesh and severely increase calculation time. In order to simulate the roughness introduced in the wind tunnel experiment, element faces of the Eulerian mesh were simulated as barriers whereby no flow of material is allowed. Several rows of these elements were added to introduce time varying vortices to develop a more time varying response. These barriers are seen in Figure 15 as well.

A coupling algorithm was utilized in DYTRAN to enable the complex fluid-structure interaction. Additionally, to simulate the effect of the frictional resistance provided by the structure as the fluid is flowing around it, a skin friction coefficient is input in DYTRAN. The skin friction coefficients can be derived from the drag coefficient, which depends primarily on the Reynolds number. A reasonable estimate of the drag coefficient for the Reynolds number for this simulation of $6e10^5$ can be taken as 1.2, which is equivalent to a frictional coefficient in Dytran of 0.095.

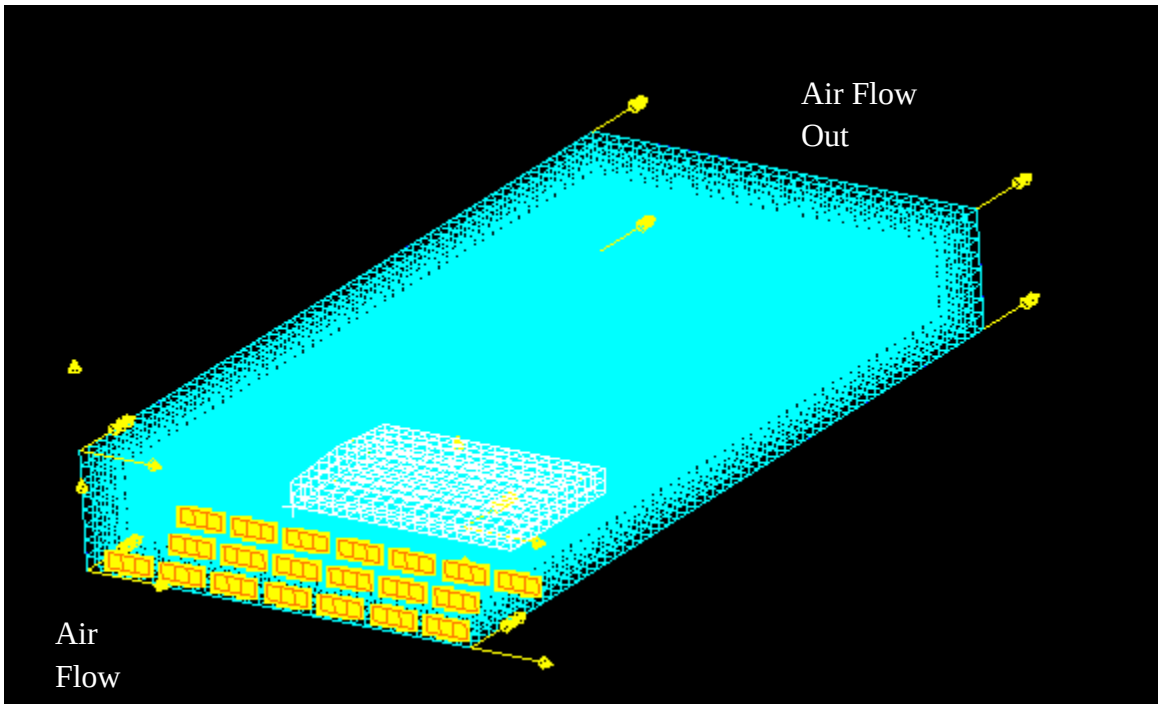

Figure 15: CFD model from DYTRAN of UWO experiment. Blue: Eulerian Elements (Fluid) White: Lagragian Elements (Structure)

One of the main benefits of the numerical simulation technique is the wealth of available data to be collected during the experiment. In this study, nodal force time histories for X, Y, Z and resultant components and Eulerian mesh parameters were recorded at a sampling rate of 500Hz. In the numerical models, a record of each nodes force time history can be recorded and converted to a pressure coefficient through the tributary area of each node. This will enable direct comparison with the wind tunnel pressure tap data. A typical CFD model was run for a 10 second duration at a sampling rate of 500Hz generating 1.5-2 GB of data. These models were run on a single core Pentium four processor, to generate the ten second duration worth of data and required 112 hours in simulation time. Due to these high computational costs, only two wind directions were used for validation with the wind tunnel. In the wind tunnel experiments,

models were rotated on a turntable to create the various angles of the wind attack. In the DYTRAN simulation, general coupling requires the meshes to be aligned in the Cartesian coordinate plane. Therefore, in the DYTRAN simulations the velocity of the air is given their respective component values, based on the angle of attack. The angle of attack that was chosen for comparison was 75 and 45 degrees from the longitudinal axis of the building, or 15 and 45 degrees transversely respectively.

To ensure that all effects of the wind pressure distribution are captured throughout the building, CFD comparisons will be conducted for five separate locations of the building. The five locations used in the comparisons will be: windward wall, windward roof, leeward walls, leeward roof, and roof peak. On each face, a node from DYTRAN was selected and a corresponding pressure transducer from the wind tunnel experiment was sampled for direct comparison. For each node, a time varying force was captured in Dytran that could be converted to pressure through its tributary area. A list of the comparisons included: mean pressure coefficient, power spectral density (PSD), autocorrelation, integral length scale, and the turbulence intensity. An outline of each measure will be made in the next section.

Mean Pressure Coefficient

During wind tunnel testing experiments, measured external pressures are typically stored in a non-dimensional form known as pressure coefficients (Cp), as shown in Equation 3. The measured pressure, (P) is normalized by the air density, (ρ) and the mean wind velocity at roof

height, (V) to obtain the pressure coefficient. From this parameter, wind pressures for any particular speed can be obtained by appropriate scaling.

$$P = \frac{1}{2}\rho V^2 C_p \quad (3)$$

Internal pressures develop in a model due to the openings in the building envelope and other leakage paths. Fluctuating internal pressures are not measured in wind tunnels directly however they can be determined through an empirical relationship given in Devenport et al. (2007) from the external pressures. Therefore the net load on the cladding can be determined as the difference between the internal and external pressures. This information is used for determining design pressures for cladding and glazing components of buildings.

Data provided from the wind tunnel experiments at the UWO laboratory were given in the pressure coefficient form. However, in the CFD simulation Dytran generates force measurements that were converted to a pressure using each nodes tributary area. The velocity at the boundary was defined as (26.831m/s, 60mph) but this velocity is not the velocity seen at the mean roof height, when the air interacts with the structure. No measurements of wind velocity are taken during the simulations on the building however, the Eulerian mesh was inspected to observe the wind velocity. This value was found to be around (17.1m/s, 56.1ft/s) at the roofline and was used for all calculations.

Another important characteristic for comparing mean pressure coefficients is to ensure that averaging time is consistent, as described by Main and Fritz (2006). ASCE 7-05 uses pressure

coefficients derived from a 3 second gust at (10m, 33ft) above ground in current design standards. However, due to the model and prototype scaling, wind tunnel mean pressure coefficients are derived under a time window of approximately 1 hour (once converted to prototype scale) (Main and Fritz, 2006). During the verification studies as discussed previously Dytran mean pressure coefficients were derived from a ten second signal due to the high computational demands.

Power Spectral Density (PSD)

The power spectral density (PSD) of a random process describes the power distributions of the signal in the frequency domain. Thus it shows at which frequencies variations are strong and at which frequencies variations are weak. Mathematically, it is defined as twice the Fourier Transform of the autocorrelation sequence of the time series, or the squared value of the Fourier transform of the time series as shown in Equation 4.

$$S_u(n) = \lim_{T\to\infty}\left[\frac{2}{T}|X_T(n)|^2\right] \quad (4)$$

Simiu and Scanlan (1996) showed that the spectral density of the signal can be used to describe the energy spectrum of the turbulent motion (Yu, 2008). Turbulent energy fluctuations on the building can be seen as the superposition of numerous winds eddies that combines and contributes to the total kinetic energy. Each eddy is characterized by a periodic motion of circular frequency ($\omega = 2\pi$n) or wave number (λ) (Yu, 2008).

Thus, to ensure that Dytran has captured all turbulent eddy contributions of the wind, a PSD was then computed for both signals and compared. To smooth the PSD plot a Hamming window was applied to a Welch PSD (Yu, 2008). This method is based on the direct Fast Fourier Transform (FFT), which was implemented in MATLAB. The plots were then normalized by the standard deviation of the longitudinal wind component (σ_u), Integral Length scale (Lu_x) and the mean wind speed (U). Due to both positive and negative deviations, the value is first squared and before averaging them, and finally the root is taken to given consistent wind speed units. Mathematically the formula for the standard deviation can be found in Equation 5.

$$\sigma_u = \left\{ \frac{1}{T} \int_0^T [u(t) - \bar{u}]^2 \, dt \right\}^{\frac{1}{2}} \tag{5}$$

Additionally, to ensure accuracy in both numerical and experimental wind modeling techniques, the respective spectra was compared against established methods for estimating the spectrum for design purposes. These established methods include Von Karman, Eurocode I and Busch and Panofsky et al. (1968) (Holmes, 2001).

Autocorrelation

Autocorrelation is a statistical tool used to measure the correlation of two values in the same data set at different time steps. The autocorrelation coefficient can detect non-randomness in data

as it is closely related to the spectral density. The autocorrelation coefficient is also used in calculation of the integral length scale.

The calculation of the autocorrelation function is shown in Equation 6 where T is defined as the length of time for the record and τ is defined as the time lag.

According to Yu et al. (2008), the autocorrelation coefficient/function and integral length scale are affected by the length of record being analyzed (Yu, 2008). Therefore, for the autocorrelation comparison, only ten seconds of data from both the wind tunnel and CFD simulations will be used.

.

$$R_{xx}(\tau) = \lim_{T\to\infty} \int_{-T}^{T} x(t)x(t+\tau)dt \tag{6}$$

Integral Length Scale

Another measure of the turbulence of the signal is the calculation of the integral length scale. The integral length scales of turbulence are measures of the average size of the turbulent eddies of flow. There are 9 scales corresponding to the three dimensions and three types of eddies (longitudinal, transverse and vertical). According to Simiu and Scanlan (1996), the integral length scale can be calculated according to Equation 7 where U is the mean wind speed, τ is the time lag, $\bar{u}^2$ is the longitudinal turbulence fluctuation and ρ_{uu} is the autocorrelation coefficient. The longitudinal turbulence fluctuation is based on an empirical constant β and squared value of the friction velocity.

$$\mathrm{L}u^x = \frac{U}{\overline{u^2}} \int_0^\infty \rho_{uu}(\tau) d\tau \tag{7}$$

Turbulence Intensity

One of the most straightforward characteristics of the atmosphere's turbulence is described in a quantity termed the turbulence intensity. The turbulence intensity is defined mathematically as the ratio of the standard deviation of each fluctuating wind speed component to its mean value. Typically for wind observations, the time window used for the calculation is between 10 minutes and 1 hour (Simiu and Scanlan, 1996). For our DYTRAN simulations, the ten second record will be used for this calculation.

The turbulence intensity is also compared against an approximate relationship given in Holmes (2001). Through measurements of surface wind gusts produced by large scale depression systems, the turbulence intensity can be approximated through Equation 8. Therefore, the turbulence intensity is entirely characterized by the surface roughness length of the terrain (z_o).

$$I_u = \frac{2.5 \times u*}{\left(\frac{u*}{0.4}\right) \times \ln\left(\frac{z}{z_o}\right)} = \frac{1}{\ln\left(\frac{z}{z_o}\right)} \tag{8}$$

Single Degree Of Freedom Response (SDOF)

The last verification method used was to validate the use of CFD simulations from a dynamic response instead of a static comparison. As stated in the literature review this is critical for the use of CFD in PBHE, as little research has been committed to this topic in the CWE field. Additionally Dytran is typically performed for sudden transient impulses and well developed turbulence models for LES simulations may not be employed. These applications typically include impact, ballistic or other short duration loading situations. These time durations typically are on the order of milliseconds or tenths of seconds. However, for wind tunnel comparisons the CFD simulations were ran for 10 seconds. In order to ensure that the dynamic response of a system is not lost in the numerical simulation the response of a single degree of freedom (SDOF) system was investigated.

A program in MATHCAD was used to analyze a time dependent force input on a SDOF system with damping, according to the average acceleration method. The SDOF system was defined with a mass of (500kg, 1,100lb) which when scaled to model dimensions represents 110 kip and a natural frequency of 5Hz. The damping of the system was set to 5% of the critical damping. Due to the large wealth of collected data in 100 sec at 500 Hz (50,000 data points), only 10 seconds of the wind tunnel record was used and then the load was released for a total recording of 13 seconds. This was mimicked with the CFD simulation data, and comparisons were made of the displacement, velocity and acceleration of the SDOF system for all thirteen seconds. Finally, power spectral analysis of the response for each method was compared to verify the frequency content of the dynamic response.

Wave Tank Verification

For this study, wave basin records from studies conducted at the Coastal Engineering Facility at the University of Florida were collected (Shepperd, 2009). Using a wave tank measuring (1.8m, 6ft) wide by (1.8m, 6ft) tall and (36.5m, 120ft) in length numerous bridge configurations of various levels of complexity were investigated. In all, over 1100 tests were performed for numerous wave periods, wave heights, structure clearance height, and structural models (Sheppard, 2009).

The models used in the study were built from scale 1:8 replica of the I-10 Escambia Bay Bridge. This bridge experienced failure during Hurricane Ivan, as many of the segmented spans were pushed off their pier caps and into the bay, from the storm inundation and hydrodynamic wave forces. Figure 16 shows the progression of structural elements added to the bridge models to help quantify the effects of the wave forces on bridges. The First Model (A) only represents the slab of the bridge and further models continue to add the girders, overhang, and crash barriers (B-D).

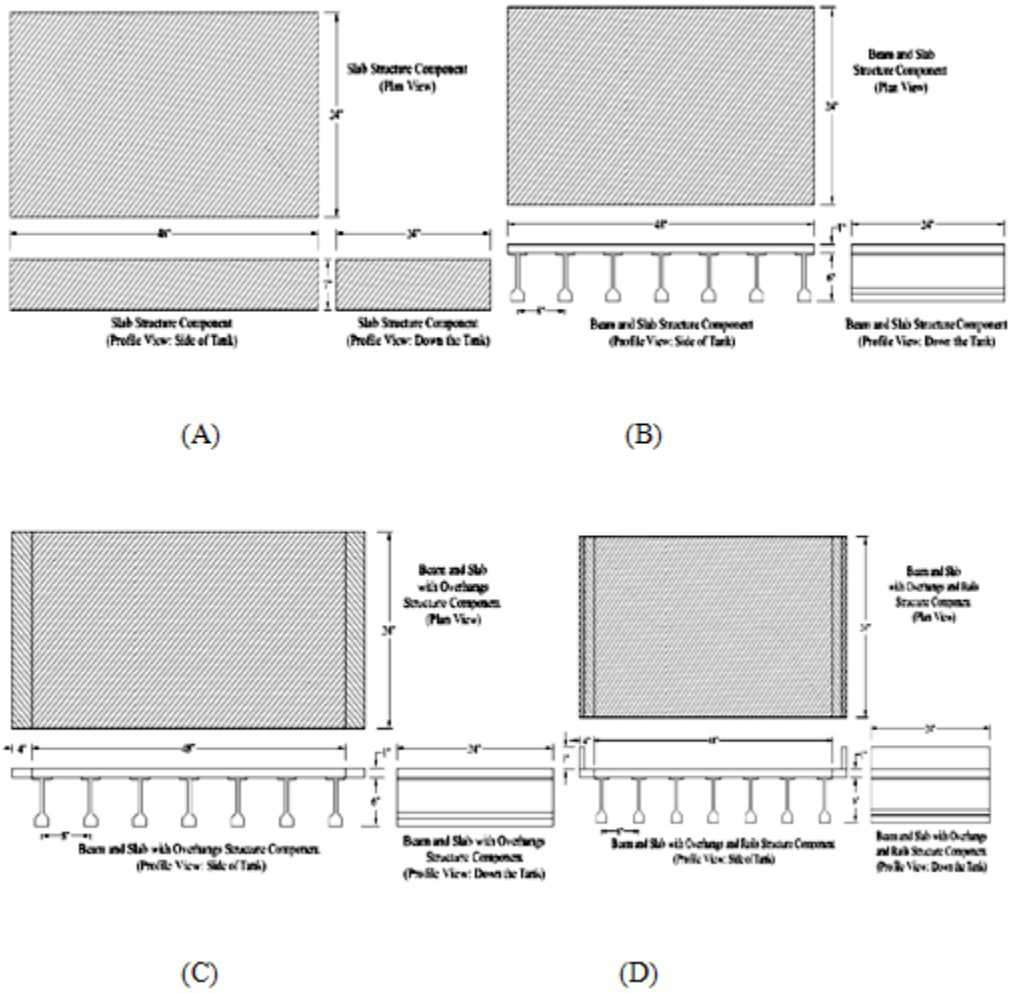

Figure 16: Bridge Deck Models used in Wave Tank Testing (Sheppard, 2009)

Bridge models were suspended from a steel bracing system in the wave tank and subjected to a series of monochromatic waves as shown in Figure 17. Measurements from the bridge model were taken by four multidirectional load cells placed on the steel support system and pressure transducers mounted across the bottom surface of models. The load cells and pressure transducers were sampled at a rate of 480 and 1000Hz, respectively.

Figure 17: Left: Steel Support Structure for Models Right: Flat Plate Bridge Model during testing in wave basin tank. (Sheppard, 2009).

Thus, in this study, only one of the bridge deck models tested was replicated numerically using Dytran. The structure chosen was the flat slab model, and test number 47 and 50 was replicated (Sheppard, 2009). For this specific test, a train of waves with a period of 1.5 to 2 seconds, wave length of (3.04m, 9.97ft), and wave height of (228mm, 0.75ft) was created in the wave tank basin. Other parameters used in study were the still water depth of (533mm, 1.75ft) and the structure clearance was (52mm, 0.17ft).

The exact bridge was replicated in DYTRAN simulations. The same 1:8 scale model was made with 492 Lagragian shell elements made of an elasto-plastic polypropylene material (DMATEP) for the slab model. However, the structure was constructed rigidly by defining a relatively thick shell, as performed in the CFD wind models. The wave tank basin was

constructed with over 77,000 Eulerian Quadrilateral Solid Elements (CHEXA). Figure 18 shows both the Eulerian and Lagragian Mesh of the CFD model used for wave tank verification.

In Dytran, all of the geometric quantities were modeled exactly and the wave was not created but rather initialized with the corresponding parameters discussed above. Therefore the only assumption required in the program was the velocity at which the water is translating forward. No information is provided about this from the report and therefore a reasonable assumption of (0.5-1 m/s, 1.64-3.28 fps) was assumed for the numerical models based on the wave period and estimated wave width.

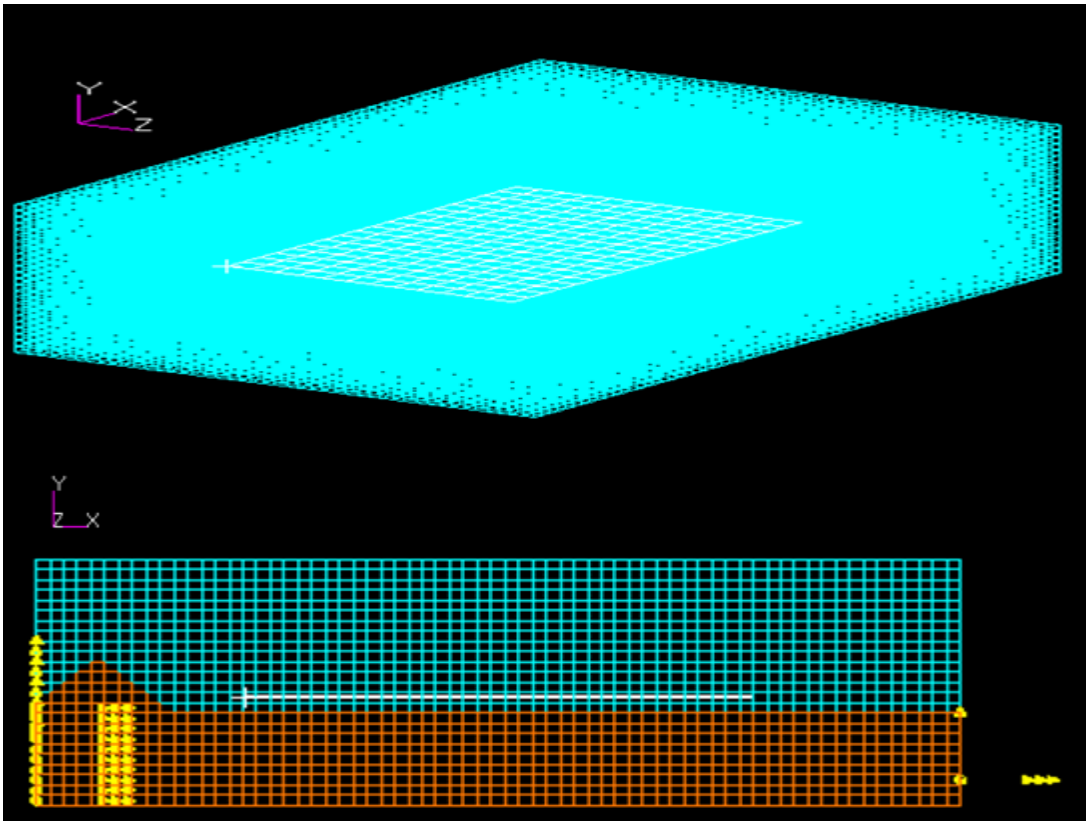

Figure 18: CFD model from DYTRAN of UF wave tank experiment. Top: Blue: Eulerian Elements (Fluid) White: Lagragian Elements (Structure). Bottom: Input shape of Setup Wave for Test Number 50. Input Wave Velocity in Positive X-Axis

To ensure that all effects of the wave loads are seen in the CFD models, a comparison was conducted on the time dependent load cell readings. In DYTRAN, several nodes were selected and a time varying force was recorded. This allowed for direct comparison of the maximum and minimum vertical forces and the power spectral density (PSD) of the signal. Additionally the load rise time t_r was observed for each event which is a determining parameter for classification of the loading as quasi-static or slamming.

Prototype Structures and Location

Performance based engineering is typically performed for a specific structure in a specified location. In this study the region of interest will be the Tampa Bay/Sarasota area. This area of the State of Florida is host to numerous coastal structures, including the Sunshine Skyway Bridge, MacDill Air Force Base, and numerous shoreline hotel structures that are typically 8-15 stories tall. Tampa Bay, has been spared from a major hurricane since 1921 in which a 100+ mph Hurricane made landfall at Tarpon Springs, causing six deaths. However, during that time Tampa Bay had a population of 135,000 and today more than 2.5 million people reside in the area. Additionally the bathymetry of the Tampa Bay Area is very conducive to excessive storm surge, which makes it vulnerable to large hurricanes. All of these factors decrease the expected performance of the empirical design based structures in the region. Therefore, results from structures in this region may substantiate the need for refinement in the current structural engineering field.

Building Model

The prototype building used in this study was obtained from a Reinforced Concrete Design Handbook. The building consists of a three story one way joist and slab system with typical bay spacing of (9.1mX9.1m, 30'X30'). Each story is thirteen feet tall and the total plan dimensions of the structure are (27.5mX45.7m, 90'X150'). The building was designed with no shear walls and uses the beam and column framing as the lateral restraint system. The building was designed in a very high wind prone region, with 145mph as the design wind speed. This design wind speed is slightly higher than the base wind speed in the Tampa-Bay region, according to ASC 7-02 which is approximately (58-60m/s, 135-130 mph). The structure was designed for typical Dead Load (DL) and Live Load (LL) of (6.22kPa, 130psf) and (2.87kPa, 60psf), respectively, that is typically found in an office building or hotel.

Using this load data, the structure was designed per American Concrete Institute (ACI) code and all reinforcing steel was sized for the columns and beams. The columns and beams were reinforced with a 5% and 3% steel percentage respectively. The concrete and steel reinforcing grades chosen were (27MPa, 4000psi) and (420MPa, 60,000psi) respectively due to their common use in the design industry.

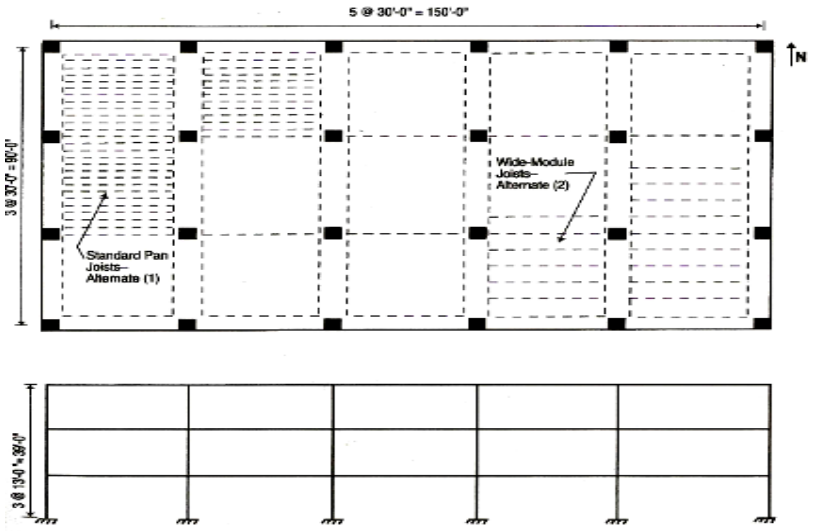

Figure 19: Plan and Elevation view of Prototype Building used in Study for Wind Tunnel and Wave Tank Testing

Bridge Model

The bridge model chosen for this study was based on the Anna Marie Island Bridge replacement project currently under consideration since 2008. The existing bridge consists of several concrete beam fixed span segments and a bascule type span in the main channel approximately (5.3m, 17.5ft) above the mean water high. The bridge connects the Anna Marie Island to the mainland near Bradenton, Florida, as seen in Figure 20. During the Project Development and Environment (PD&E) study, wind tunnel testing was carried out on several different bridge deck configurations on a 1:60 scale ratio at the RWDI Miramar, Fl BLWT. Therefore this bridge was chosen due to the availability of data from wind tunnel testing and its applicability of a typical coastal bridge.

Figure 20: Left: Existing Anna Marie Island Bridge. Right: View of Anna Marie Island in Tampa Bay and Study Bridge Location (Mara & King, 2008)

The wind tunnel testing carried out at the BLWT facility was conducted on two different bridge deck geometries. These bridge deck cross sections can be seen in Figure 21. For this study the smaller cross section was chosen, with 6 girders for modeling and analysis. Measurements from the BLWT from a hotwire anemometer provided information on the mean wind speed and turbulence intensity for various elevations for the bridge deck placement. Additionally, smoke flow visualizations were conducted to see the effect of the barrier placement on the wind vortices that developed. These results will be used a validation tool for the CFD models implemented in this study.

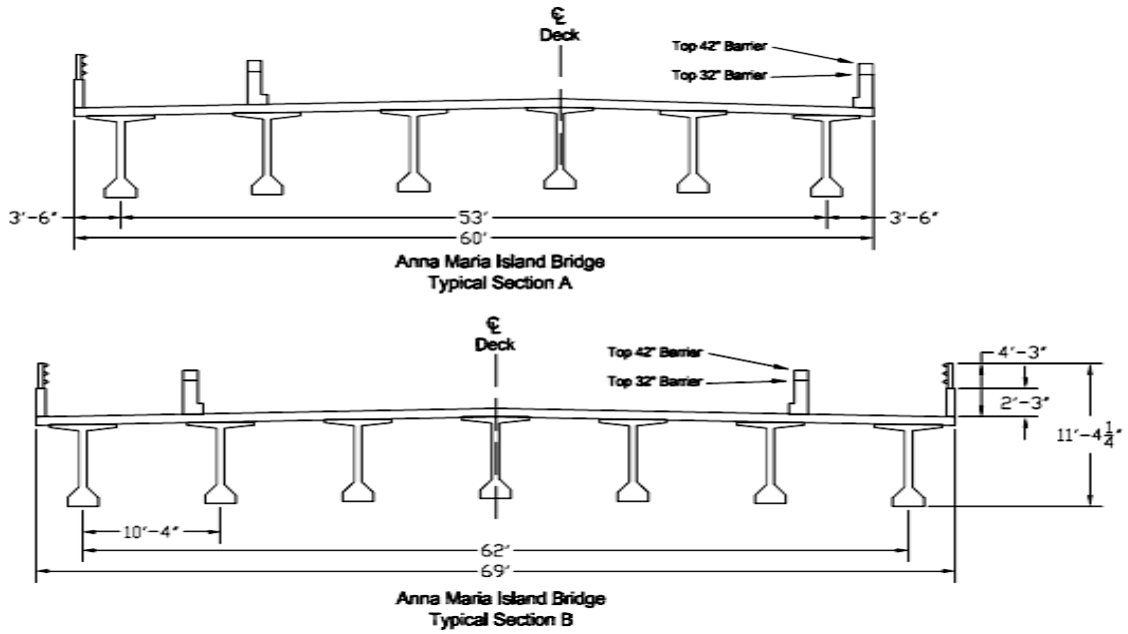

Figure 21: Section Views of Anna Marie Island Bridge Deck Alternatives (Mara & King, 2008)

Since the full design of the bridge has yet to be determined, a typical Florida Pre-stressed T-78" bulb beam was chosen for the main girders of the bridge deck. A Florida T-78" Beam was chosen due to its large span applicability (typically around (36.5m, 120ft)) and predominant use in Florida bridges. Additionally, the new bridge deck height has yet to be determined and therefore the existing deck height will be used for this analysis.

To simplify the structure for use in the wind tunnel and wave tank for software reasons, the depth change between the slab and girder was not modeled and the flanges of the beams were connected continuously, to create a smooth undersurface to the deck. The bridge model was created out of 242 Shell elements and was comprised of over 8938 quadrilateral elements (CQUAD). The properties of the shells were defined from standard concrete values used in

design. The model was constructed rigidly by defining the thickness of the shells to be large, in comparison to the dimensions. A picture of the bridge model is shown in Figure 22.

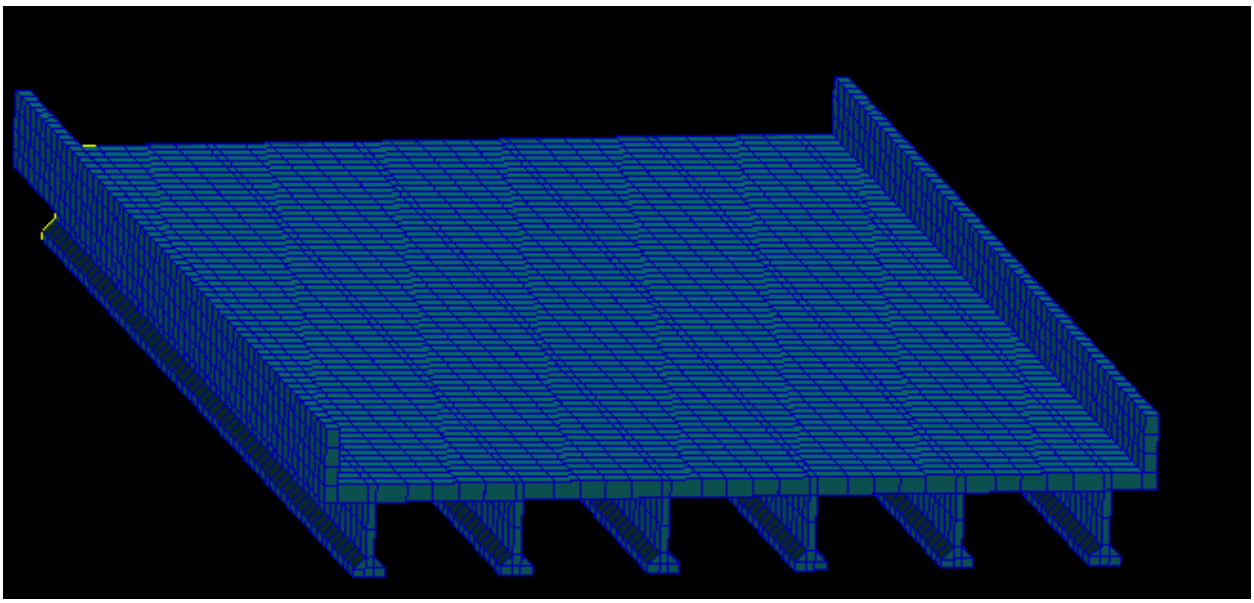

Figure 22: Bridge Model Used in Wind Tunnel and Wave Tank CFD simulations

Probability Distribution Analysis

Once a specific locations and structure of interest has been determined, the first step in hazard analysis in a Performance Based Design is to statistically define the magnitude and probability of occurrence of these hazards occurring both individually and simultaneously. Probability Distribution Analysis is a vital step in applying PBE. Since the performance of the structure is related the hazards associated with it, then full probabilistic quantities are required to map structural response/damage to category of hurricane. This step in PBHE is currently quite

well understood and can be thoroughly explained in Simiu and Phan et al. (2007). However the existence of structure specific dynamic data from hurricane hazards is currently non-existent.

Statistical information from the Tampa Bay region was collected from annual records and computer simulations through NOAA and NIST. The statistical data was not collected from actual hurricane conditions, and would only be used for identifying statistical quantities, such as the return period for damage assessment. Each hazard was then described by an appropriate probability distribution function for the given location. Once each hazard's marginal distribution has been defined, a joint probability distribution can be determined with additional knowledge of the correlation between the hazards. These results will then be combined with the dynamic time history data generated to allow for scaling of the record to any particular event.

Prototype Dynamic Time History Generation

Once the accuracy of CFD modeling were confirmed through the verification studies the generation of Dynamic Wind and Wave time history data was the main subject of this study. CFD model simulations were carried out on the MSC Dytran platform. These results were then standardized into pressure and force coefficients. This process will enable a spectrum of loads corresponding to each storm category to be created and applied to later structural models.

Extreme Winds

First, annual extreme non-directional wind speeds were collected from NIST for the Tamp Bay region from 1951-1990. A 10m corrected 3-second annual extreme wind gust was reported. This data was collected for insight into the historical wind records available.

Next, dynamic data was created using CFD wind tunnel simulations of the building and bridge under consideration. Both structures were placed in the Dytran Fluid Solver to develop time history records of wind pressure on various sections of the models as shown in Figure 23 and Figure 24. From each time history record, the forces/pressures can be converted to pressure coefficient as typically done in wind tunnel testing. From this non-dimensional coefficient, a time history of pressure can be obtained for each storm category by scaling the pressures by the appropriate expected mean wind speed.

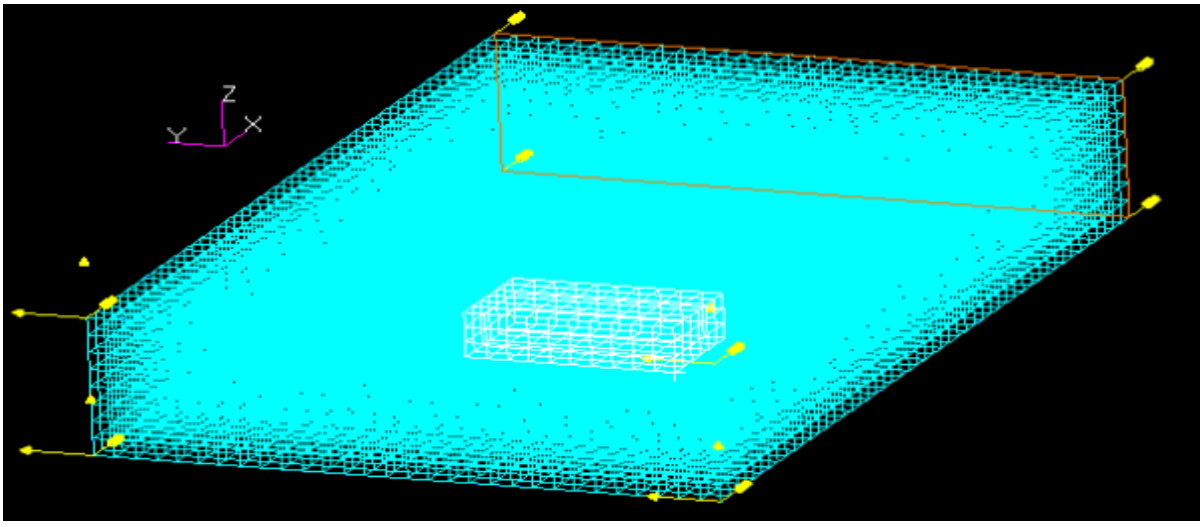

Figure 23: Building Model in Wind Tunnel CFD simulation. Flow in the positive x-direction.

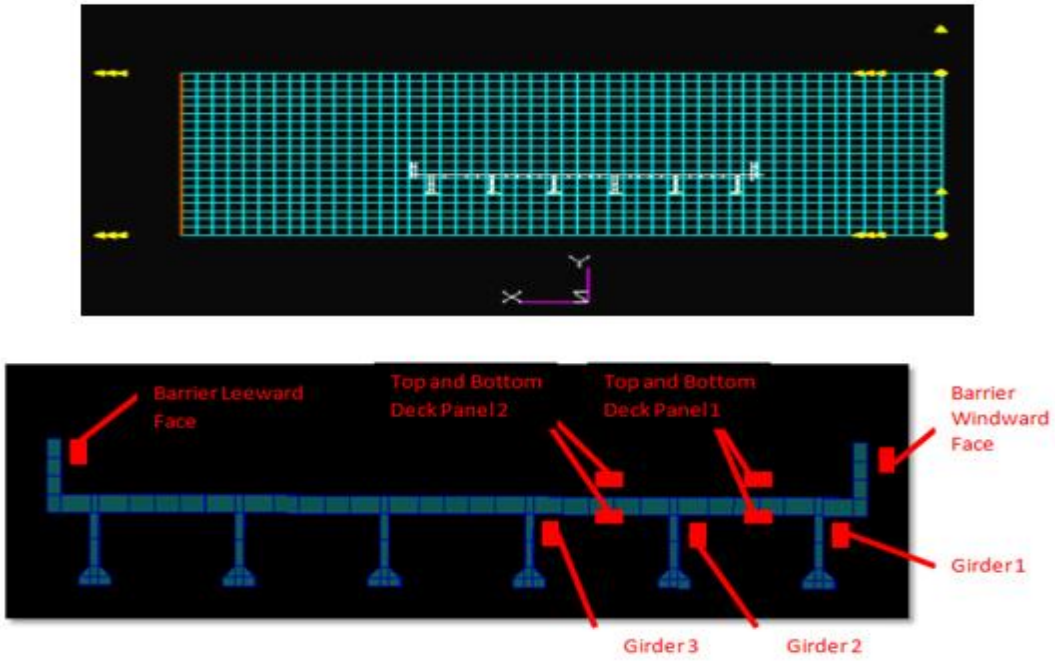

Figure 24: Top: Bridge Model in Wind Tunnel CFD simulation. Flow in the positive x-direction. Bottom: Location of Pressure/Force Readings taken during simulation.

Surge Height

For the present study, SLOSH generated storm surge data was utilized for analysis. The Tampa Bay basin was used and the corresponding SLOSH grid for the basin is shown in Figure 25. The SLOSH program employs a telescoping polar grid coordinate system within each coastal basin. As a result, good resolution data is provided for areas of interest along the coast and inlet bays, while conserving computer resources.

The SLOSH Grid for the Tampa Bay Region consists of approximately 58 radial and curved lines, making up approximately 3100 regions. Each grid region covers approximately 1.5 square miles. The SLOSH model requires only the category of the hurricane, direction of wind

speed and landfall tidal condition (high, medium, low) for calculation of anticipated storm surge heights. All possible surge conditions were recorded for the prototype building and Anna Marie Island Bridge.

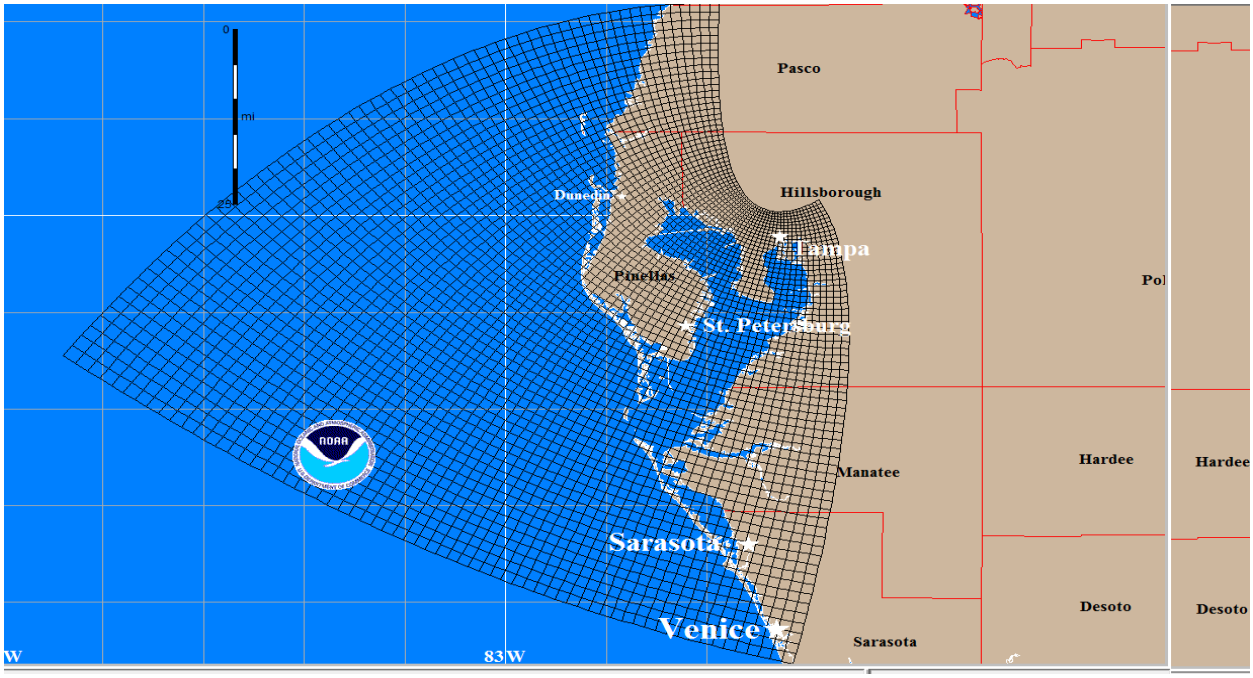

Figure 25: Tampa Bay region SLOSH Grid

Time dependent surge heights were generated not in this study and rather it is suggested that it should be treated as a static load. Storm surge is typically relatively constant for the study location, and the only fluctuation in the height is due to the astronomic tidal heights. Therefore the expected storm surge can be drastically different if the storm is expected to make landfall during high, low or normal tide conditions. Therefore, taking a look at the astronomic tidal variation in the Tampa Bay region was conducted using SLOSH and shown in Figure 26. As

you can see from the Figure, the fluctuation in tidal height is relatively constant over a 1-2 hour window, which is the expected extreme loading duration of the hurricane event for a structure. The change in astronomic tides is very small and typically around (30-60mm, 0.1-0.2ft) during this window.

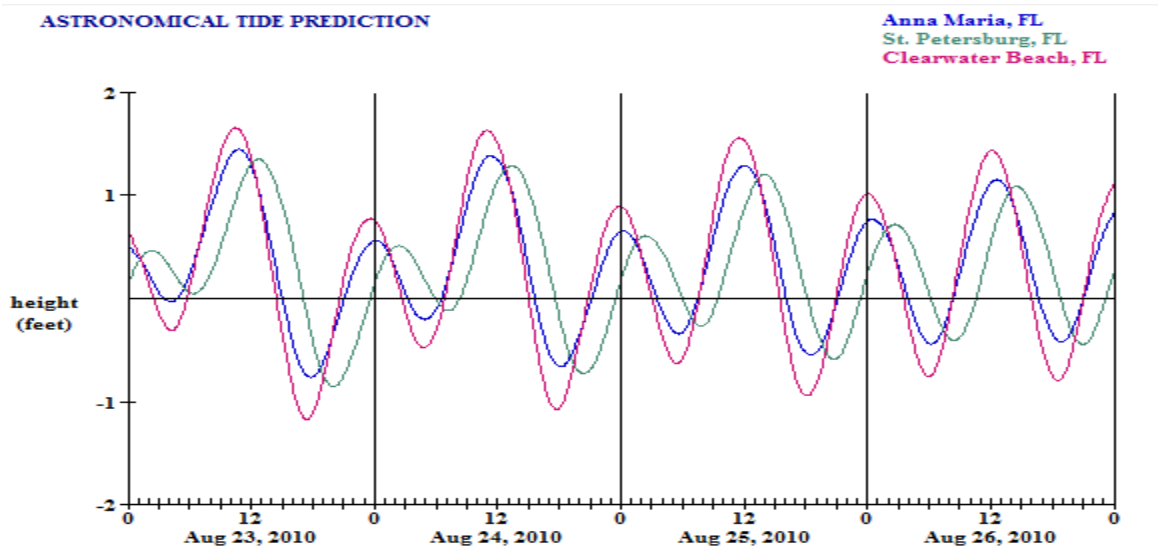

Figure 26: Astronomic Tidal Predictions for Tampa Bay region from SLOSH

Wave Simulations

Similar to the extreme wind speed hazard, both annual extreme wave data was collected and numerical modeling of wave loads was conducted. First significant wave heights were collected from NOAA buoy number 42099 located in the St. Petersburg area as shown in Figure 27 for a three year period. The significant wave height is calculated by averaging the top 1/3 of

the entire wave heights recorded during a 20 minute interval. The wave height intensity data was appropriately described by the log-normal distribution.

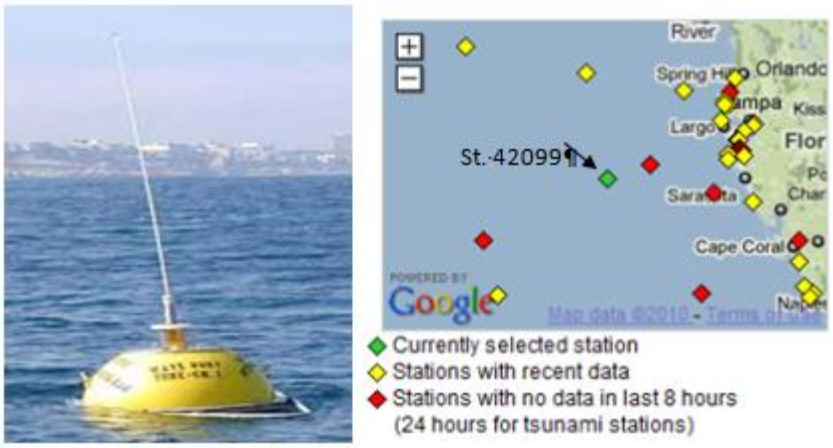

Figure 27: Picture and Location of NOAA Wave Buoy Number 42099

Next, dynamic data was created using CFD wave tank simulations of the building and bridge. A single wave height and period was modeled and measured forces were converted into a non-dimensional force coefficient. This was performed by scaling the load by the water density (ρ_w), acceleration of gravity (g), significant wave height (Hs), and tributary area (A). Then estimates of the anticipated wave forces for each category of hurricane dynamic wave forces can be developed for each model by scaling the appropriate non-dimensional force coefficient.

However, the full dimensions of the building were not modeled in a wave tank but, rather a square shape representing the column will be modeled This approach was taken due to the

high likelihood of building envelope failure and loss of the curtain wall for the first story with the presence of wave action. Therefore, only the primary structural members, such as the columns, would be subjected to wave forces for the first story. This assumption was also used for all of the wind loading calculations for the building.

Finite Element Structural Models

Once Dynamic Loads were generated for both prototype structures, a detailed FEM was created for linear structural analysis. To simplify the structural analysis process due to time constraints, a 2-D model of a frame was constructed of the three story building and a single span of the Anna Marie Island replacement bridge was modeled. Each model was created in SAP to full scale, utilizing frame and shell elements. A short description of each model is given below followed by a figure of each model.

The 2-D building model was constructed entirely of frame elements, which were given their respective cross section dimensions and reinforcement properties previously determined from ASCE 7-05 wind design procedures. Fixed support conditions were enforced along the base of the structure. Wind Loads were applied at floor locations where the building's facade or curtain wall would be attached to the main structural framing. Wave loads were applied at each node, from the base of the columns of the structure to their respective wave crest plus surge height.

The Bridge Deck model was constructed of both frame and shell elements. Frame sections were modeled for each girder and were given AASHTO Beam Type VI properties (72"). A (250mm, 10") reinforced concrete deck shell was then modeled (0.9m, 36") above the frame

elements which were then rigidly linked together. The (30.5m, 10ft) long by (18.3m, 60 ft) wide bridge deck was coarsely meshed into (0.3m, 1 ft) lengths to enable easy application of nodal time histories. Pin support boundary conditions were enforced on the ends of the each frame element end where each span would rests on the pier caps. Additionally, the crash barrier was not modeled in the structural model, but its tributary was taken into account when applying the loads. Wind loads were placed on the structure on several nodes and wave loads were applied to the barrier and the bottom of the bridge deck.

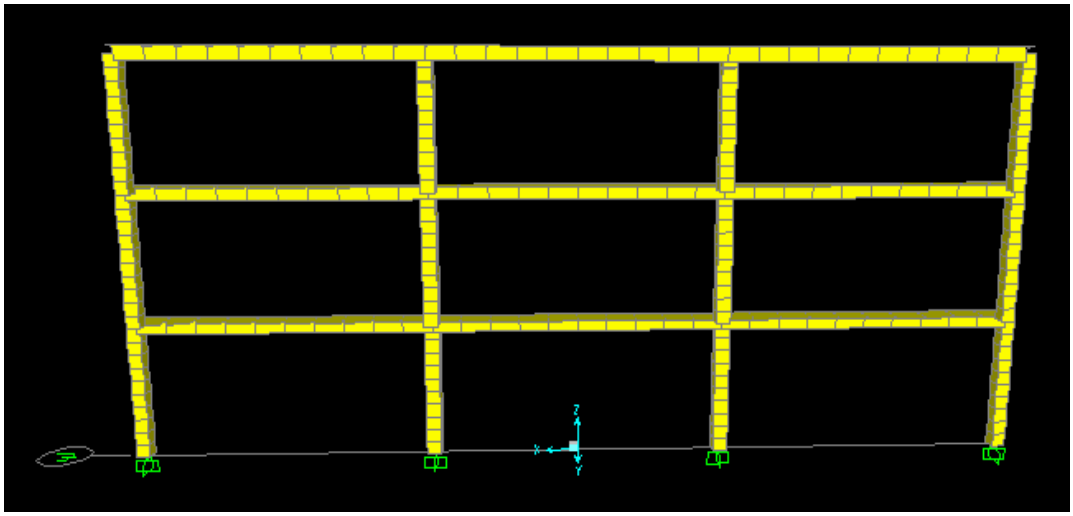

Figure 28: Building Model in SAP

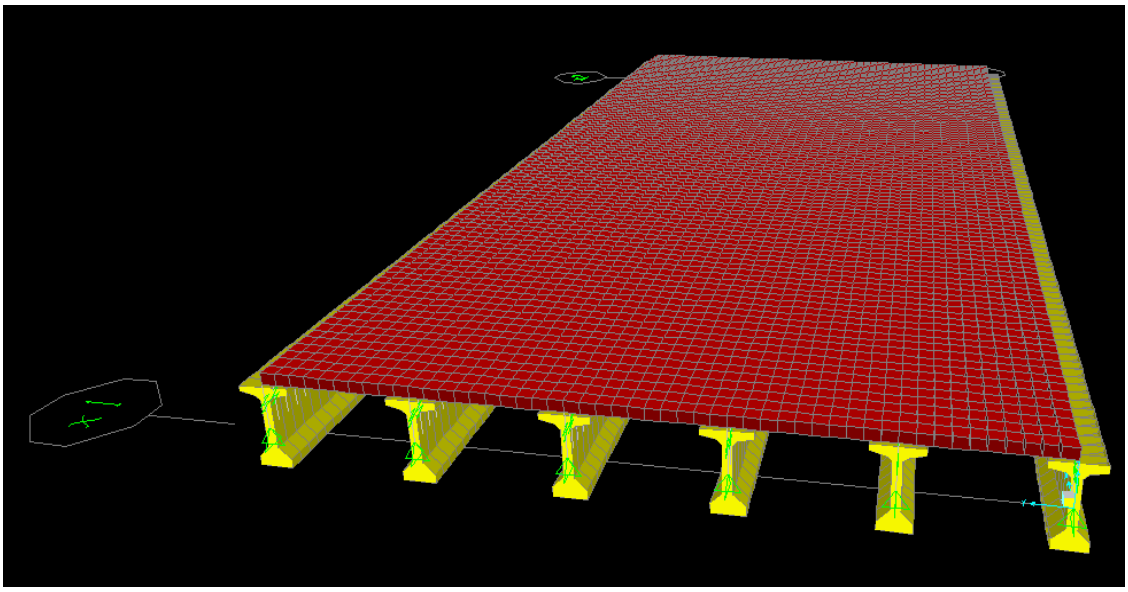

Figure 29: Bridge Model In SAP

Load Cases

Only a select number of realizations of the wind and wave hazard were investigated. For this study wind speeds for hurricane categories I-V corresponding to [33 40 49 58 67m/s, 75 90 110 130 150mph] and significant wave heights from [0.6 0.9 1.2 1.5 1.8m, 2 3 4 5 6ft] were used for structural evaluation. The resulting storm surge from each storm category was then determined from SLOSH. Each hazard was applied to the structure in separate and combined cases to see their individual and collective effects. Structural demand parameters such internal bending moment and shear were plotted against the two dynamic hazards in this study.

CHAPTER FOUR: RESULTS

Wind Tunnel Verification

A comparison of the four faces of the model is shown below in Table 1. Results are shown for both wind attack angles of 45 and 15 degrees from the longitudinal axis of the building. The Dytran signal and wind tunnel mean pressure coefficients agree well. All five faces of the structure have mean pressure coefficients in agreement on the order of 5%. This result agrees with other researchers such as Dagnew et al. (2009) and Holmes et al. (2001) in, that accurate static mean pressures can be achieved through numerical wind tunnel modeling techniques. However, a more scientifically precise description of the loading is required for PBE and therefore dynamic characteristics of the signal are vital.

The frequency content of the signal was investigated next using the PSD. An example of a comparison of the PSD of the various methods described is shown in Figure 31, for the windward wall. PSD comparisons for all five locations are included in the Appendix. From the PSD comparisons, a very good agreement is seen between the wind tunnel and Dytran simulation. No difference is seen in the magnitude of the power of each signal, but a small horizontal shift is seen in the frequency axis occurs due to normalization of the PSD. If no normalization is used on the horizontal axis, these two curves align. Additionally, the established wind spectrum equations approximated the two methods accurately. Some minor differences are seen in the higher frequency range between the predicted spectrum and the two modeling techniques. This pattern was seen in all of the PSD comparisons, which can be found in the Appendix. This result may be attributed to high sampling frequency use for the

experiment. A desirable upper limit is 200Hz (Holmes, 2001), which was used for down-sampling.

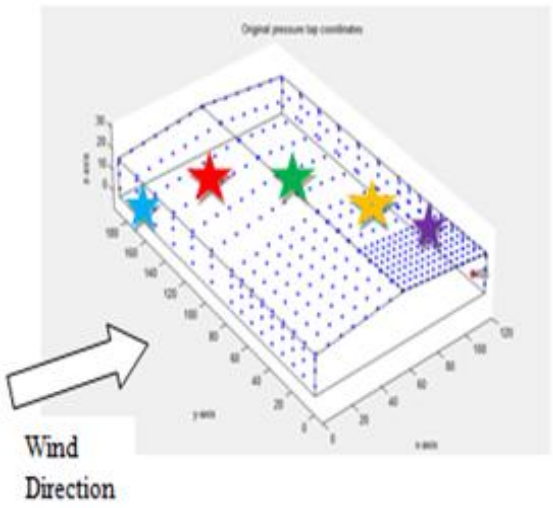

Figure 30: Location of Signal Comparisons on Barn Structure

Table 1: Mean Pressure Coefficient Comparison

Structure Location	**Mean Pressure Coefficient Wind Tunnel**		**Mean Pressure Coefficient DYTRAN**		**ASCE 7-05 Analytical Procedure**
WIND ATTACK (°)	45	15	45	15	-
Windward Wall	0.22	0.56	0.19	0.54	0.40
Windward Roof	-0.27	-0.45	-0.32	-0.50	-0.69
Roof Peak	0.32	0.53	0.35	0.49	-
Leeward Roof	-0.19	-0.27	-0.15	-0.22	-0.37
Leeward Wall	-0.37	-0.21	-0.30	-0.20	-0.29

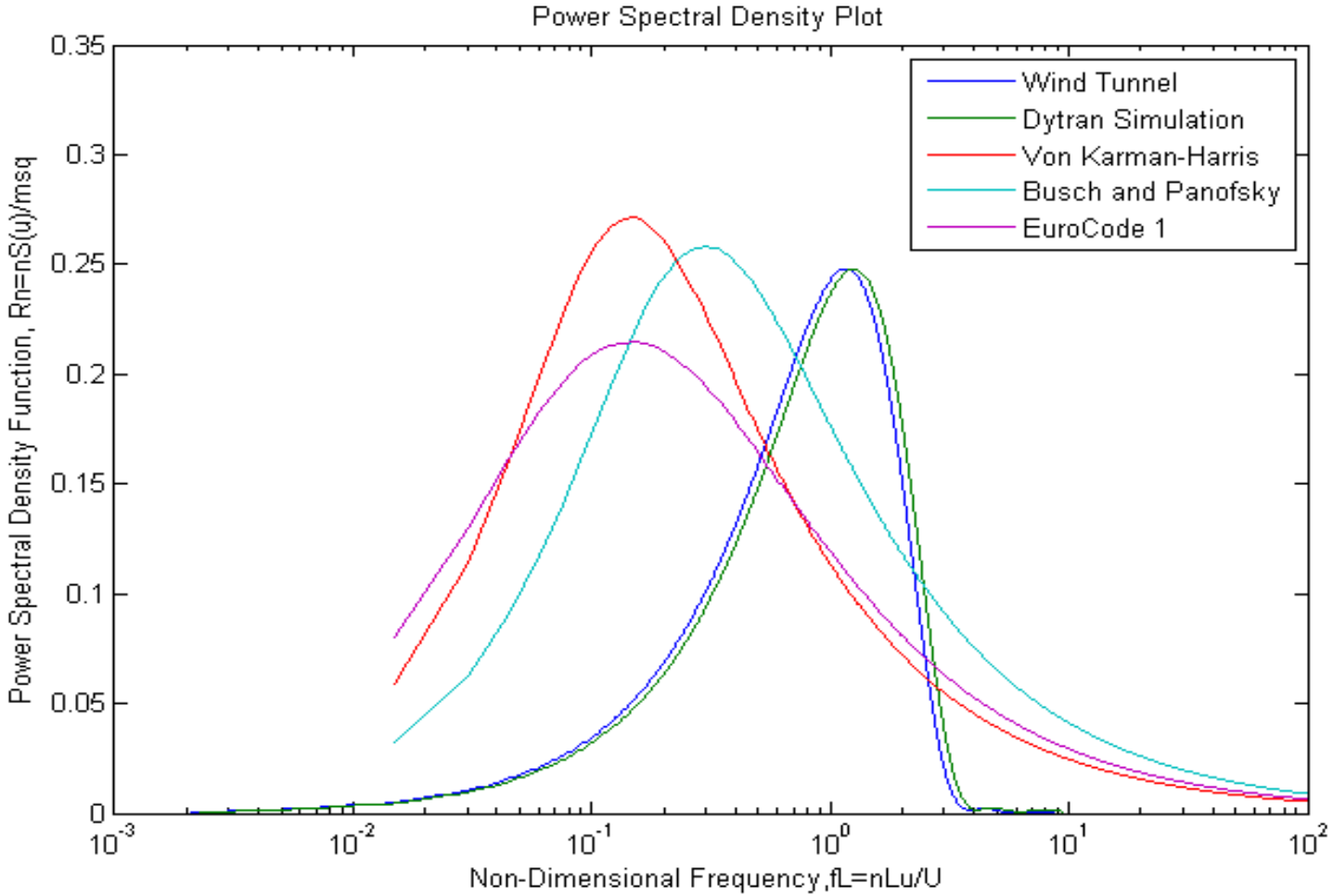

Figure 31: PSD Comparison of Wind-Ward Roof

An example of an autocorrelation function comparison is shown in Figure 32. In the Figure, the windward roof autocorrelation functions of the two modeling methods are compared. Only minor differences are seen in the magnitude and the shapes are identical. Again, all of the comparisons are provided in the appendix.

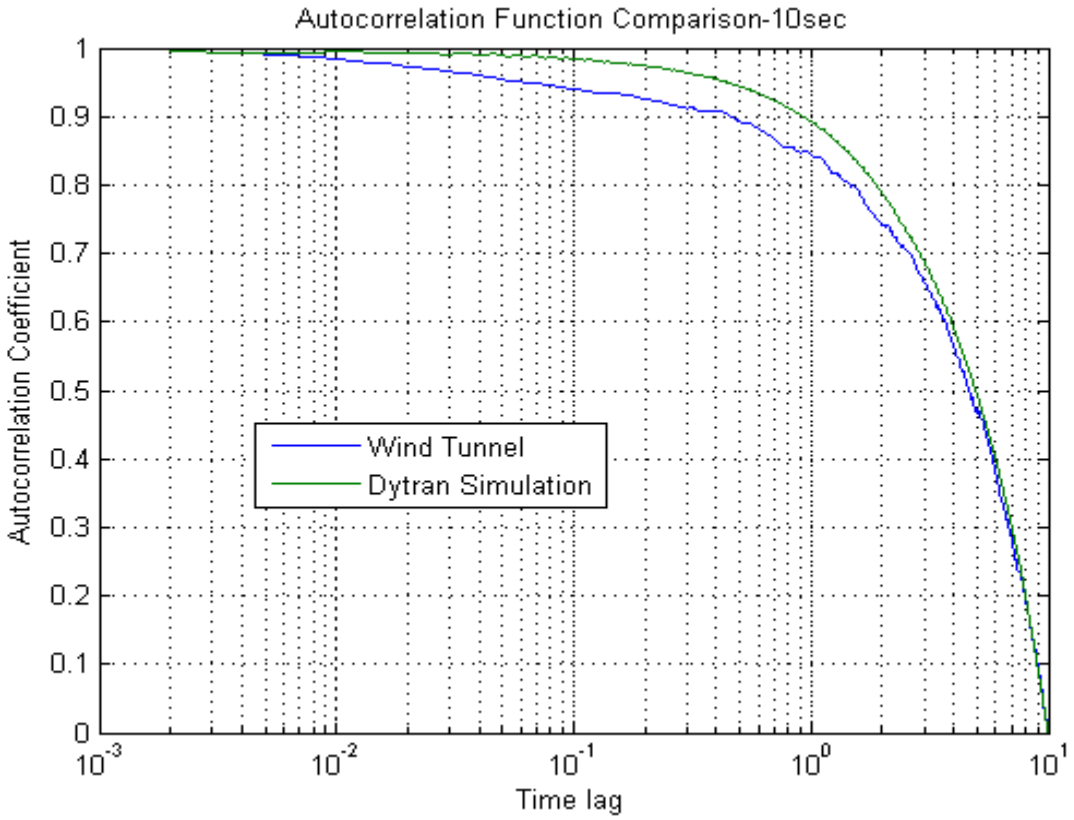

Figure 32: Autocorrelation Function Comparison of Windward Roof Pressure

A comparison of the integral length scale of the various faces of the structures is shown below in Table 2. The agreement between the two is not as accurate as the previous parameters compared. This deviation give rise to the horizontal scale shift of the PSD plots discussed

earlier. One reason for this discrepancy may be due to the fact that the longitudinal turbulence fluctuation is based on the frictional velocity (u*), which is further derived from the surface roughness of the wind record. The surface roughness is not a definitive quantity and was merely estimated from dimensions of roughness elements, using a primitive method that has been updated very little in the last 30 years. Additionally, the surface roughness in the wind tunnel models could not be replicated in the numerical simulations, due to the tremendous computational demands it would require.

Table 2: Integral Length Scale Comparison

Structure Location	**Integral Length Scale Wind Tunnel (m)**		**Integral Length Scale DYTRAN (m)**	
WIND ATTACK (°)	45	15	45	15
Windward Wall	.040	.086	.087	.293
Windward Roof	.033	.017	.063	.024
Roof Peak	.026	.043	.014	.025
Leeward Roof	.023	.020	.098	.017
Leeward Wall	.035	.012	.012	.014

The values of the turbulence intensity for the two different models, as well as the predicted intensity given in Equation 5, are shown in Table 3. The comparison shows that Dytran is consistently measuring lower turbulence intensity values than the wind tunnel models. This finding suggests that fluctuating pressures are not being accurately captured in the Dytran

simulation. A source of the discrepancy may be due to the fact that no randomness of the velocity profile is input into Dytran, and only a constant velocity profile is allowed. Therefore the lack of turbulence is attributed to the limited number of roughness elements use to develop vortices. Also, the turbulence intensity predicted by Equation 8 is appreciably different than both sets of collected data. Equation 8 was based on measurements produced by large scale depression systems (Holmes, 2001). Therefore it is not entirely applicable for BLWT modeling conditions.

Table 3: Longitudinal Turbulence Intensity Comparison

Structure Location	**Longitudinal Turbulence Wind Tunnel (%)**		**Longitudinal Turbulence DYTRAN (%)**		**Longitudinal Turbulence Equation 8 (%)**	
WIND ATTACK (°)	45	15	45	15	45	15
Windward Wall	12.3	31.8	4.6	19.4	46.5	
Windward Roof	15.6	25.6	8.6	13.4	49.6	
Roof Peak	18.1	29.8	9.8	15.6	58.9	
Leeward Roof	10.5	15.3	8.3	7.9	49.6	
Leeward Wall	21.0	11.7	5.1	10.1	46.5	

Next, comparisons of the SDOF oscillator are shown in Figure 33. The response of the two systems is quite different. Consistent with the turbulence intensity measures, the Dytran response reaches a steady state after several seconds of duration and that is not seen in the wind tunnel. The initial responses of the two methods are merely identical, and differ in magnitude by

5-10%. After approximately one second of loading the Dytran system has reached a constant position and exhibits relatively no dynamic response. The wind tunnel SDOF oscillator continues to display dynamic movement for the entire loading duration of ten seconds.

DYTRAN WIND TUNNEL

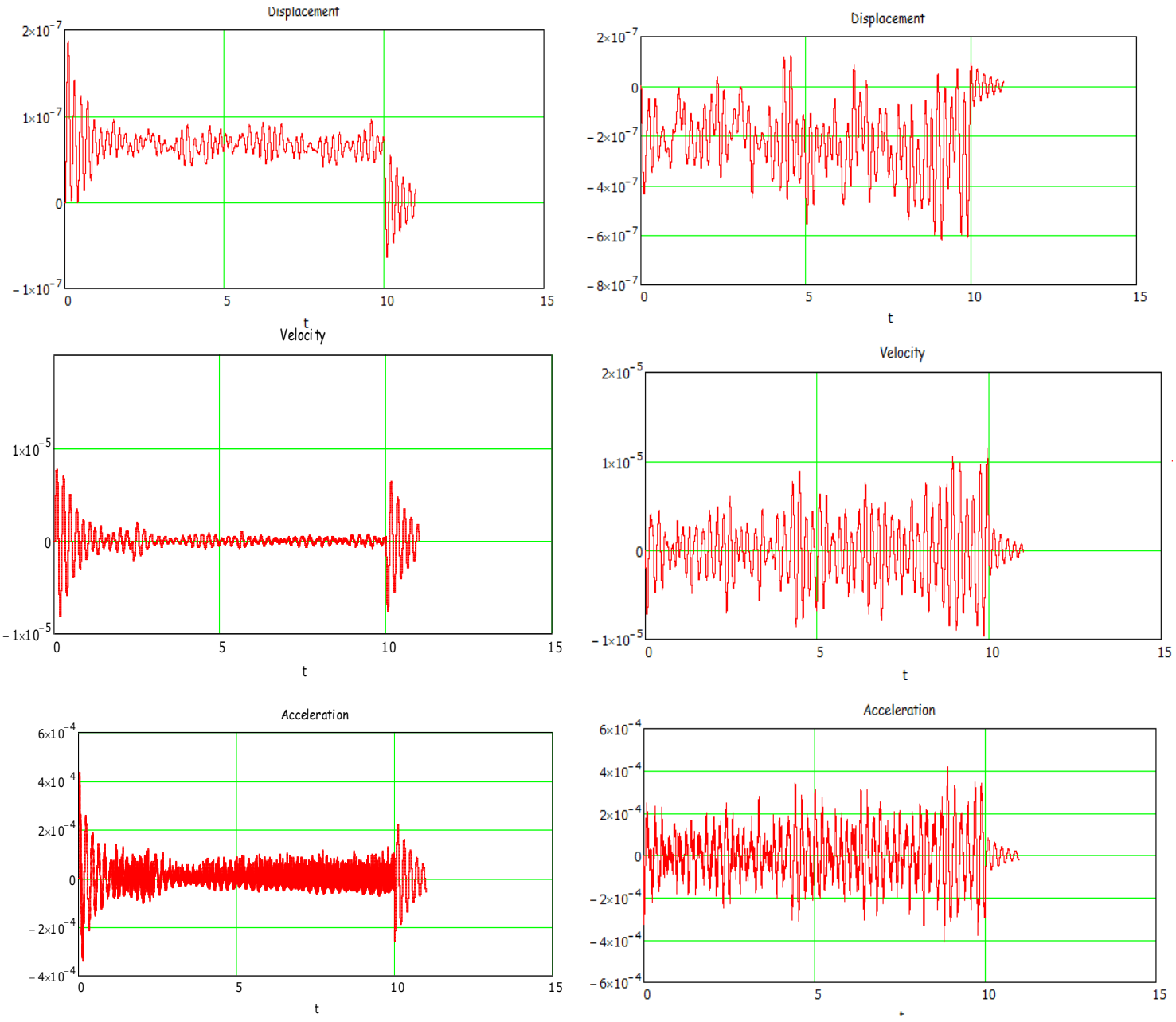

Figure 33: SDOF Comparisons for Wind Wall. Left: Dytran. Right: Wind Tunnel

From these results, an investigation was performed on the Eulerian mesh to ascertain why Dytran results approach steady state after such a short duration. Figure 34 shows the development of the air vortices over time as the program is running. The velocity profile over the building is relatively constant after the initial front. The flow of the air over the structure is limited to streamlines of constant velocity and relatively no mixing or creating of eddies are visible after the initial front. Additionally vortex shedding in the wake of the building is the only source of turbulence seen in the mesh. This phenomenon occurs regardless of the turbulence of the upstream flow and is simply related to the Strouhal number (Holmes, 2001).

Therefore, from these results the Eulerian mesh was inspected to give hints as to why the Dytran results reach such a steady state. Therefore, it is believed that these vortices that are created in the experimental wind tunnel are created due to the non-ideal creation of the wind flow. Typically, wind tunnels are constructed with a series of large fans or blower systems that create the flow striking the structure over a long roughness surface. The roughness elements used in the numerical simulation were limited and the true wind tunnel testing has a series of over 25-30 rows of these elements. These additional elements may help create the additional vortices that are lacking in the numerical simulations. However, the addition of more roughness elements is not feasible in this study due to the increased simulation runtime. To combat this issue, the idea of random pulse generation (RPG) was investigated.

Random pulse generation is typically performed in seismic research to create synthetic time dependent ground motion and has been shown to be a very versatile tool for simulating a large class of physical phenomena (Lin and Cai, 1995). The signal is considered to be composed of a series of

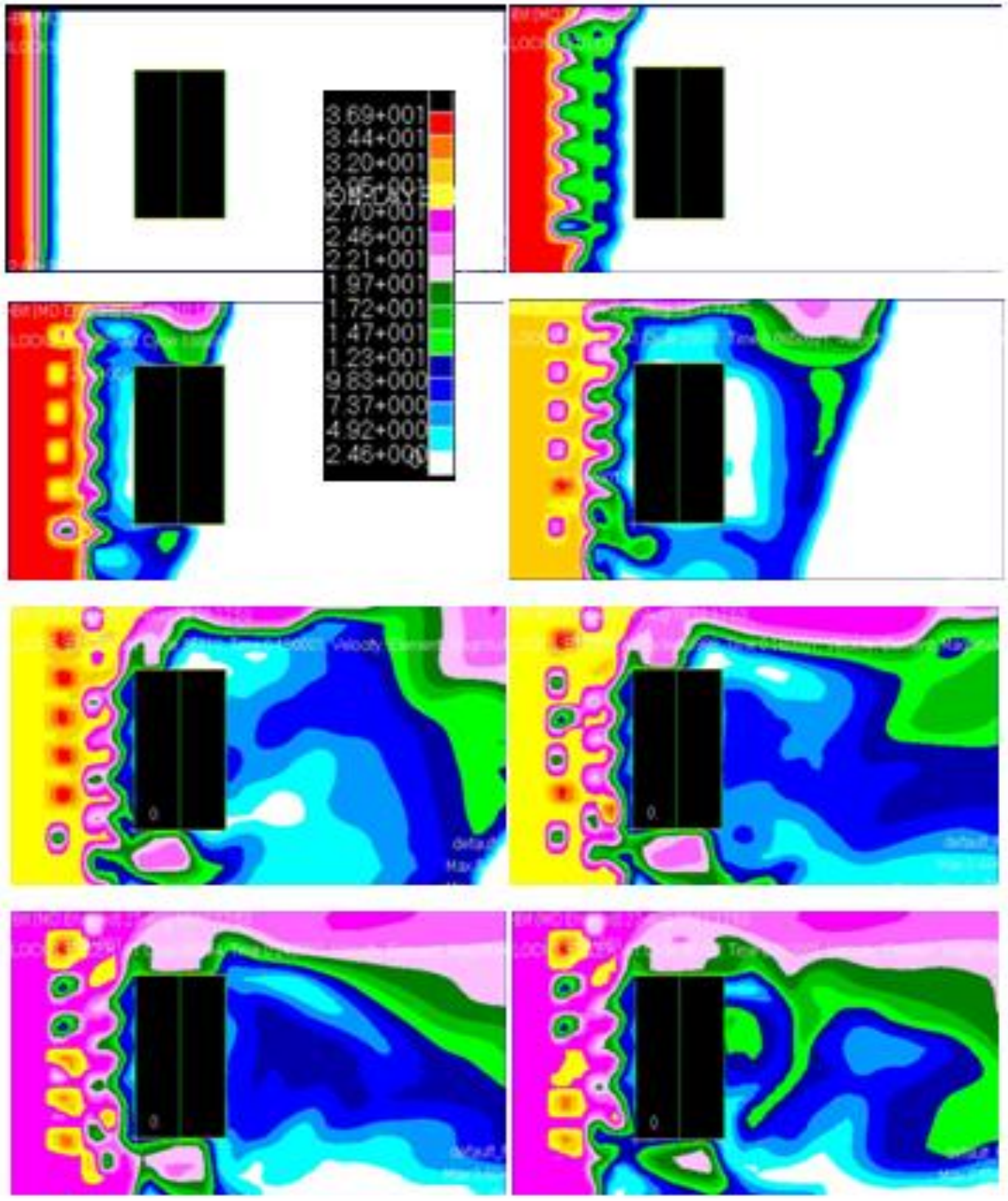

Figure 34: Development of Wind Turbulence (eddies) in Eulerian Mesh of Barn Wind Tunnel Study. Velocity of Wind (m/s) is shown in Contours

pulse trains, which are a repetitive series of random magnitude pulses (Y_j) that are separated in time by a random arrival time (τj). If a linear assumption is valid for the combination of the pulses and each random pulse magnitude (Y_j) is independent of the arrival time, then a series of (N) pulses can be combined to obtain the signals evolutionary spectral representation (X). This result allows for synthetic generation of a random seismic signal in the frequency domain from a series of single pulses as shown in Equation 9. Where $w(t-\tau)$ is a deterministic pulse shape function satisfying the condition $w(t,\tau)=0$ for $t>\tau$ (Lin and Cai, 1995).

$$X(t) = \sum_{j=1}^{N(T)} Y_j w(t - \tau_j) \tag{9}$$

However, the Navier Stokes equations are a set of non-linear second order differential equations and therefore the direction superposition of signals arriving at each timeframe will not recreate a signal with 100% accuracy. However, it will allow for turbulence to be introduced into the signals. Therefore, it was conceivable that the combination of several simulations of the same structure under different obstacle placements would allow random pulse generation to be applied to the signals. Numerous simulations would be required to produce enough data to generate a full 10 second record. To accomplish this, ten computers were simultaneously programmed to run various placements of barriers on the barn structure. Random pulse generation was then applied to the various data sets to create a suitable final signal.

For random pulse generation, the most important quantity needed for a synthetic signal generation is the time/source relationship. Through this relationship, the time/delay between

successive arrivals of signals is used to create the final signal. For this study, the time/delay of the arrival of wind vortices was calculated from the speed of the wind and the upwind distance. This time was found to be about 0.25 seconds and corresponds to approximately 50-100 samples depending, on the velocity of the wind. Additionally, due to the fact that the measured pressures oscillate about a mean instead of zero, the mean value of the entire signal was subtracted when two signals were added together. Using this idea, a synthetic signal was constructed with a varying arrival rate of successive signals.

Comparisons were then recomputed for the mean pressure coefficient, autocorrelation and PSD to ensure that the signal was not significantly altered using this technique and only the turbulence component is affected. All of these results are shown in the Appendix with the subtitle RPG. The dynamic response does not reach a steady state and the numerical values are very comparable to the wind tunnel response for the entire length of the record. The frequency content of the displacement response was compared with a FFT based PSD.

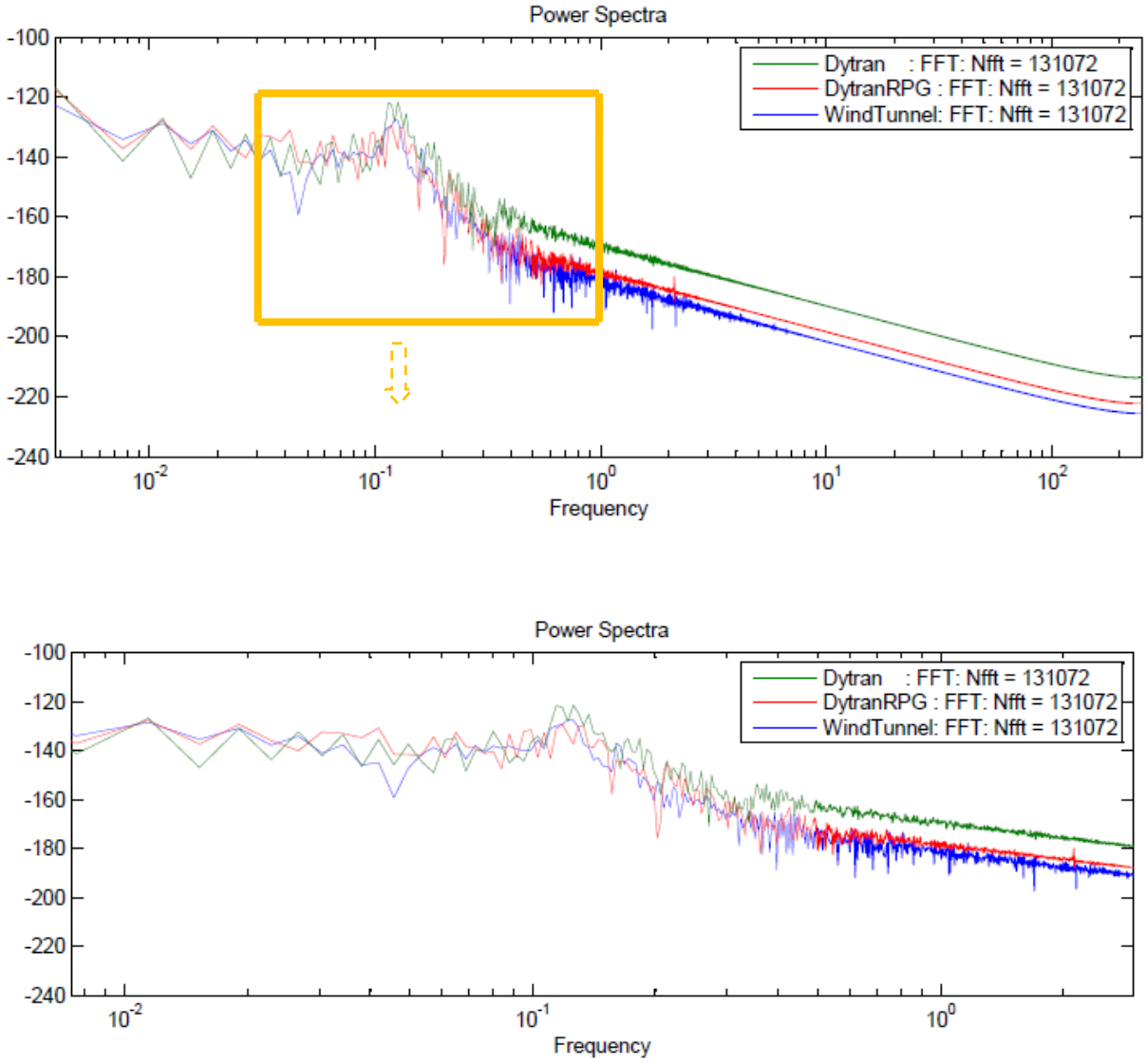

Figure 35 PSD comparison of Displacement Response of SDOF

Figure 35 shows that the RPG addition to the Dytran signal shifted the shape of the PSD plot in line with the wind tunnel response. The original raw dytran signal had a significant amount of higher frequency response. From these results, it was concluded that the CFD technique could be combined with RPG to create a suitable dynamic signal without adverse

affects on the frequency content of the signal as shown in the PSD plots. In all three signals a distinct peak is seen around 0.2Hz which is less than the natural frequency of the barn of 5Hz.

Wave Tank Verification

To ensure that the wave loading phenomenon is accurately captured, both the time and frequency domain content were examined. First, the signal was passed through a Chebyshev low-pass filter which was used to remove the excessive high frequency content obtained in the raw signal. Chebyshev Filters have a steep roll-off but, have more passband ripples than Butterworth filters (Daniels, 1974). A cutoff frequency of 25Hz was used as to not induce excessive extension of the loading time history. Once completed, the maximum and minimum loads recorded from the experiment and numerical simulations were compared for both the horizontal and vertical directions. A typical comparison of the two methods is shown in Figure 36 and Figure 37.

Dytran captures additional high frequency slamming forces that are associated with waves. The quasi-static varying load is also not as apparent in the numerical simulations, but is quite similar to slamming force shown in the experimental study. The recorded peak load is approximately (325N, 73lbf). This value is quite comparable to the records from Sheppard, in which a maximum slamming force of (333N, 75lbf) was recorded for Test #50 (Sheppard, 2009). This was also representative of the horizontal load comparison as a (8N, 0.48lbf) difference (approximately 10%) was measured. A summary of the vertical and horizontal load comparisons can be found in Table 4. The variation was not of a great concern, due to the large deviations in

both magnitude and shape of wave time histories reported for similar test conditions by numerous laboratory basin studies (Cuomo, 2007).

Table 4: Force Comparisons for Wave Tank Modeling

	Test #47		Test #50	
	Dytran	Experiment	Dytran	Experiment
	(lbf)		(lbf)	
Vertical	72.8	60.06	73.06	75.07
Horizontal	1.8	2.23	3.60	4.08

Once the maximum and minimum peak loads were compared, each force time history was converted into a non-dimensional time history. Each time history was normalized by the density of water, acceleration of gravity, tributary area, and significant wave height. This process will enable the recreation of simulated peak pressures for any wave height, and further comparison against other researchers such as Cuomo et al. 2007. These plots are shown in the appendix under Bridge Wave tank verification. For the two test simulations, the vertical peak pressure was found to follow the empirical relationship given in Equation 10. This result is quite comparable to other peak vertical forces in which the range of (1.8-7.6) is given. However, more simulations are required to give a definite empirical relationship.

$$P_v = (1.5-2)\rho_w g H_s \tag{10}$$

For the frequency domain comparison the power spectral density computed using two methods is compared, as shown in Figure 38 and Figure 39, the numerical simulation shows a much higher frequency loading distribution than the wave basin studies. This high frequency loading is not typically found in natural wave phenomena, as shown from a PSD plot from the wave buoy data collected (Figure 40). Wave buoy data doesn't suggest any wave frequencies above the 0.5 Hz range. However, this data was not collected from impact studies, and is a measure of the natural wave cyclic frequency.

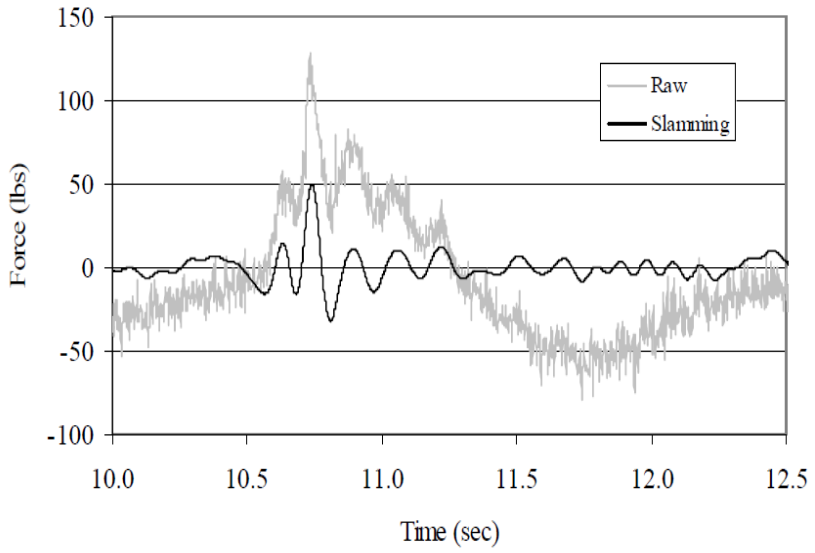

Figure 36: Vertical Time History from Flat Slab Structure Test (Sheppard, 2009)

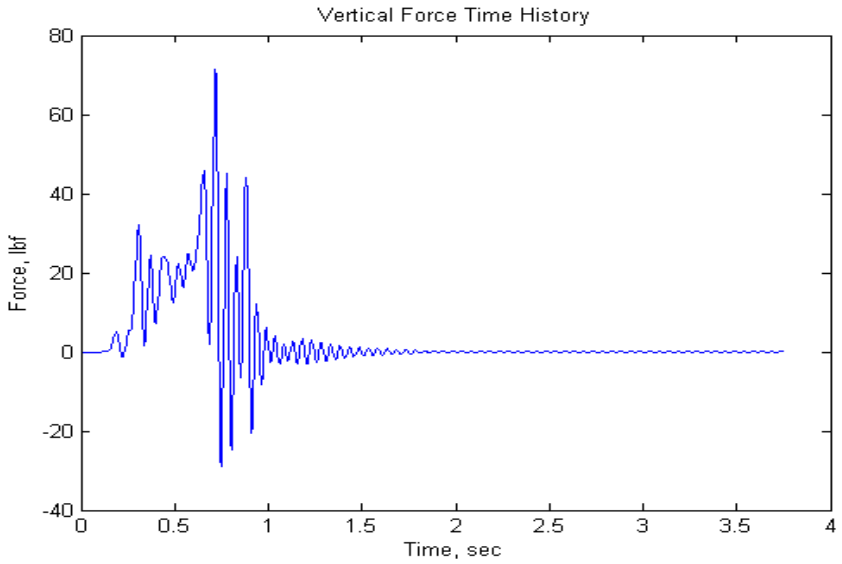

Figure 37: Vertical Time History From Dytran Simulation

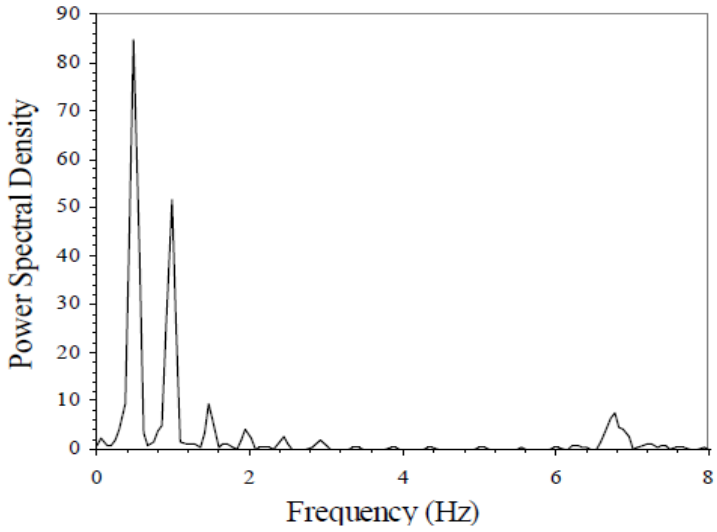

Figure 38: PSD Plot From Wave Basin Study on Vertical Load Cell (Sheppard, 2009)

.

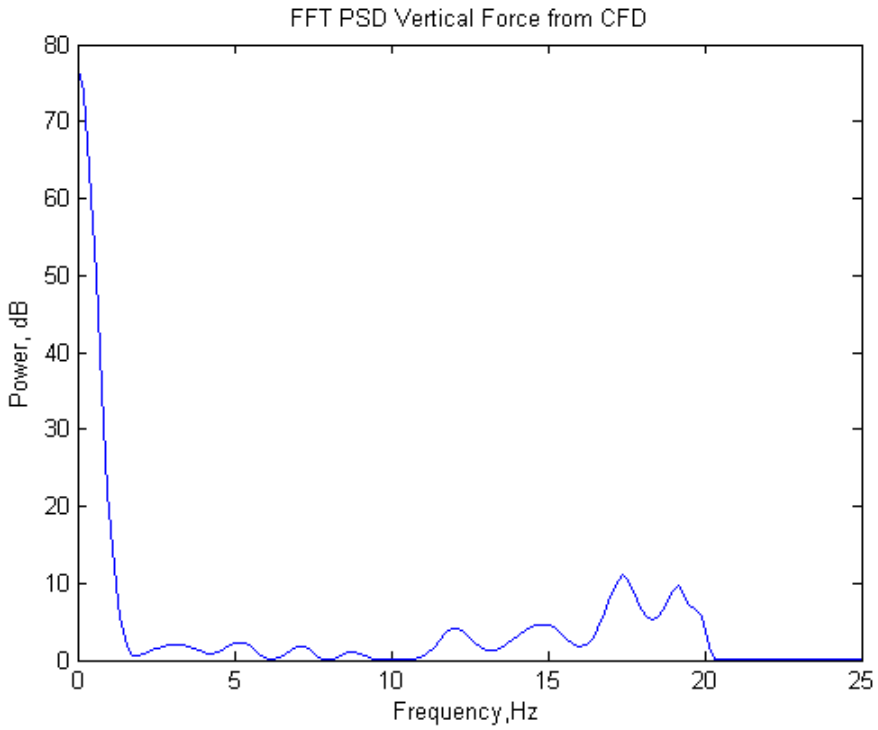

Figure 39: PSD Plot of Dytran Time History Force

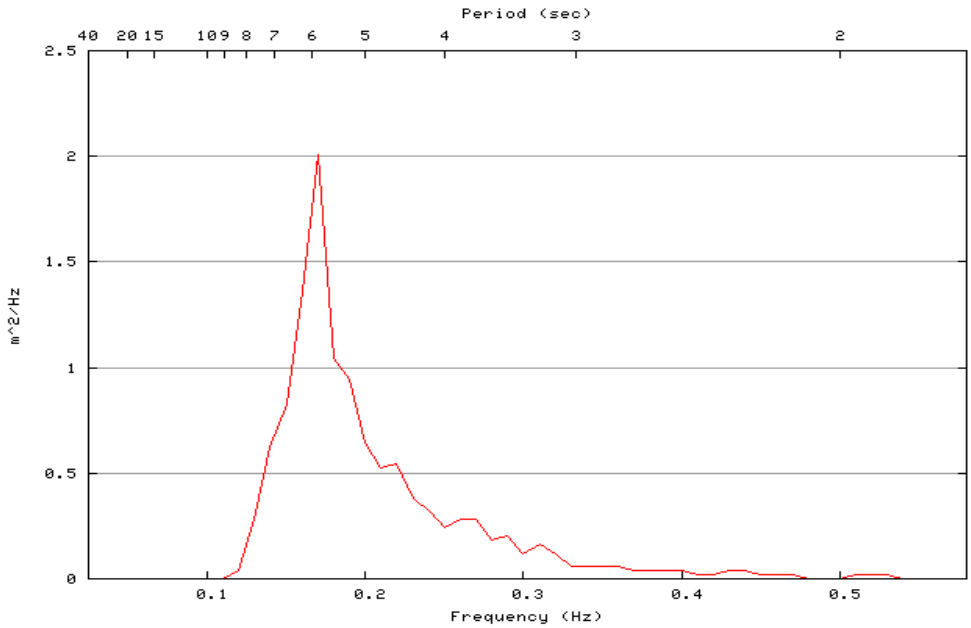

Figure 40: PSD Plot from Wave Buoy 42099 (NOAA)

After a thorough examination of these verification studies, it was concluded that an accurate quantification of the wind and wave hazard can be performed with CFD numerical simulations. Although slight differences are seen in the time and frequency content of the signal provided by the numerical approach, the margin of error of 5-10% is considered acceptable. The CFD simulation approach is then extended to study the hurricane hazards for two structural systems typically found in the State of Florida.

Probability Distribution Analysis

Probability Distribution Analysis was carried out for all of the hazards included in this study. First, an appropriate distribution fit to a measure describing the intensity of each hazard and then joint probability analysis was carried out. The correlation between the various hazards was assumed in this study and the Nataf method for joining correlated multivariate distributions was utilized, as described in Der Kiureghian et al. (1986).

For the extreme wind speed records gathered the Gumbel/Type I Largest Distribution was found to fit the data accurately. Gumbel (1954) introduced the methodology for fitting recorded annual maxmima events, which has been typically applied to flood prediction and extreme wind speeds (Holmes, 2001). The parameters of the distribution, along with a plot of the fit is shown in Figure 41. The return period for wind speeds (31m/s, 70mph), (40m/s, 90mph) and (49m/s, 110mph) is 8, 80 and 250 years respectively.

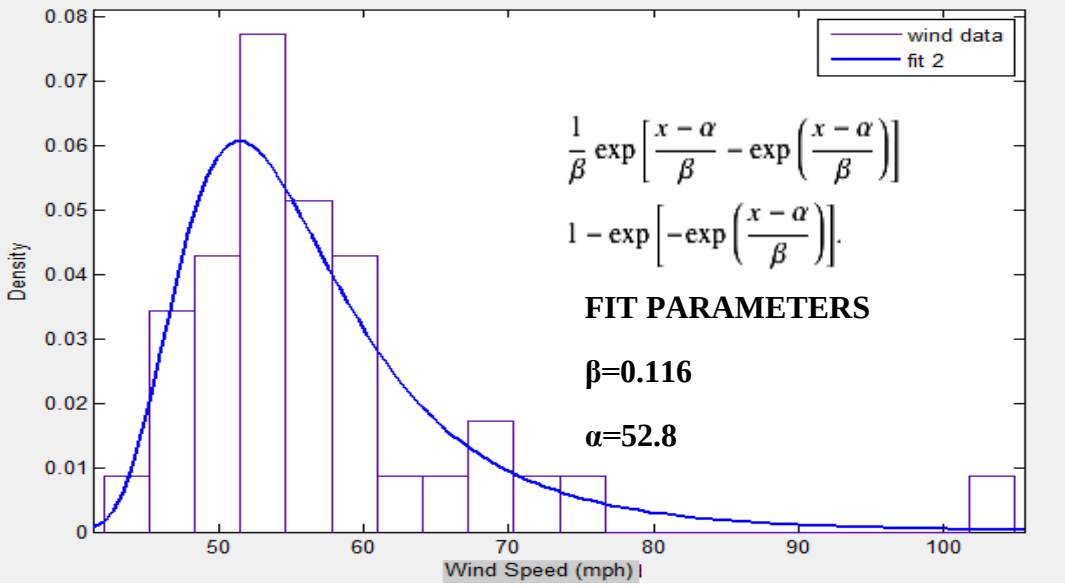

Figure 41: Gumbel Distribution fitting to Extreme Wind Speed from Tampa Bay (1951-1990)

For the surge height data collected from SLOSH, the exact coordinates of the structures location was extracted for all storm levels, forward directions and tidal conditions resulting in over 200 combinations. An example of the significant storm surge expected in the Tampa Bay region is graphically shown in Figure 42.

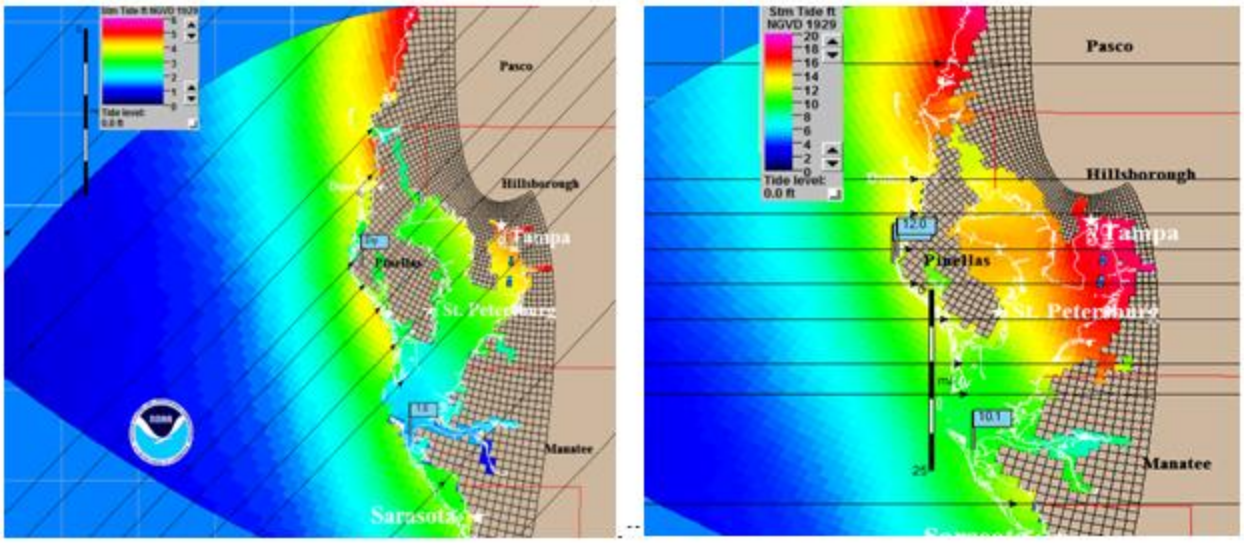

Figure 42: SLOSH Surge Height Results from Category I at mean tide on Left and Category IV at mean tide on Right.

Once the data was extracted, the generalized extreme value distribution accurately fit the Tampa Bay surge data, as shown in Figure 43. However, this approximate distribution is only valid for the specific location of the structures, as surge heights in the the next grid basin may be drastically different.

Significant wave heights in the Tampa Bay region were accurately described by the lognormal distribution, as shown in Figure 44. However, this data was collected from an offshore buoy and the expected wave height that may reach the inland structures, such as the building under consideration, is significantly reduced. According to Wu et al. (2006) due to wave decay once reaching shore, the typical wave height that reaches an inland structure is only 10-20%.

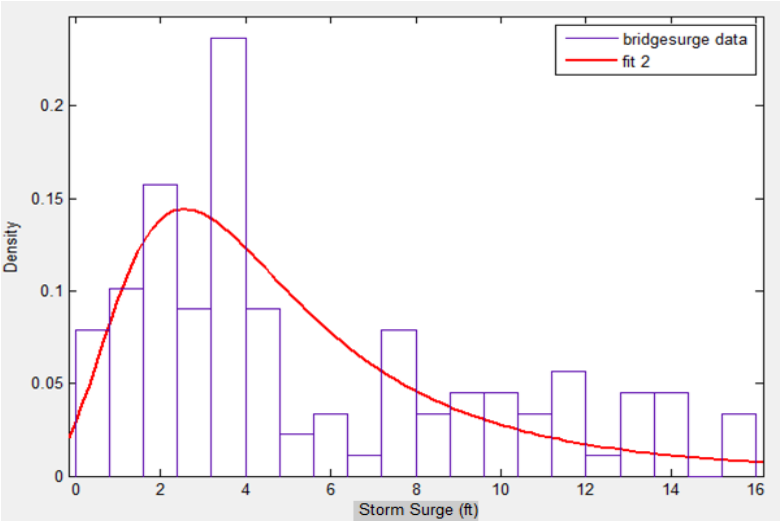

Figure 43: Extreme Value Probability Density Function Fits to Surge Data

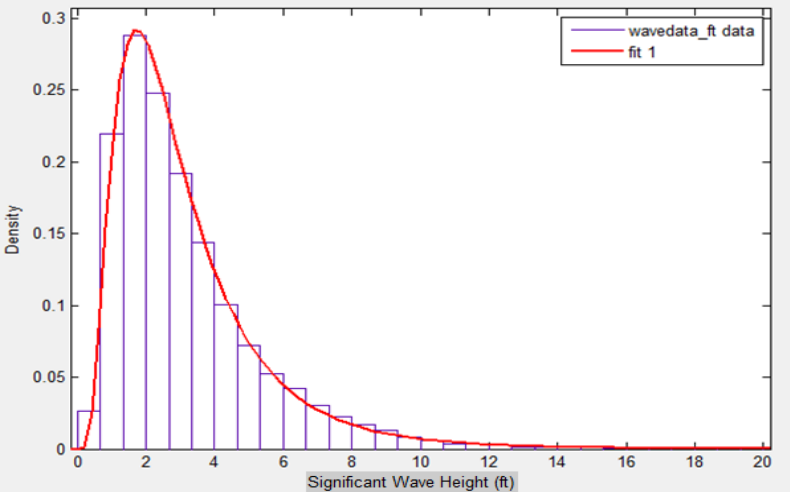

Figure 44: Log Normal Probability Density Function Fit To Significant Wave Height Buoy Data from Station 42099 (2007-2009)

Once each hazard has described by an appropriate density function, a joint probability analysis was carried out. For this analysis, the correlation coefficient between wind and wave hazards and wind and storm surge was assumed to be 0.5. This is a relatively strong correlation

between the hazards, as one would expect that the influence of wind has a drastic effect on storm surge and waves generated in a hurricane. The results of the joint density distributions are shown in Figure 45.

(A)

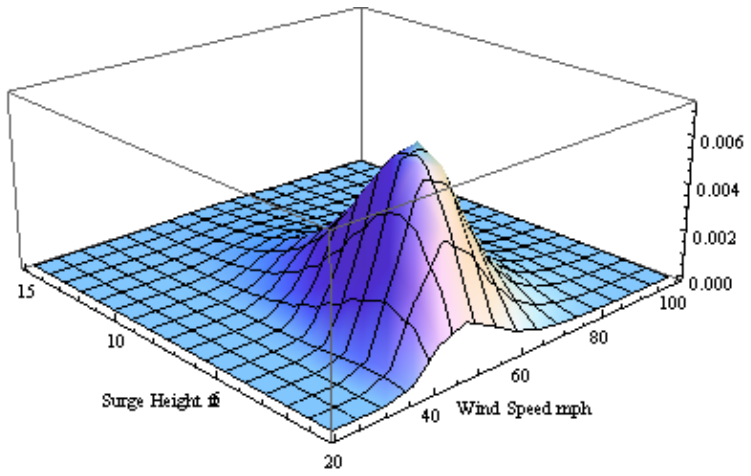

(B)

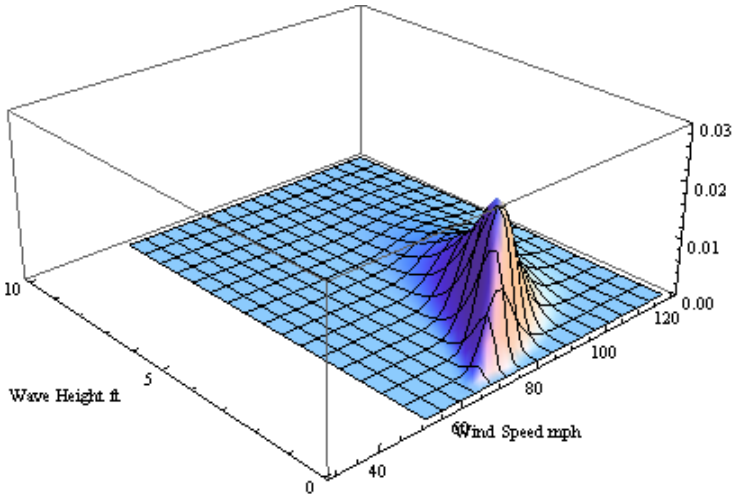

Figure 45: Joint Probability Density Function (A) Wind and Storm Surge (B) Wind and Wave Hazards

Dynamic Wind and Wave Load Generation

Dynamic wind loads were generated for both prototype structures considered in this study. Therefore, no experimental or full scale pressure coefficients were available for comparison. The sampling frequency and the input velocity were the only parameters changed from verification models. Each parameter was set as 200Hz. and (12m/s, 39fps), respectively. Only one angle of attack was used to create the time history data, due to high computational demands of each simulation.

The data was then assembled through RPG into a suitable 25 second signal which was then analyzed in both the time and frequency domain. Nodal time histories were converted into a non-dimensional pressure coefficient for application to each FEM. An example result is shown in Figure 46 and Figure 47 for the second floor windward wall of the building model. Results correlated well with previous verification studies as the pressure coefficient varies around 0.50. The wind PSD plot aligns with the established design code spectrum and only a slight shift is seen in the frequency domain due to the normalizing terms. These findings were typical for all locations recorded for the building and several more results are provided in the Appendix.

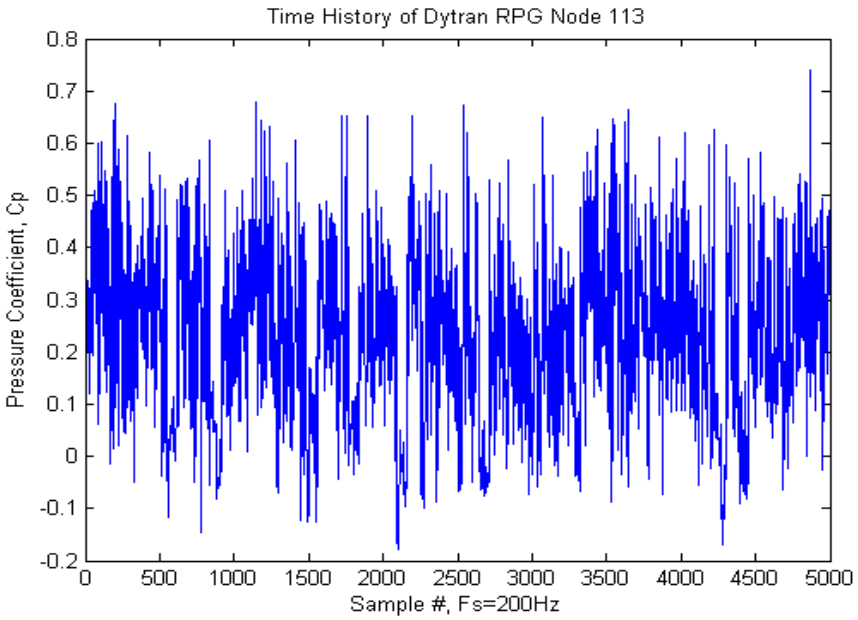

Figure 46: Second Floor Time History Windward Wall

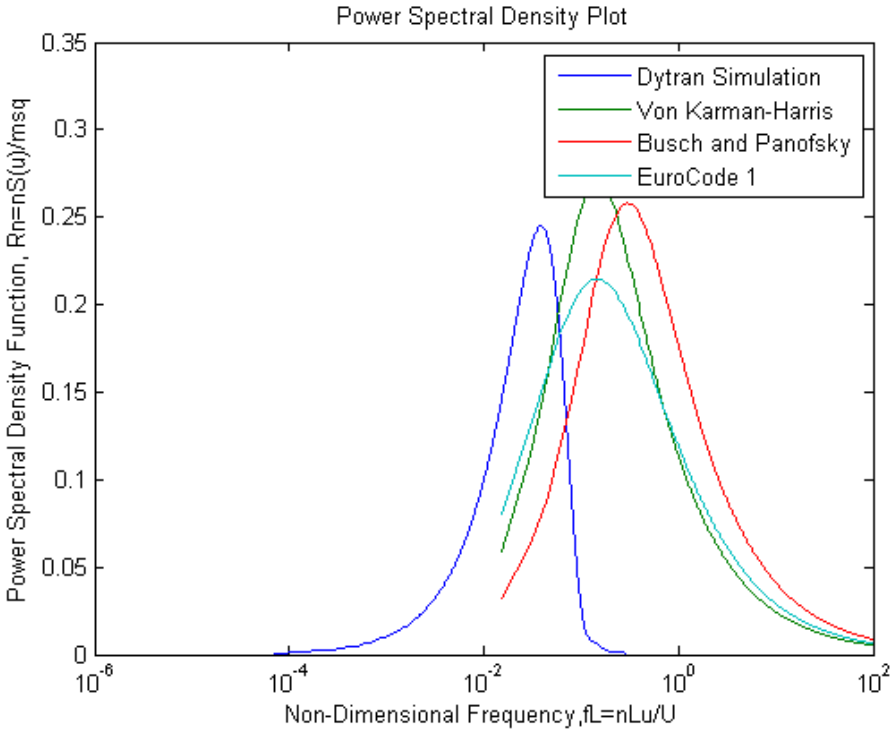

Figure 47: Second Floor Windward Wall PSD Comparison

Dynamic wave loads were also generated for both the bridge and building in this study. Scaled models were placed in the numerical wave tank, and a particular wave height and period impacted each structure. Horizontal and vertical forces were then sampled at 200Hz and passed through the Chebyshev Type I lowpass filter. Similar to the wind loads, a non-dimensional force coefficient was created and sample results are shown in the appendix. Additionally the wave time histories were visually inspected for the number of the slamming pulses. Various studies such as Sheppard et al. (2009) indicate that the number of slamming pulses is directly related to the number of air chambers. Figure 48 and Figure 49 show that Dytran is accurately reproducing 5 distinct slamming pulses for the six girder bridge.

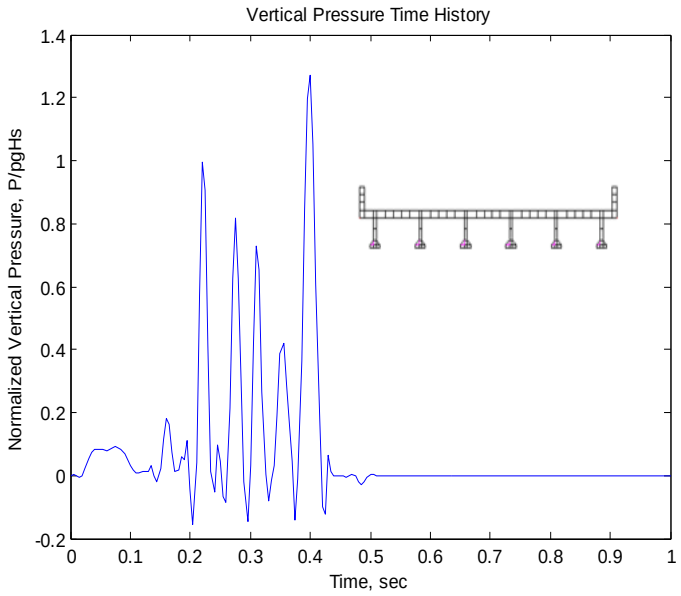

Figure 48: Dytran Vertical Time History for 5 Chamber Bridge

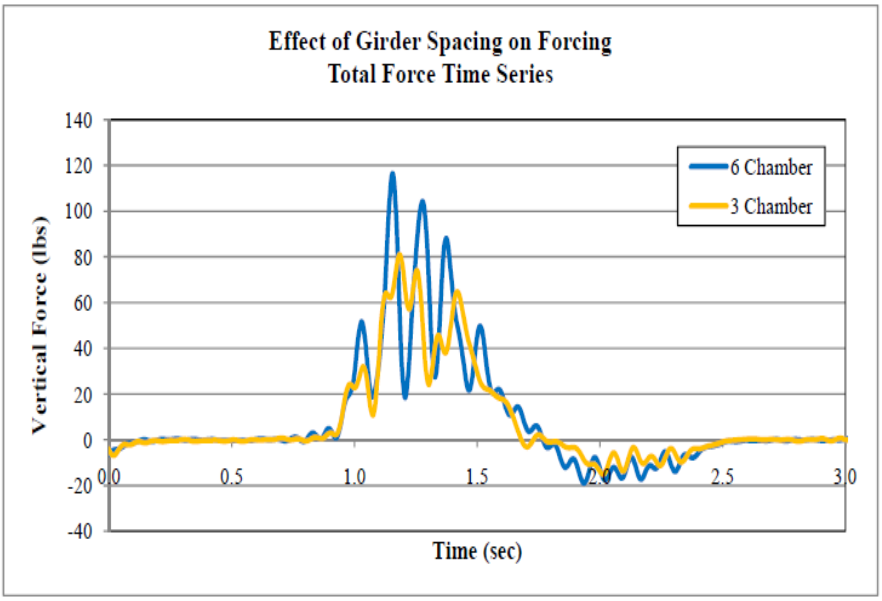

Figure 49: Girder Spacing Effects on Wave Forces (Sheppard, 2009)

Dimensional Scaling

Before application of the dynamic loads to each FEM, scaling effects due to Froude and Reynolds number modeling were considered for the wave and wind hazards respectively. Due to prototype and model scaling ratios both the time and magnitude of the loading signal must be performed.

For wind tunnel modeling a total of sixteen dimensional quantities such as the mean wind speed (u), roughness length (z_o), and density of air (ρ_a) must can be described in thirteen dimensionless quantities such as the Jensen number and Reynolds number (Holmes, 2001). For accurate modeling of the wind effects between model and prototype structures these dimensionless quantities should be equivalent. Due to these effects, results from the wind tunnel must be modified in the frequency domain due to the reduced frequencies at model scale and at

prototype scale as shown in Equation 11 (Main and Fritz, 2006). Where the model-scale frequency (f_m), model wind speed (V_m) and length scale (λ_L) are fixed due to wind tunnel modeling conditions, and the prototype sampling frequency (f_p) is proportional to the desired prototype wind speed (V_p).

$$f_p = f_m\left(\frac{V_p}{V_m}\right)\lambda_L \tag{11}$$

For wave tank modeling dimensionless quantities such as the Mach number, Weber number, Froude Number and Reynolds model can be chosen to obey similitude laws. Historically the Froude number has been used exclusively for scaling ratio used for offshore structures and ship testing (Cuomo, 2010). Therefore using this similitude law scaling factors for the measured pressures and forces are shown in Table 5.

Table 5: Froude Scaling Laws

Froude Scaling	
Length	λ
Mass	λ^3
Force	λ^3
Time	$\sqrt{\lambda}$

However from a comparison of laboratory and full scale pressures by Allsop et al. (1996) suggested that Froude scaling overestimates measured wave loads by 92-99%. Froude scaling

laws don't consider the air effects that have been shown to influence the magnitude and duration of impulsive loads. Therefore Bagnold et al. (1939) suggested modeling the compression of air by water against a vertical surface, with a water hammer compressing air in a piston (Cuomo, 2010). Building on this idea, Takahasi et al. (1985) presented a method for scaling vertical pressures based on a parameter known as the Bagnold number. Both the model and prototype Bagnold number is computed and then using Figure 50, the appropriate scaling factor can be evaluated. Therefore for this study Bagnold scaling will be used to scale the vertical pressures obtained from simulations.

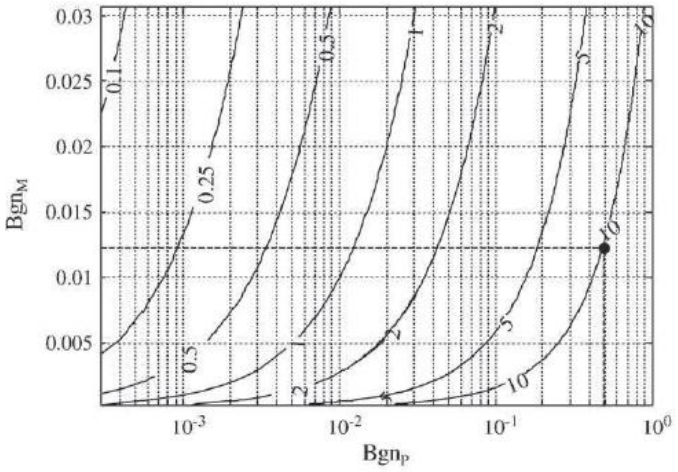

Figure 50: Scale factors as a function of the Bagnold number for model and prototype (Cuomo, 2010)

Dynamic Analysis

Using the loading cases described before response spectrum curves were created for both prototype structures. Before response curves were generated for each structure, the necessity to collect and conduct dynamic structural analysis was performed. Using the wind tunnel generated

dynamic time history data the frequency was scaled and corrected according to the reduced sampling frequencies at model scale. This data was then transformed into the frequency domain to obtain the dominant forcing function frequency. This value was found to be approximately 0.5Hz. Then the reduced sampling frequency was reduced further to obtain dominant wind frequencies of 0.1Hz, 0.08Hz and 0.03Hz. All of these forcing functions were then applied at the same wind speed to the building model and third floor response was recorded. These plots were then simultaneously plotted in Figure 51.

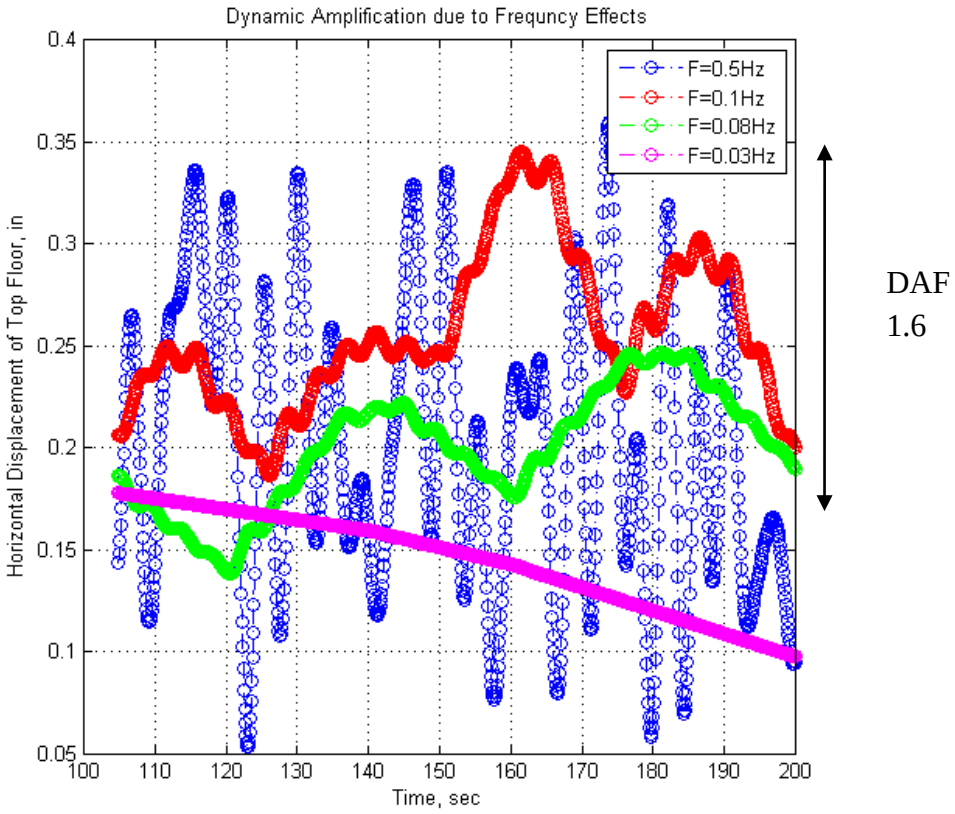

Figure 51: Dynamic Amplification of top floor displacement with dominant wind Frequency (F)

From the figure a clear dynamic amplification factor can be seen. The response is approximately 1.6 times the lowest dominant wind frequency which is approximately static. This result confirmed the need to consider the dynamic effects of the hurricane hazards

Next, response curves for the building and bridge were created for all loading cases considered. Results for the building can be found in Figure 52 and Figure 53 and results for the bridge can be found in Figure 54 and Figure 55.

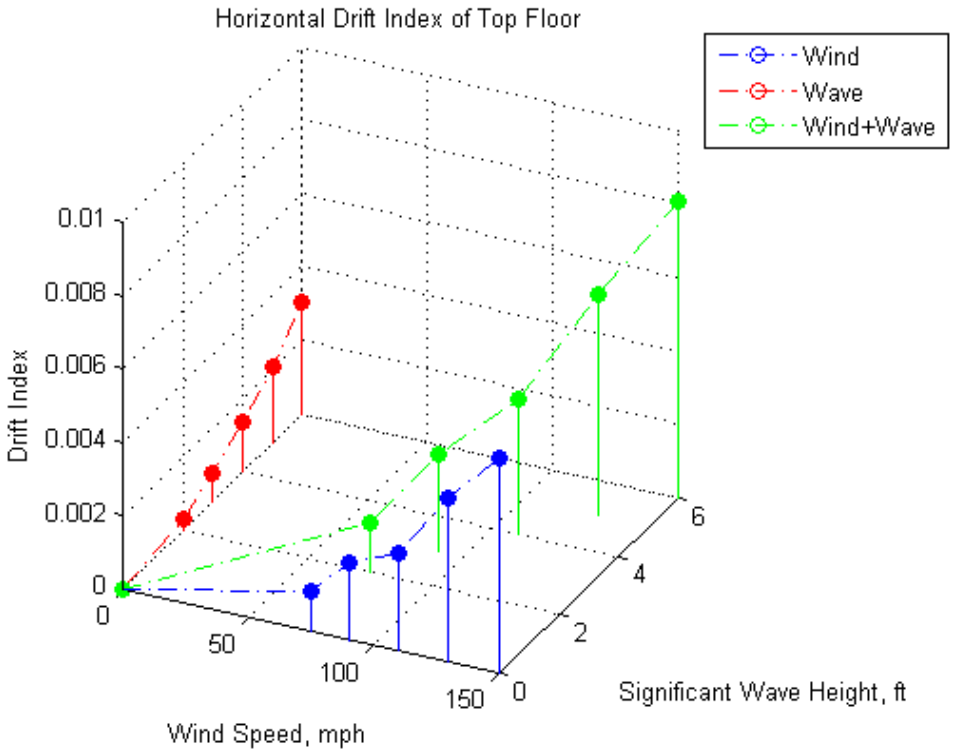

Figure 52: Drift Index Response Curve

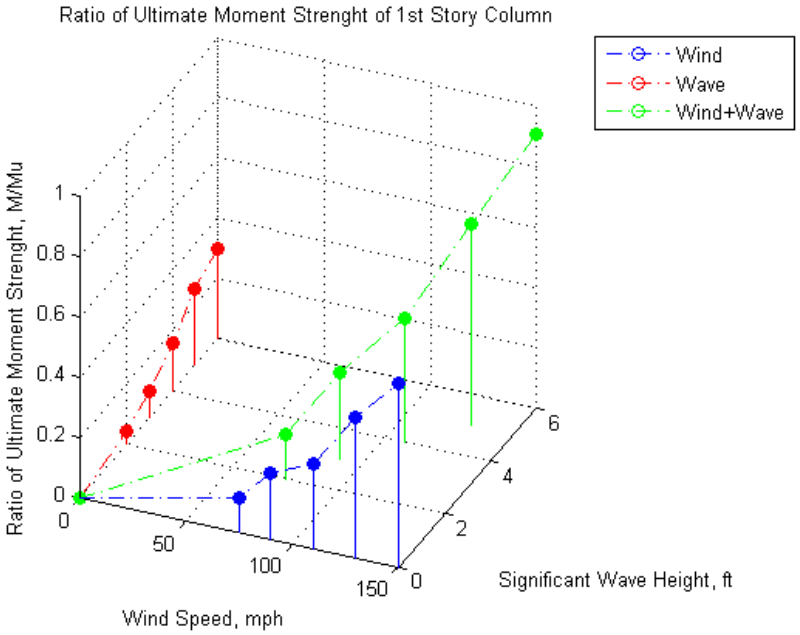

Figure 53: Ratio of Ultimate Moment Strength for First Floor

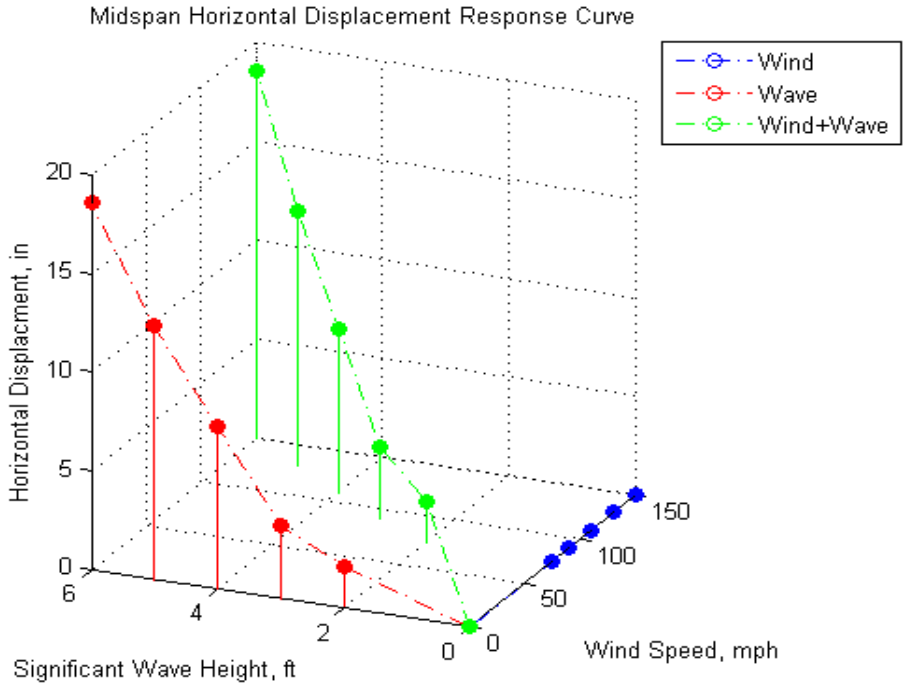

Figure 54: Bridge Horizontal Displacement Response Curve

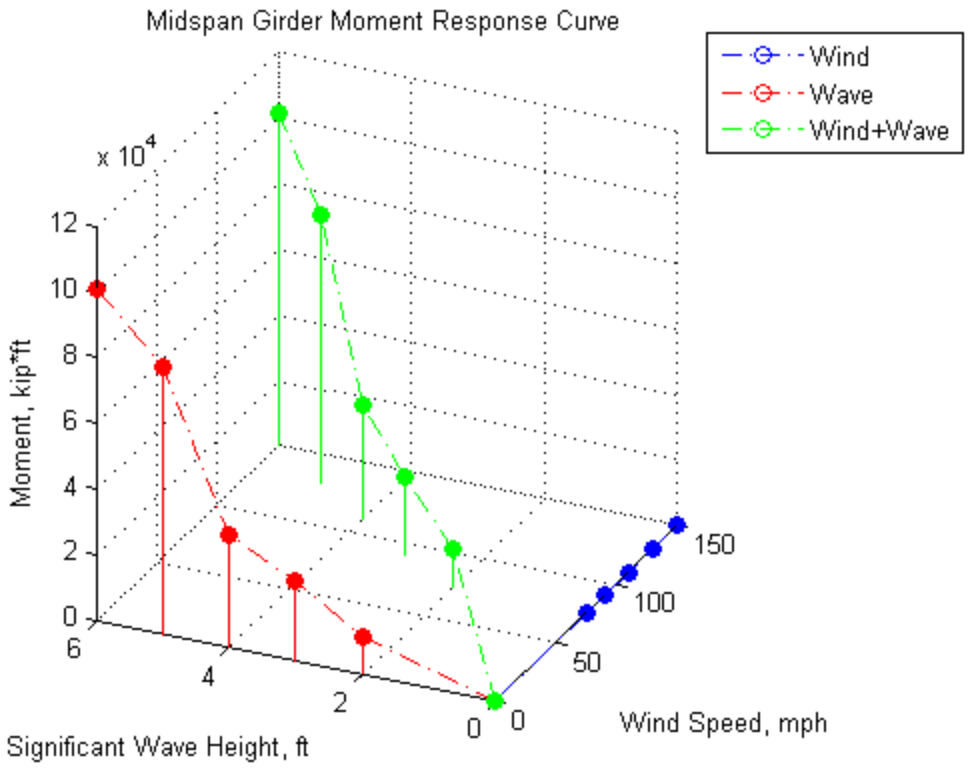

Figure 55: Bridge Midspan Moment Response Curve

From the building plots one can see the threat the wind and wave hazard have on structure. Here both the wind and wave pose and equally threatening risk on the structure. Figure 52 shows the drift index of the building is near exceeding acceptable design levels from the wind and wave hazard alone and is far exceeded if the all hazards are combined. This result is also confirmed with Figure 53 as the first floor column has reached its ultimate moment capacity and is near failure without considering dead or live load effects.

The bridge response curves show hurricane induced response is dominated by the wave hazard. This result was expected due to the reduced amount of surface area compared to a typical building. The displacement of the bridge due to the maximum significant wave height

was (450 mm, 18 in). However, it is believed failure would have been initiated or very close, as a moment of over (13,500 kN-m, 10,000 kip-ft) at midspan.

CHAPTER FIVE: DISCUSSION AND CONCLUSIONS

In this study, the primary focus was to establish a method for generating time varying dynamic, structure-specific hurricane hazard data, for use in PBE studies. Currently modeling of extreme winds and waves, such as those present from a hurricane, are performed using BLWT and wave tank basins. No actual recorded data is available from existing structures subjected to hurricanes. To address this issue, computational fluid dynamics simulations are used to generate synthetic time history records for different hurricane scenarios in this study. Before implementing such an innovative technique, the accuracy of the results provided by the numerical simulations was verified for cases were existing experimental prototypes and recorded data were available.

Previous experimental laboratory study data from wind tunnel and wave tank basin facilities were collected. Comparisons were conducted on both the time and frequency content of the signals. Mean pressure coefficients/force coefficients were shown to be in relatively good agreement for wind tunnel testing and wave tank loads. Although some variation is seen between the two results, the error is on the order of 5-10%. Additionally, wind mean pressure coefficients were compared against ASCE 7-05 code and shown to be slightly lower, as expected.

The frequency content of the wind and wave numerical simulations was found to be appreciable to their experimental counterparts. The normalized frequency of the wind was predominantly found to 0.1Hz. The wind spectra plots also agree with code generated spectra, such as EuroCode I and Von-Karmen and Harris (Holmes, 2001). On the other hand, the wave loading frequency content suggests that Dytran is only capturing the impact loading, as much

higher frequency content in the 10-20Hz. is obtained when compared to experimental and historical records of waves. This issue is not very detrimental as the quasi-static wave load is quite well understood, and is simply related to the wave height, period and structure properties. Thus, this loading function could be added to the slamming force obtained from Dytran. These results demonstrate that CFD is a viable alternative to laboratory testing with much more simulation capability to reproduce experiments with multiple structures, locations, and configurations.

This finding was extended into two typical structural systems found in Florida. Linear FEM models results for the individual and combined effects were constructed into response curves. These curves showed the most dominant hurricane hazard for each structural system. The building model is controlled by both the wind and wave hazard while the bridge is dominated by the wave hazard. The building model is pushed to the limits of its design as the wind and wave hazard approach a category 5 storm. The drift index for the top floor is exceeding the design limit for the wind hazard alone at 0.005 and up to 0.01 for all three hazards combined. The moment capacity of the first floor is nearly met at (339kN-m, 250ft-kips) when all three hazards are combined. The bridge model recorded a maximum displacement of over (450mm, 18in) and midspan moment of (13500kN-m, 10000kip-ft) for a six foot significant wave height. This finding suggests that the capacity of the girders have been reached without considering the significant horizontal reaction force. Significant horizontal forces would be subjected to any lateral restraint system. Therefore the response curves demonstrate the poor performance of the prototype structures designed through a deterministic approach and need to consider all hurricane hazards for structures located in coastal areas.

In this study, a major issue in implementing CFD modeling for producing dynamic wind loads was experienced. Holmes et al. (2001) stated that fluctuating and peak pressures cannot be accurately reproduced using CFD techniques at this time. This statement was confirmed by the steady state solutions that were produced for the wind loading spectrum. The lack of evolving vortices in the flow over time causes this phenomenon to occur, as shown in numerous simulations. The lack of pressure fluctuation is primarily attributed to the over simplification of the turbulence in the discretization and solution of fluid flow equations (Holmes, 2001). Therefore, RPG was utilized to introduce additional vortices in the flow, which may prove to be useful in further applications. Once RPG was combined with the Dytran simulations, a suitable dynamic signal could be created for further structural analysis

Upon verification of the program, the numerical modeling method was extended into two typical Florida structures. The Tampa Bay region was selected for this study and a prototype bridge and building were selected for detailed hurricane hazard identification. These structures were then modeled in numerical wind and wave simulations. Before generating dynamic time history data, historical annual extreme records of the wind, wave and storm simulations were collected for joint probability analysis. This information was used to identify the most likely combinations of wind, surge and wave heights anticipated for specific return periods. Additionally, this data would be coupled with the dynamic time history data, as pressures/forces could be scaled to any specific combination and applied to a structural model.

Time history data produced from the two prototype structures displayed similar results to the verification studies. Slamming forces were mainly recorded from the wave tank simulations, and a steady state wind tunnel signal was generated. These results show that CFD modeling can

be accurately applied to civil engineering structures for characterization of the wind and wave loading. This finding is a very important step in PBHE, as structure specific hurricane hazards can be generated without the high cost of experimental laboratory setup, equipment and personnel. This ability may help in the widespread application of PBE in the structural engineering design field. Additionally RPG generation was applied to CFD results to introduce turbulence due to the lack of an accurate sub-grid model. This finding may suggest an alternative method to introducing turbulence into CFD simulation.

CHAPTER SIX: RECOMMENDATIONS FOR FUTURE STUDIES

In this study, the field of CFD was applied to two specific hurricane hazards, namely wind and waves. To verify this technique, a comparison was made with laboratory wind tunnel data. Only typical gabled structured buildings have been tested and compared against full-scale measurements. Therefore, to fully verify this technique requires comparisons to be made with full-scale real life wind measurements using different geometric configurations. This data is currently unavailable but, a new study known as FCMP is employing numerous wind measurement techniques to obtain full scale hurricane data (Masters, 2010).

In the meantime, verification of Dytran with wind tunnel tests of a standard tall building model is required. Only low-rise structures and short span bridges were considered in this study, and it is suggested that the CAARC building model be investigated using Dytran. This building is suggested due to its widespread use in wind industry, which will allow results to be compared against other researchers such as Dagnew et al. (2009).

In this study, several computational costs prevented the development of a fully accurate reproduction of a BLWT and Wave tank basin. Computational hardware was limited to individual computers with 2-4 Core Processors and limited RAM capability. This drawback prevented a true recreation of the BLWT, as its length and size would require element numbers on the order of 10^8 and thousands of surface roughness elements. This ability can only be accomplished with a cluster of CPU's and improved computer hardware, which is recommended for future studies.

The lack of pressure fluctuation is primarily attributed to the over simplification of the turbulence in the discretization and solution of fluid flow equations (Holmes, 2001). Sub-grid models such as the k-ε model are introduced to capture the turbulent flow. These models have shown to be not stable enough and capable of capturing these effects. Therefore research into more accurate sub-grid models is a major concern and goal for CFD development.

Also included in this study was extension of the CFD method to typical prototype bridges and buildings. Structure-specific hazard data were generated from Dytran for use in later structural analysis. Only linear time history analysis was performed on the two prototype structures. However, this data should be applied to a detailed FEM of each structure and non-linear dynamic analysis be performed. Once completed the structural response quantities such as displacement, stress, and moment can be mapped to damage costs and quantities. These costs can then be statistically defined to allow for the overall performance of the structure to be assessed. These results shall show the possibility of CFD in PBHE and standards of care to improving the overall performance of our coastal infrastructure.

APPENDIX: ADDITIONAL RESULTS AND PLOTS

Explanation of Verification Plots

Pressure Coefficient Comparison

Top plot shows the original individual 10second record from Dytran (raw). Middle plot shows a 10 second window of tunnel data from the same location. Bottom plot shows the generation of a synthetic wind signal through RPG. All three plots have ASCE 7-05 derived pressure coefficients in red.

Power Spectral Density Plot (PSD)

Plot shows comparison of Welch based PSD plot of experimental and numerical results, along with established wind code spectrum such as Von Karman-Harris, Busch and Panofosky and Eurocode I.

Autocorrelation Coefficient

Plot shows the comparison of autocorrelation coefficient of wind tunnel, raw Dytran, RPG signal. All plots have a similar time record of 10second.

SDOF Comparison

Displacement, Velocity and Acceleration response of idealized barn structure from wind tunnel, raw dytran and RPG signals.

Force Comparision

Plot shows force time history of wave tank simulation results.

Wind Attack 15 Degrees

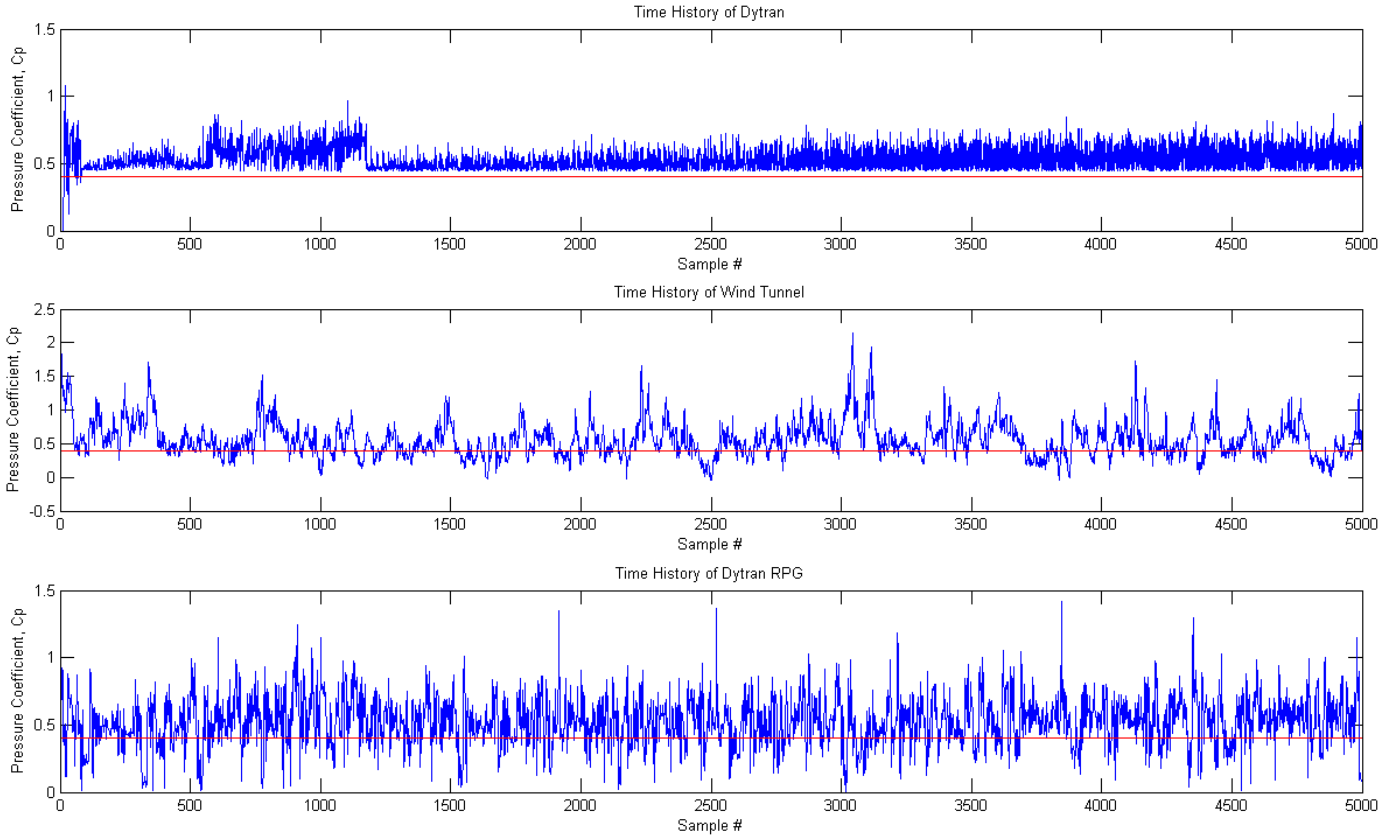

Figure 56: Windward Wall Pressure Coefficient Comparison

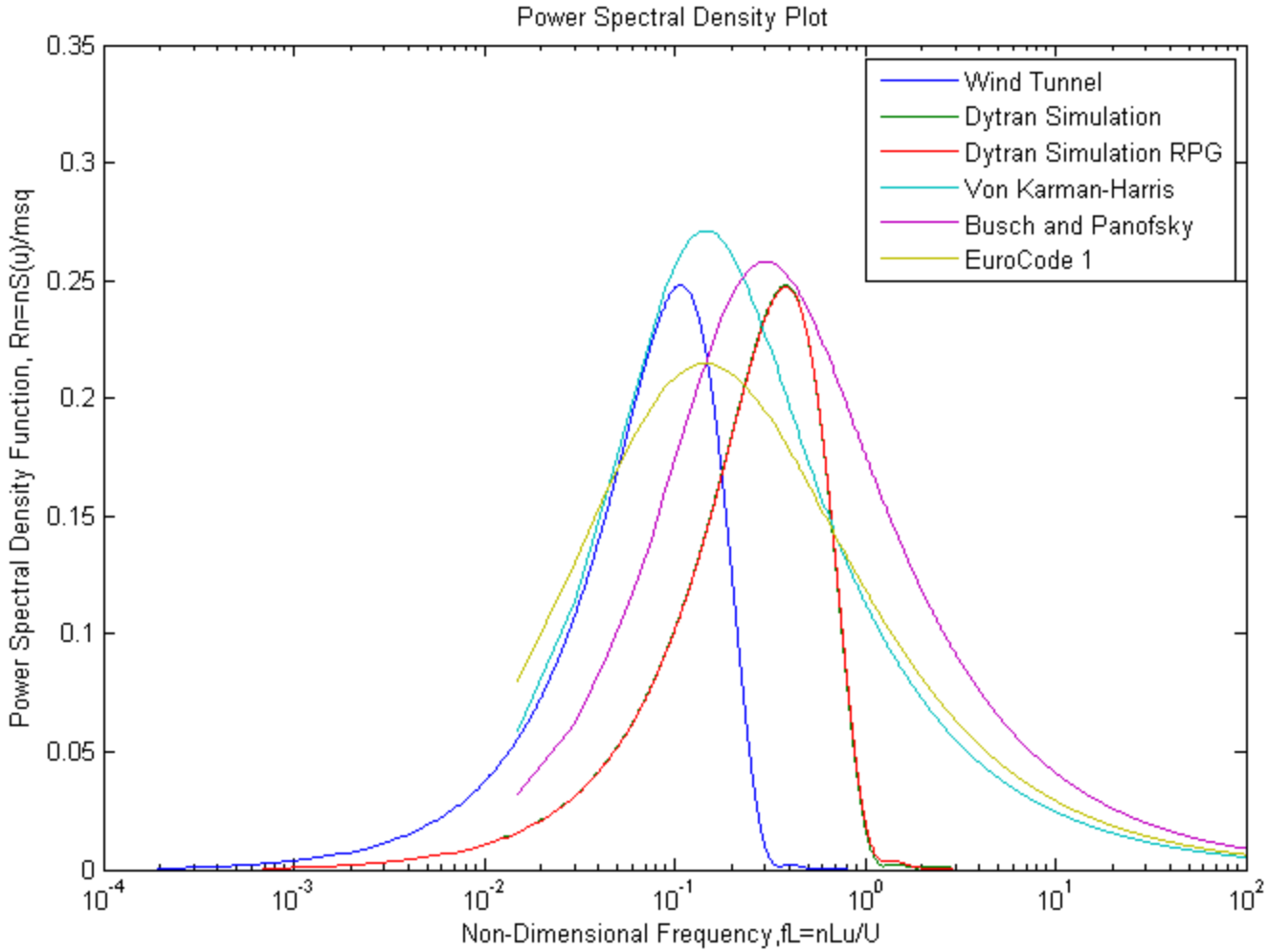

Figure 57: Windward Wall PSD Comparison

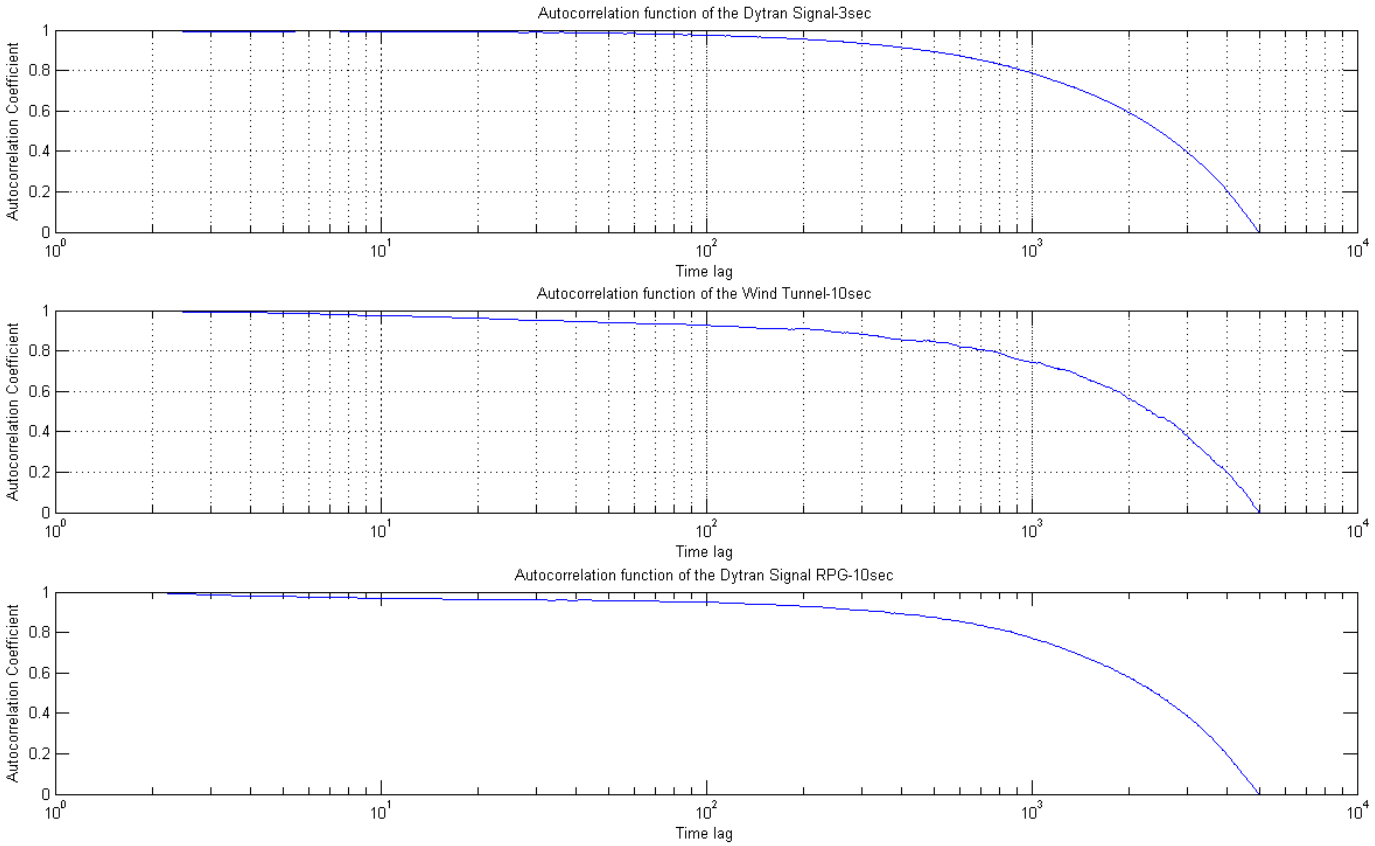

Figure 58: Windward Wall Autocorrelation Coefficient Comparison

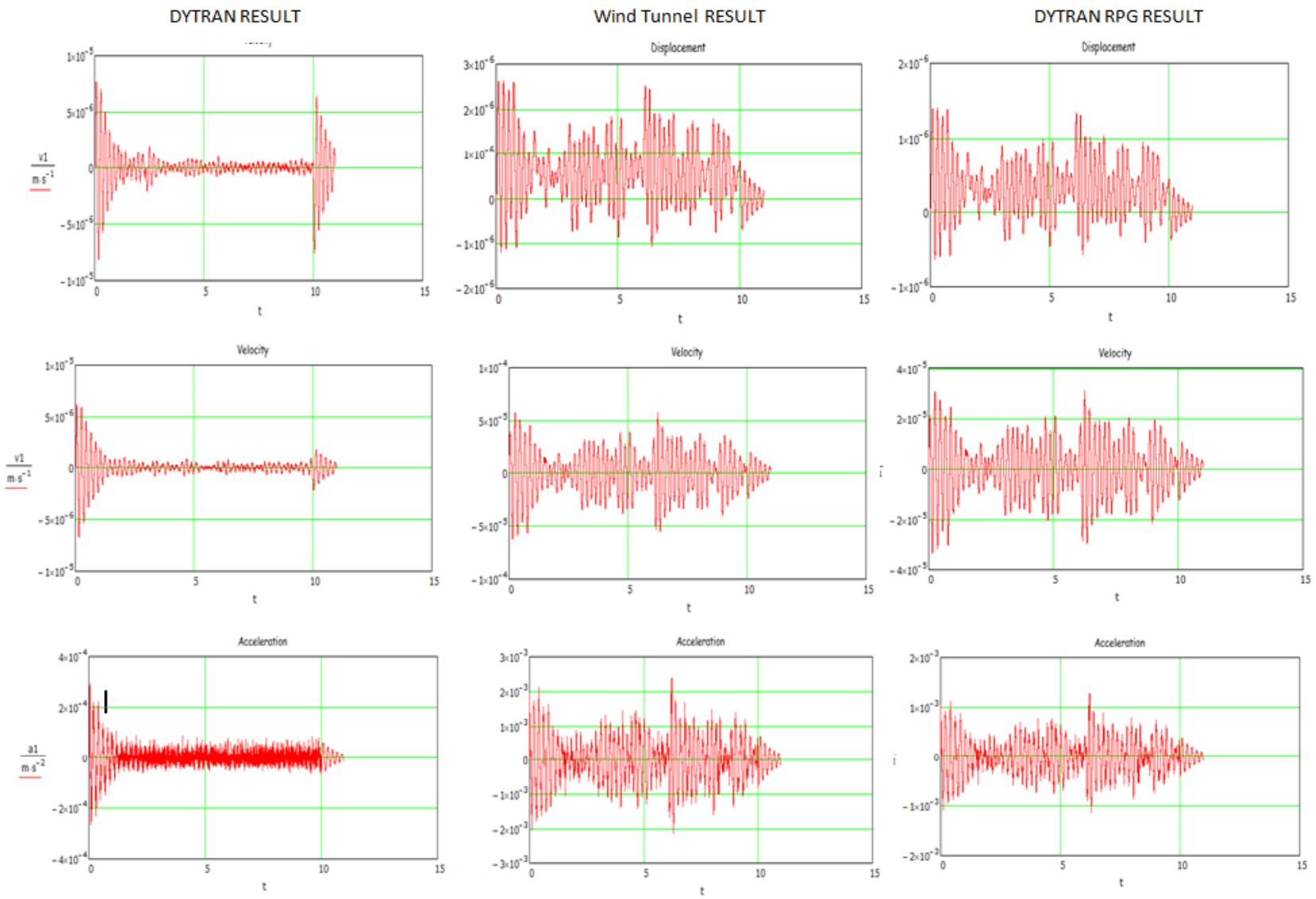

Figure 59: Windward Wall SDOF Comparison

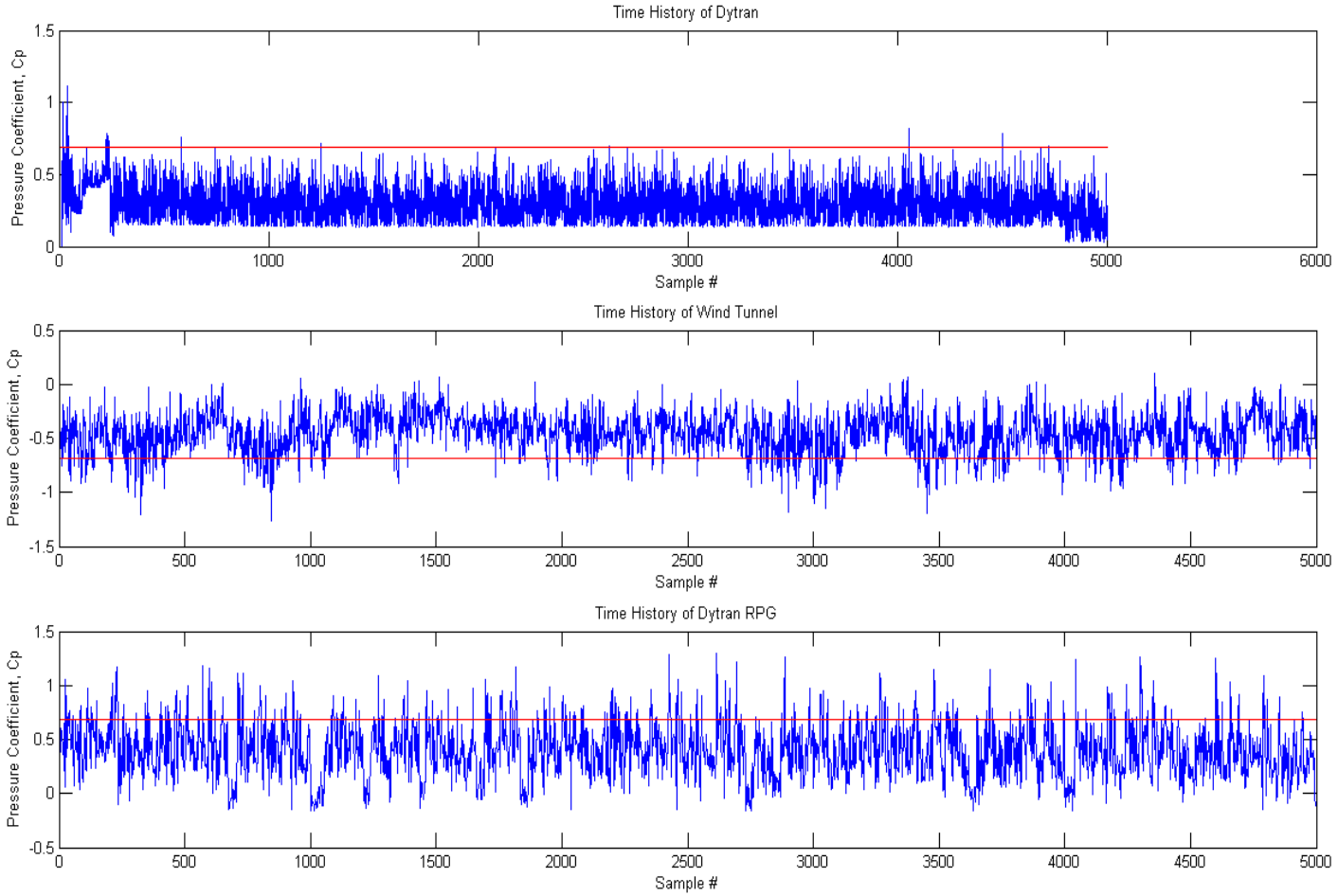

Figure 60: Windward Roof Pressure Coefficient Comparison

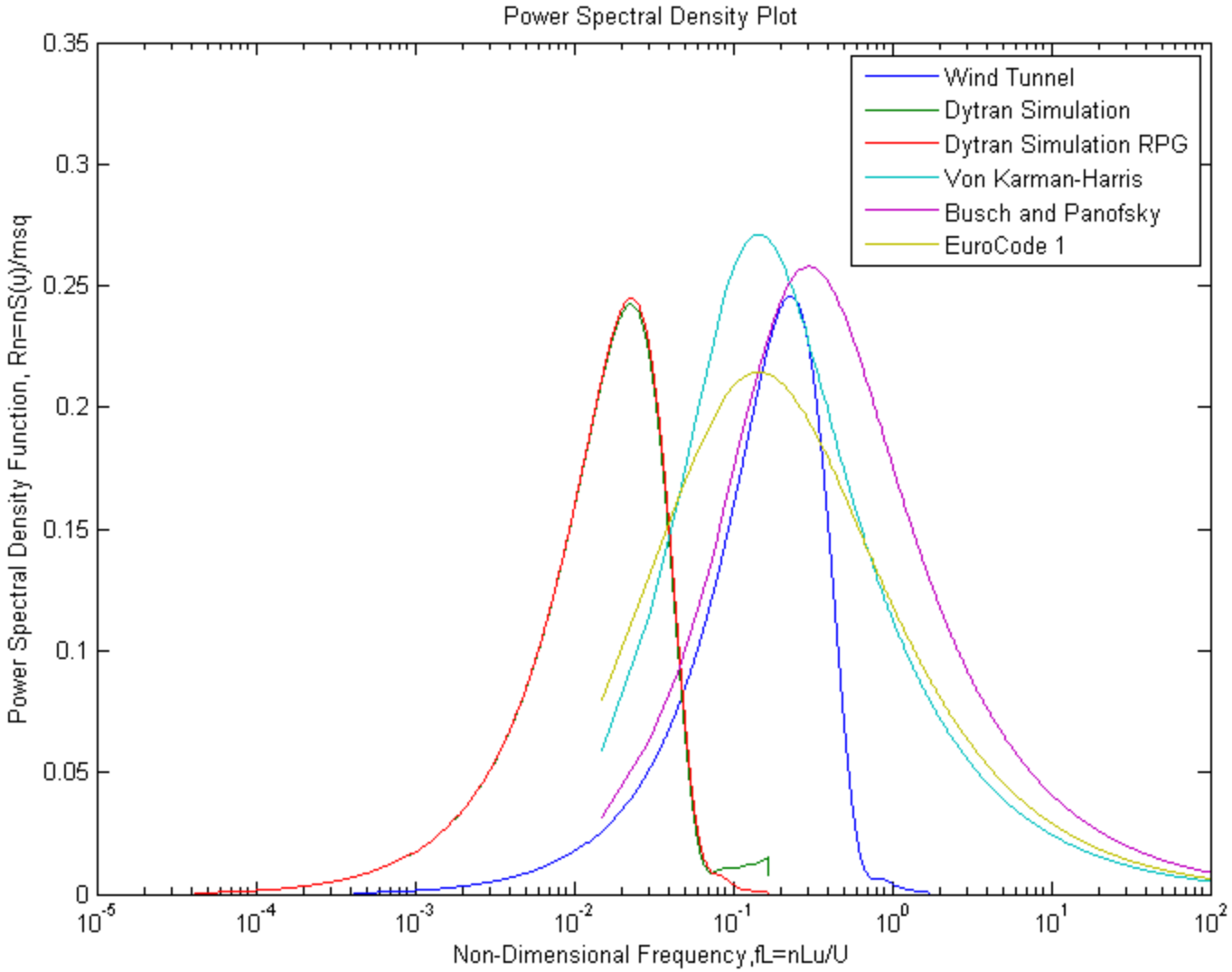

Figure 61: Windward Roof PSD Comparison

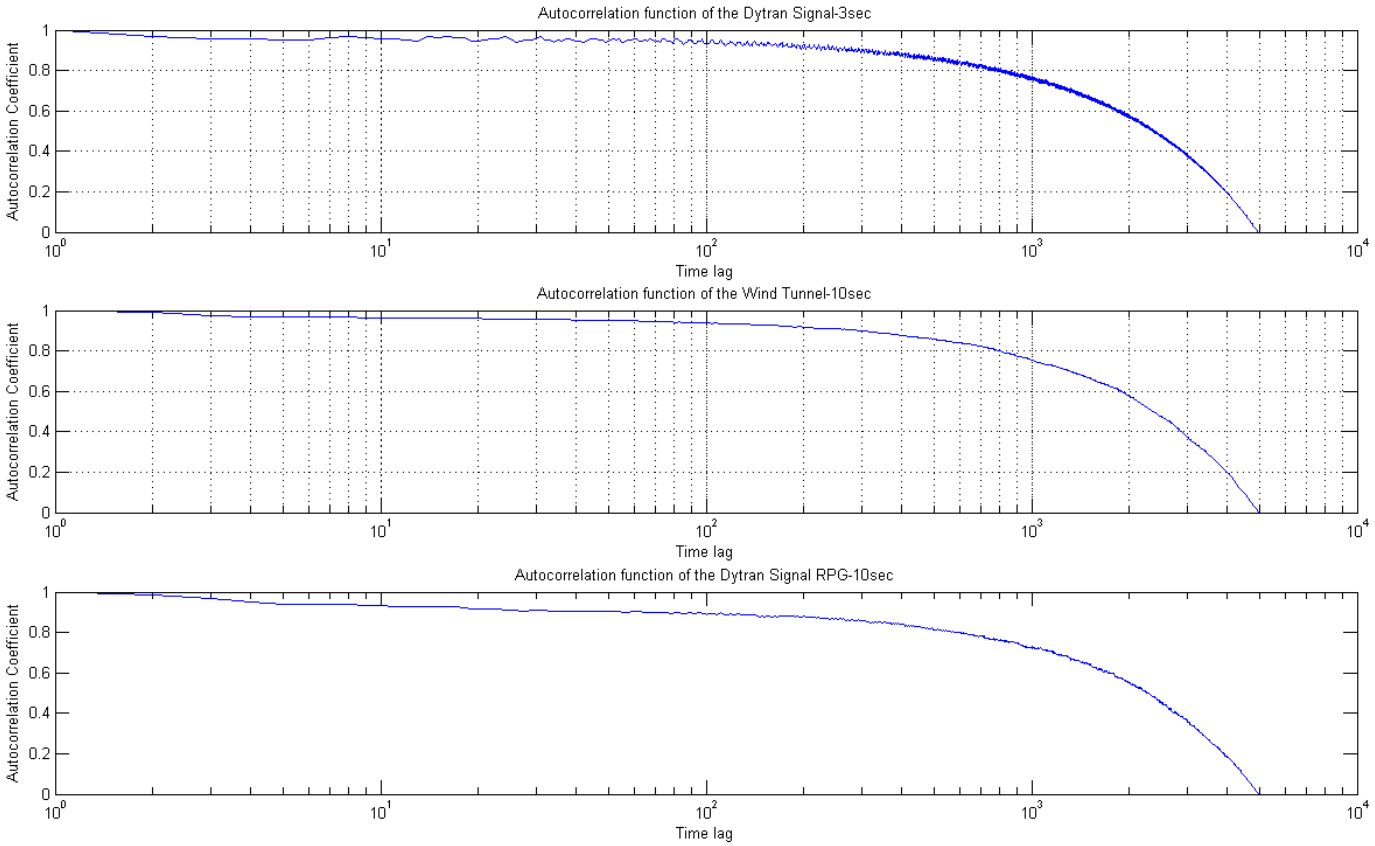

Figure 62: Windward Roof Autocorrelation Coefficient Comparison

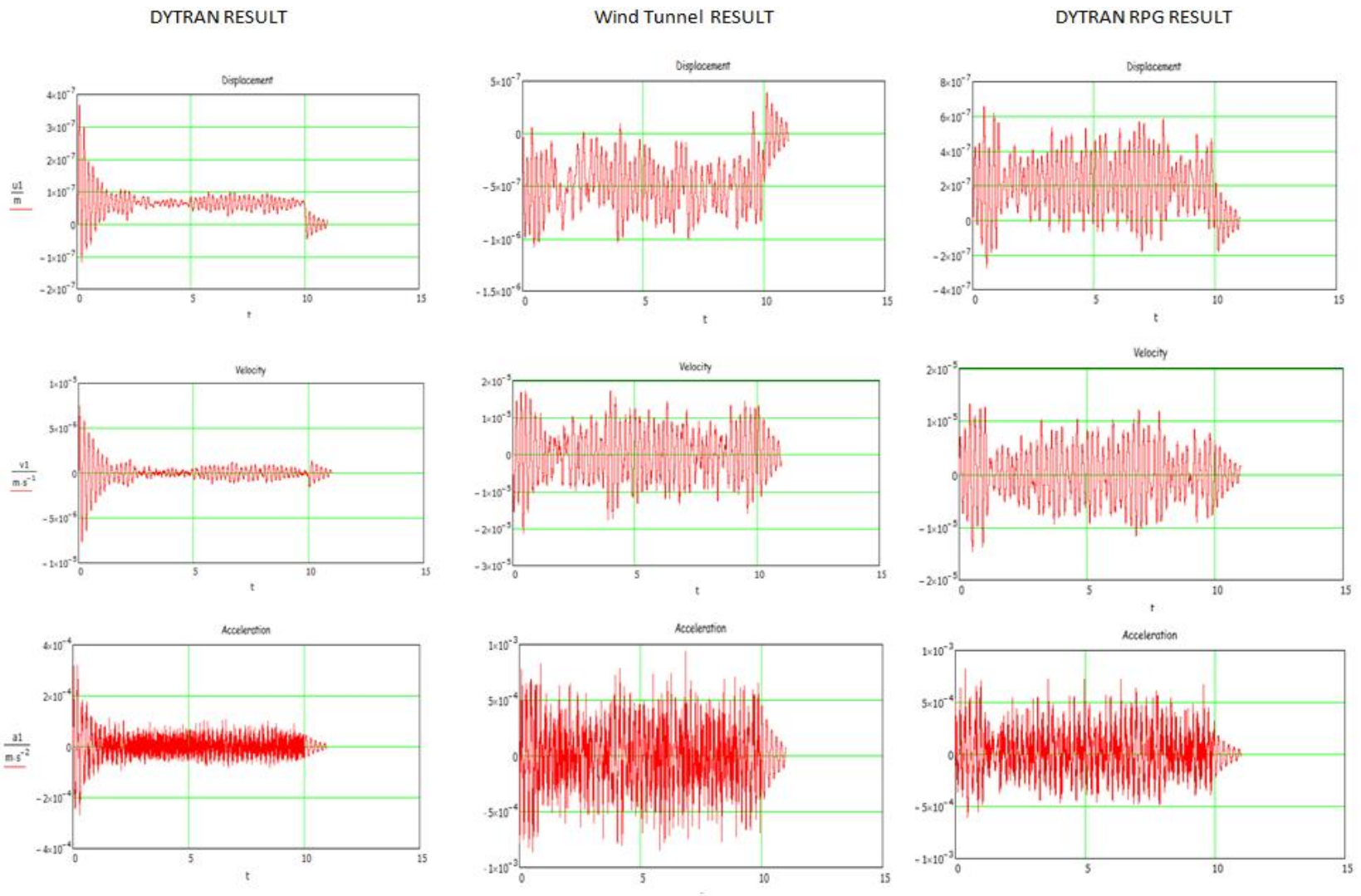

Figure 63: Windward Roof PSD Comparison

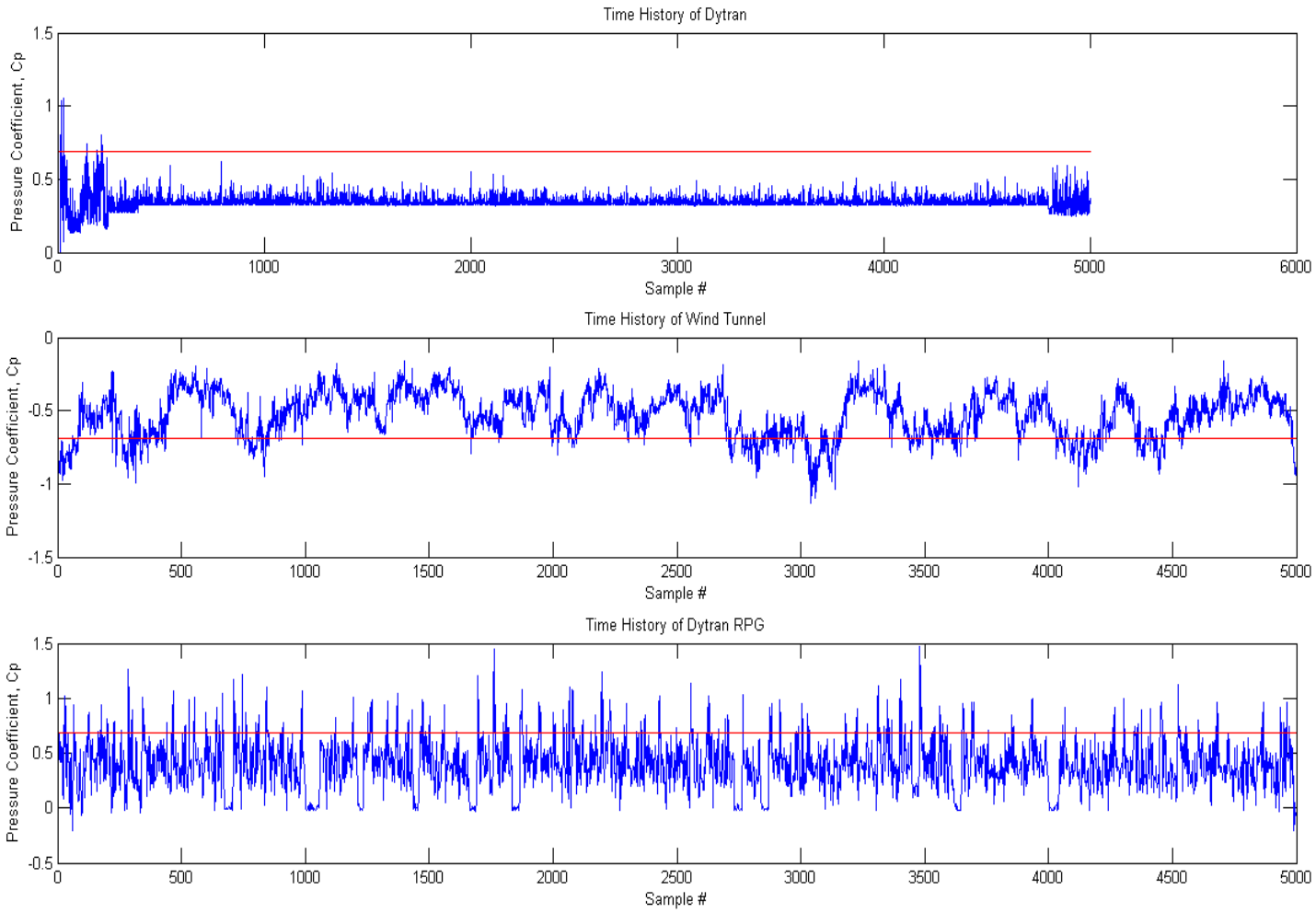

Figure 64: Roof Peak Pressure Coefficient Comparison

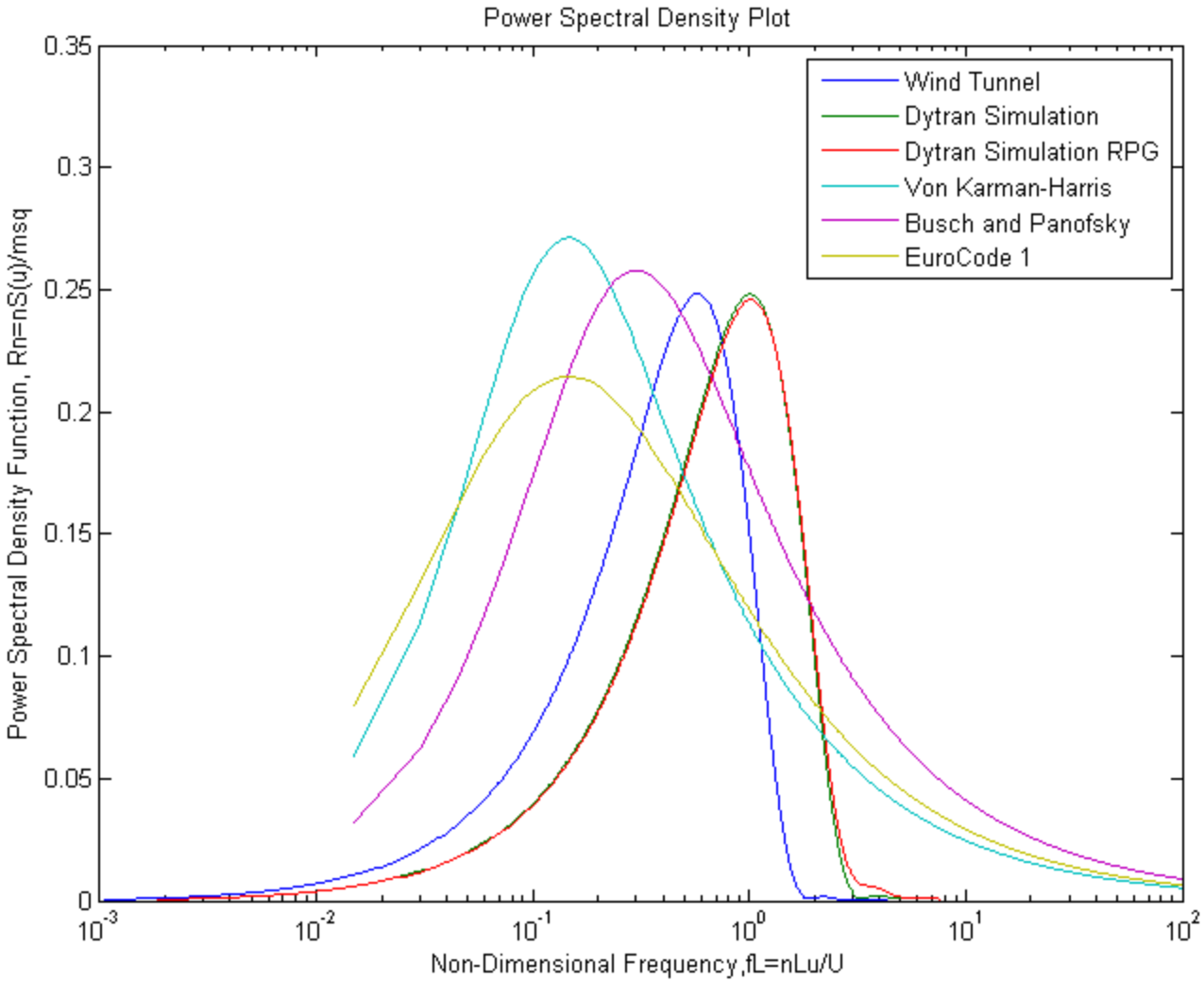

Figure 65: Roof Peak PSD Comparison

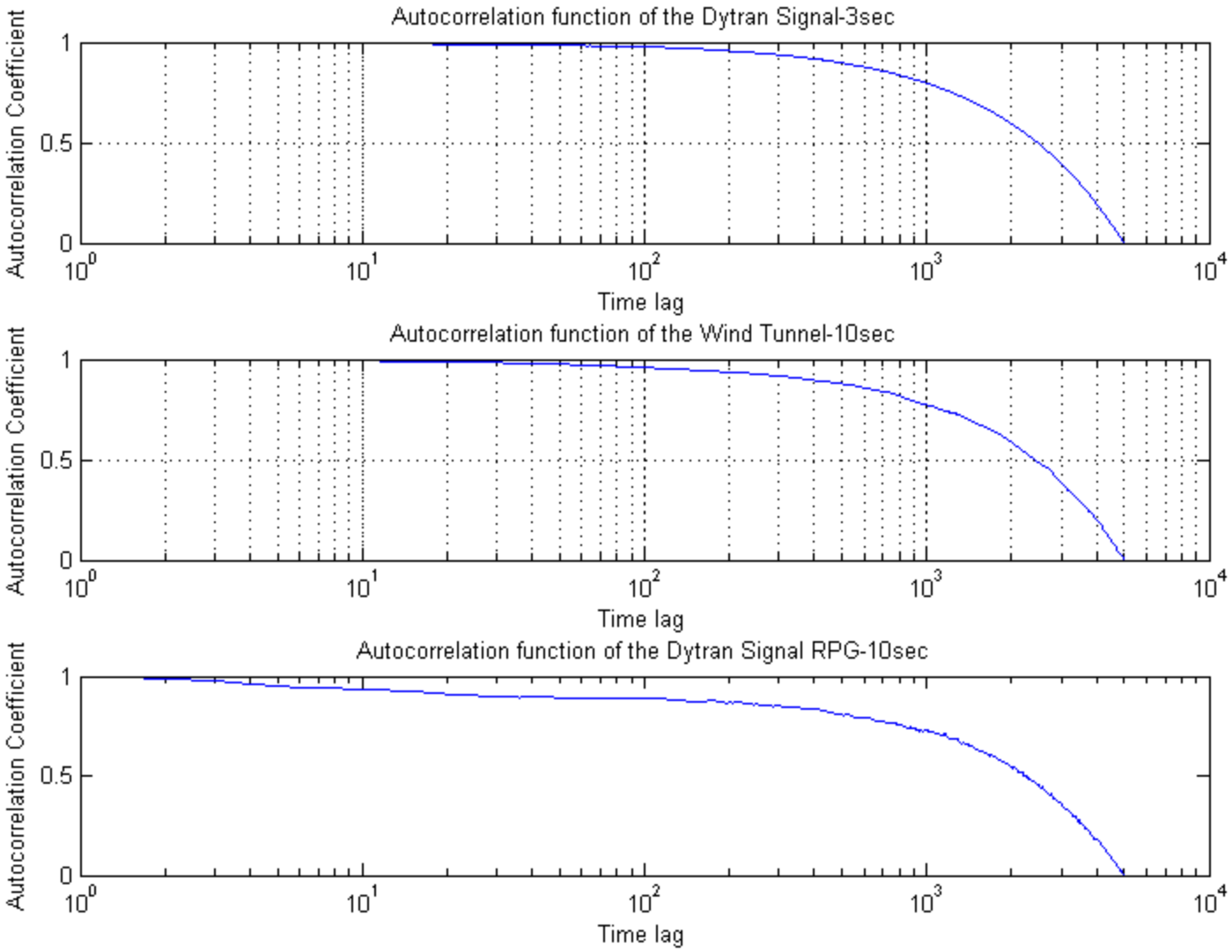
Autocorrelation function of the Dytran Signal-3sec
Autocorrelation Coefficient
Time lag
Autocorrelation function of the Wind Tunnel-10sec
Autocorrelation Coefficient
Time lag
Autocorrelation function of the Dytran Signal RPG-10sec
Autocorrelation Coefficient
Time lag

Figure 66: Roof Peak Autocorrelation Coefficient Comparison

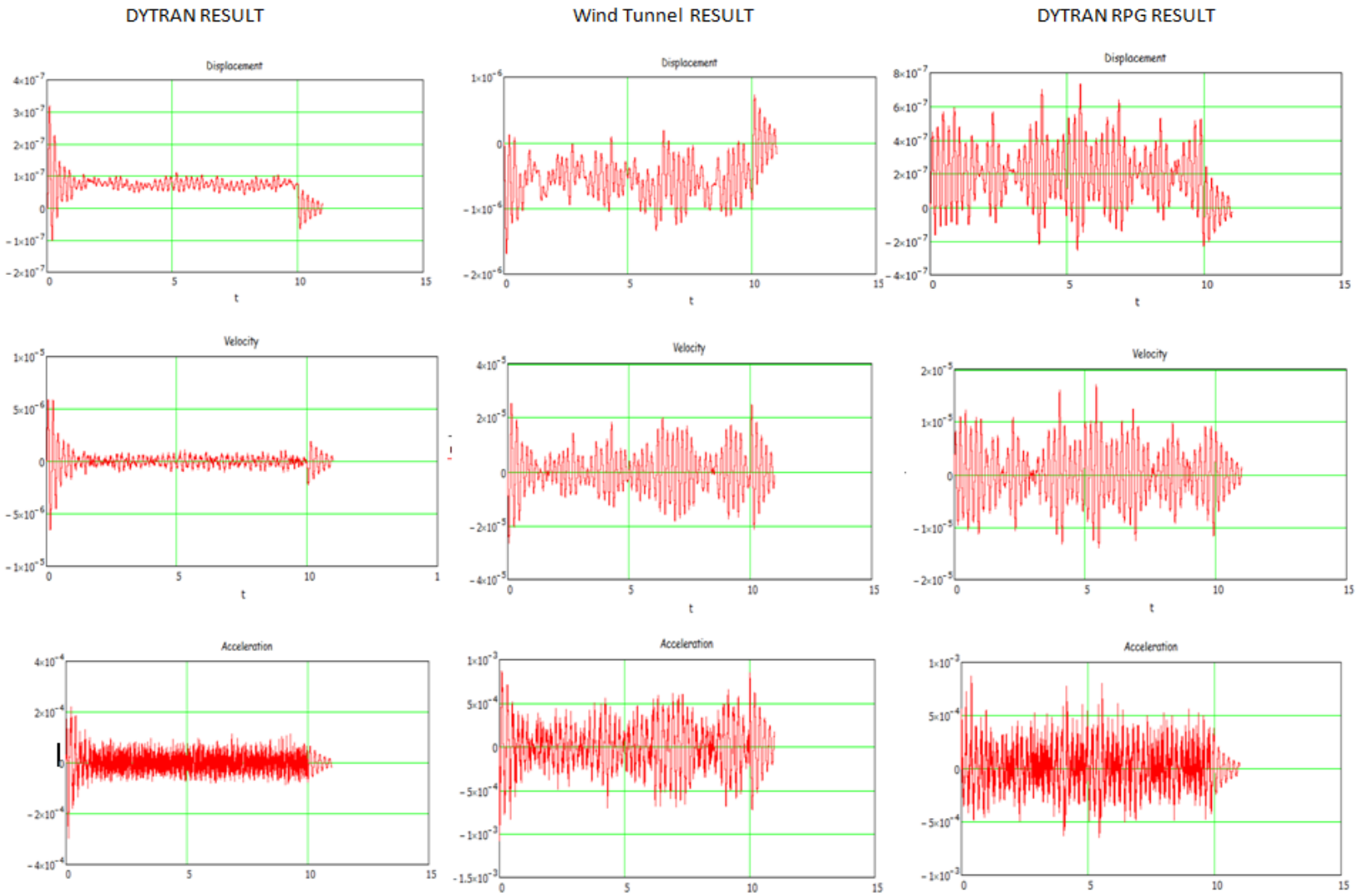

Figure 67: Peak SDOF Comparison

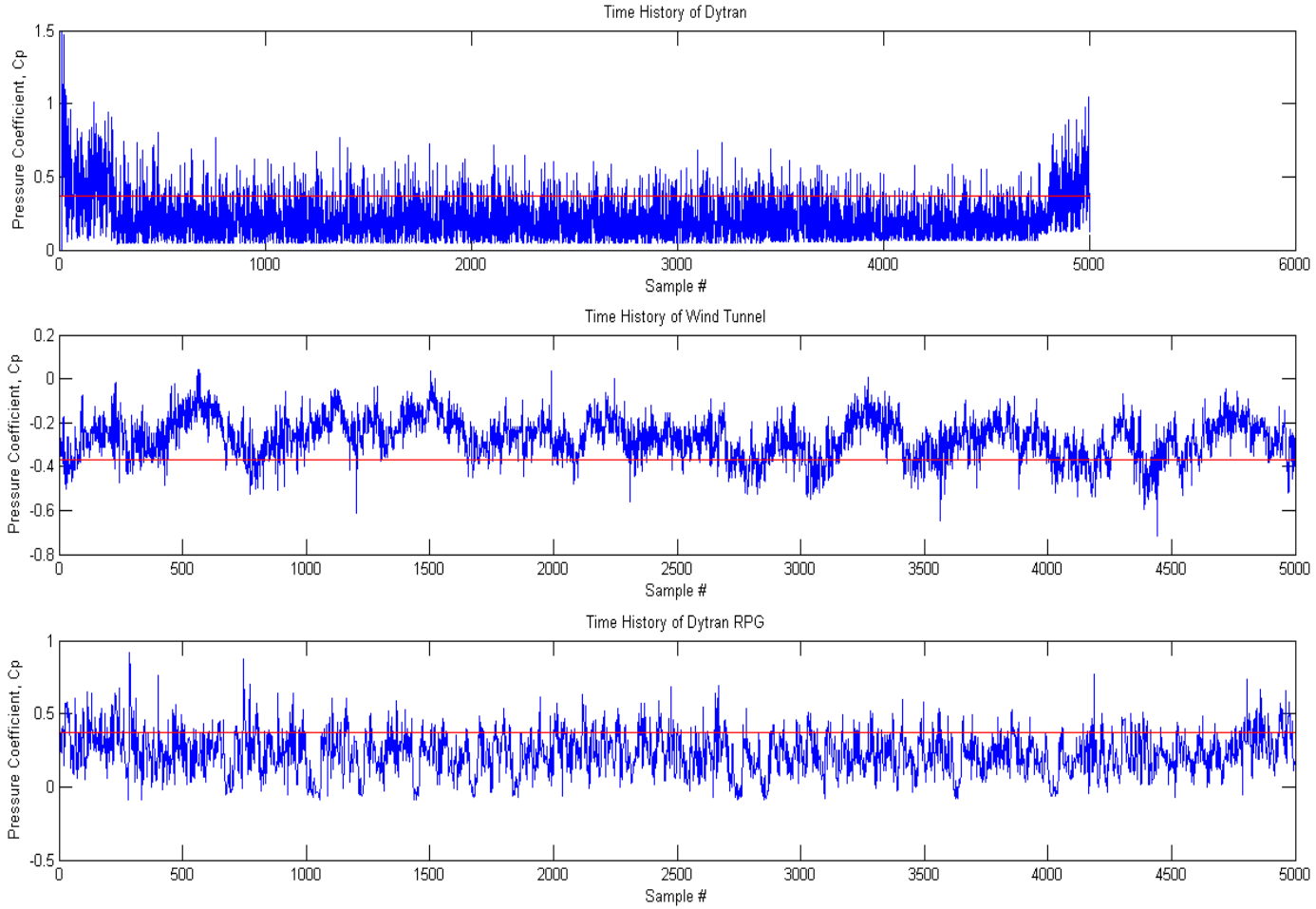

Figure 68: Leeward Roof Pressure Coefficient Comparison

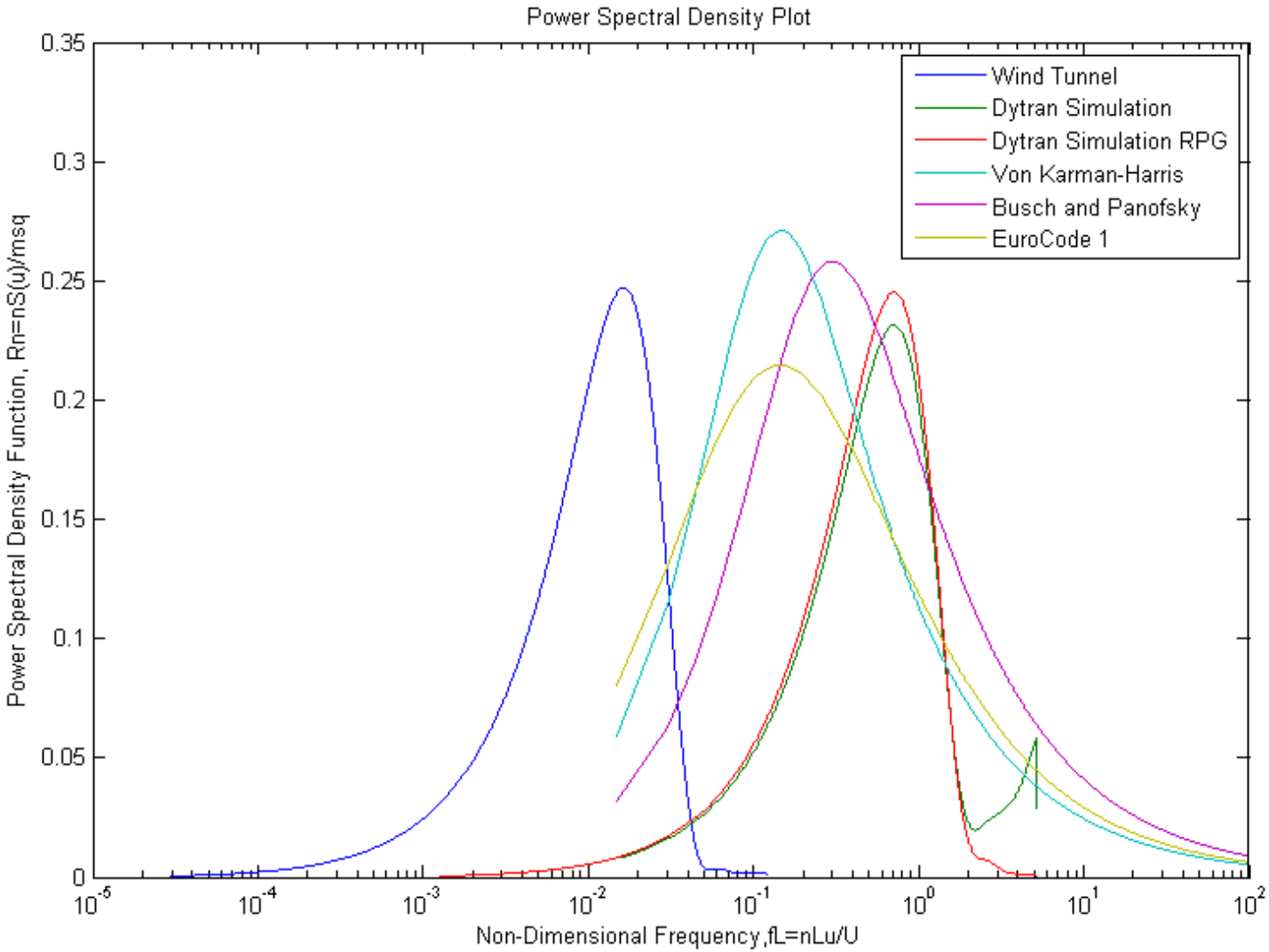

Figure 69: Leeward Roof PSD Comparison

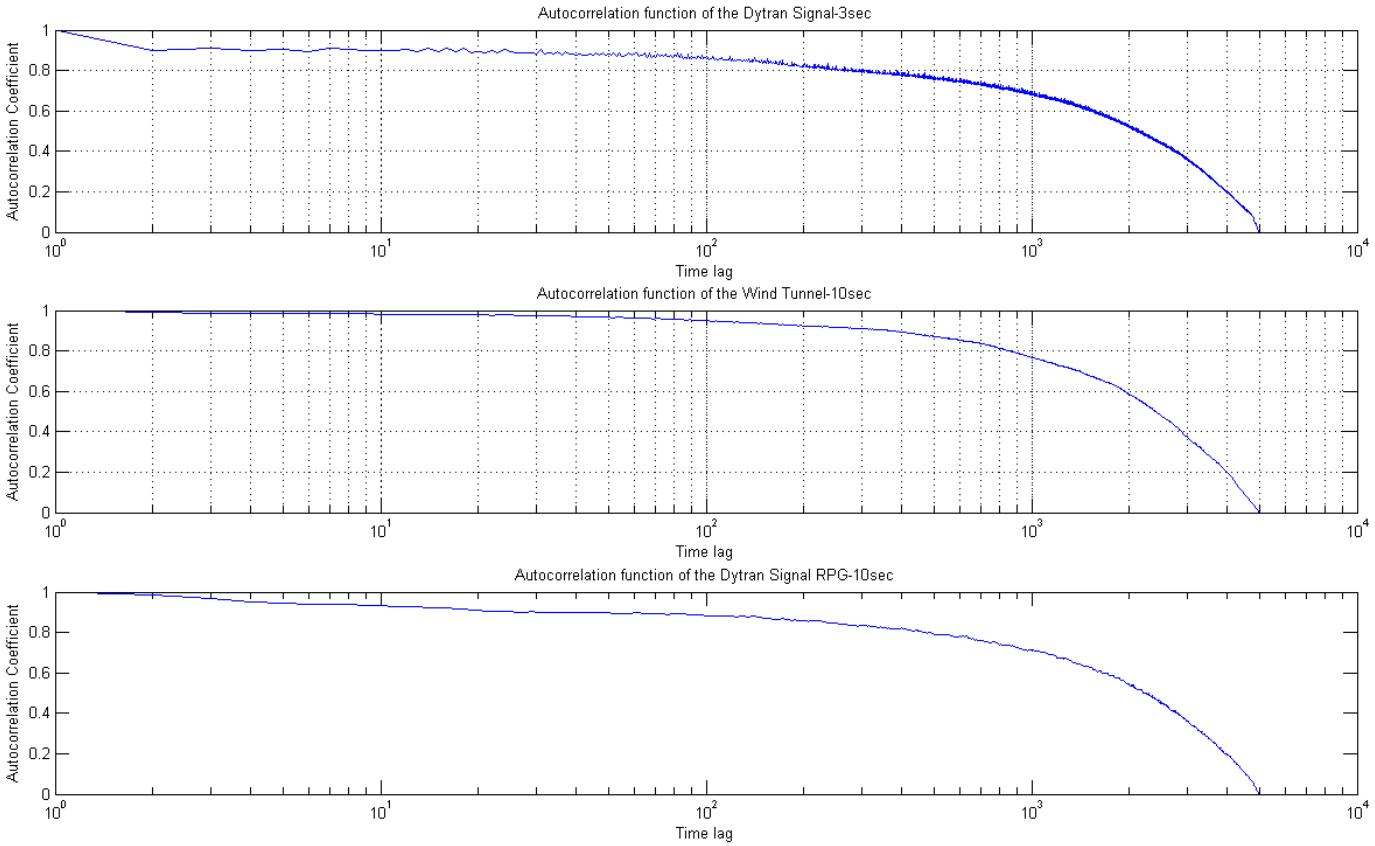

Figure 70: Leeward Roof Autocorrelation Comparison

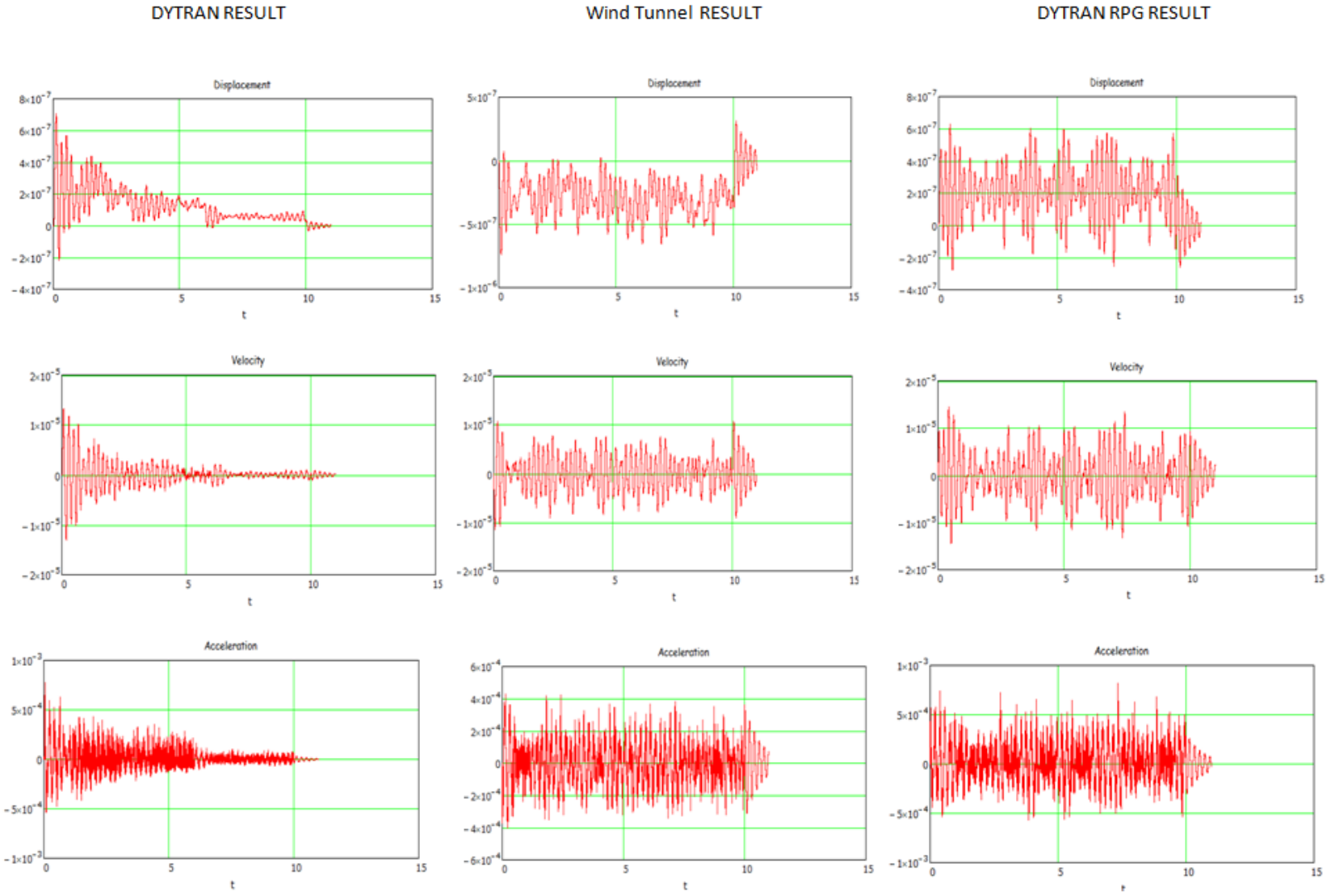

Figure 71: Leeward Roof SDOF Comparison

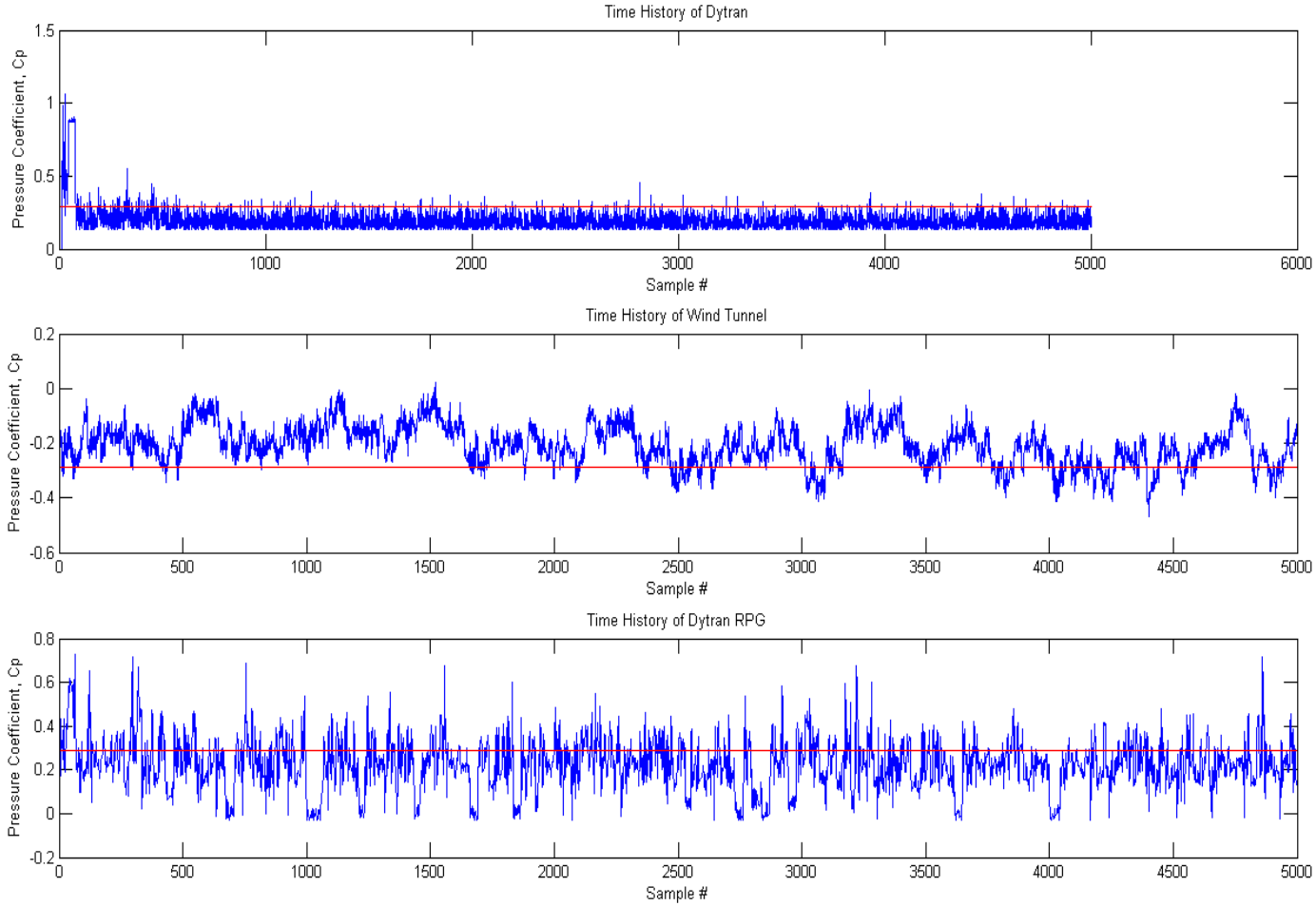

Figure 72: Leeward Wall Pressure Coefficient Comparison

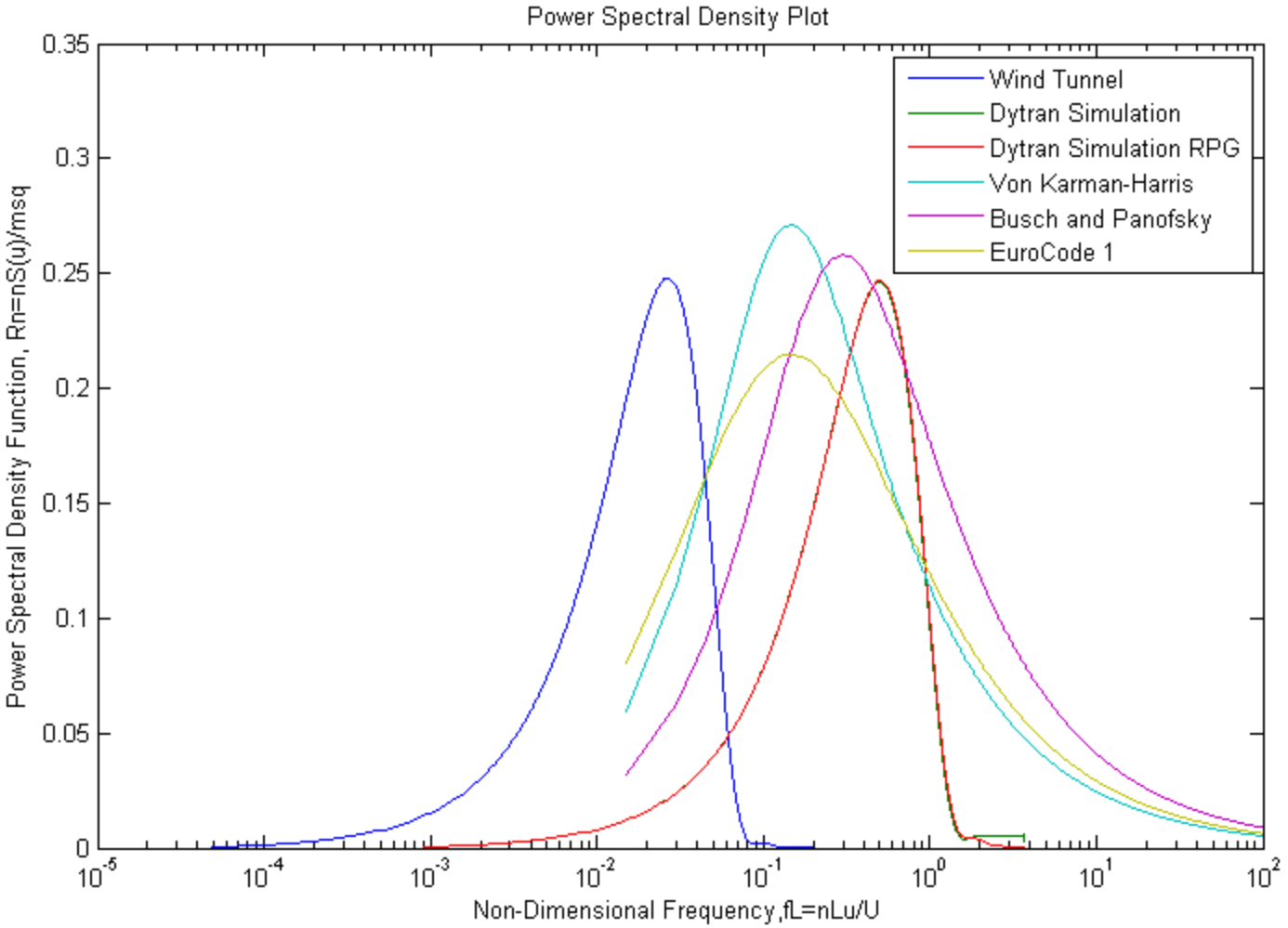

Figure 73: Leeward Wall PSD Comparison

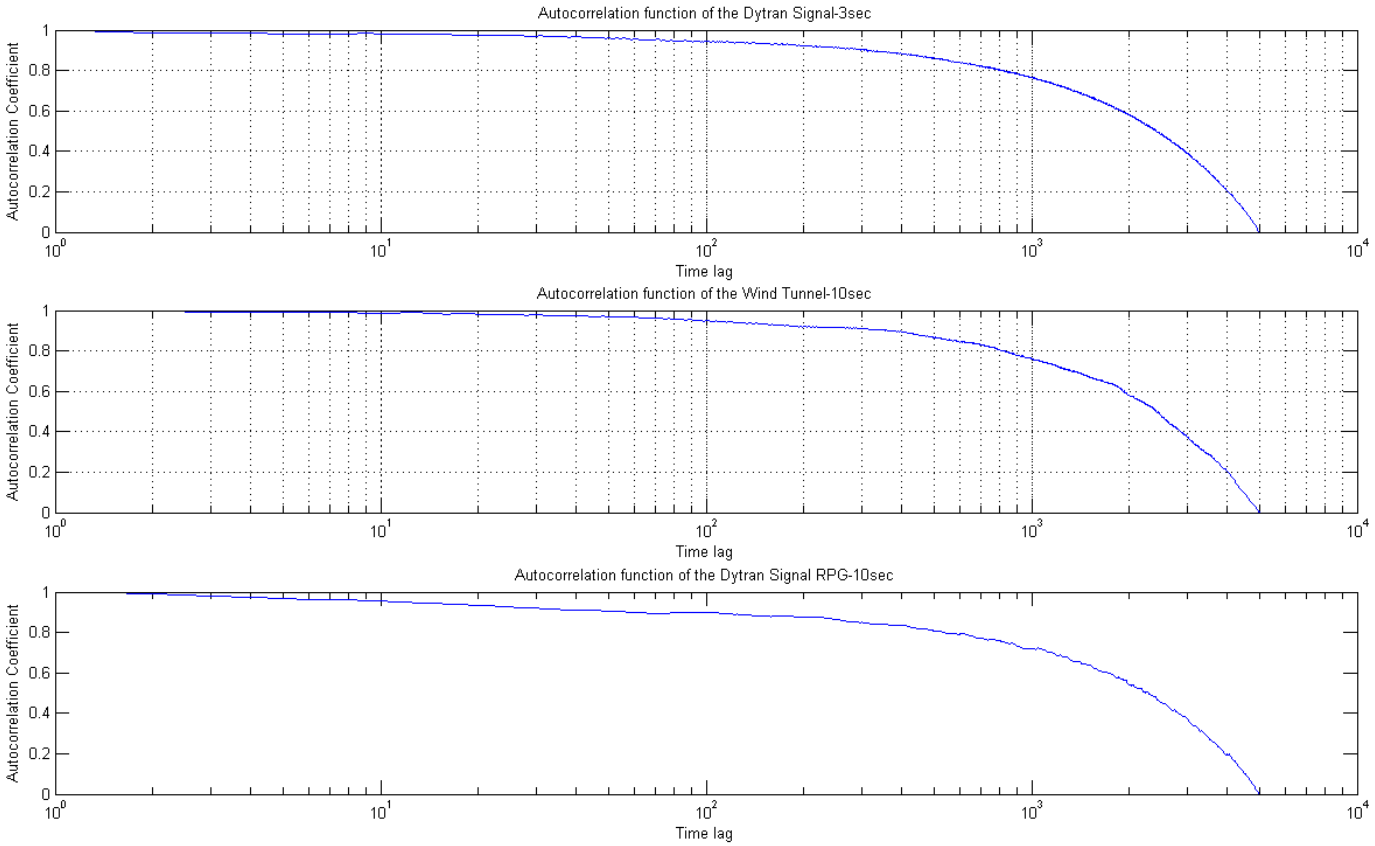

Figure 74: Leeward Wall Autocorrelation Comparison

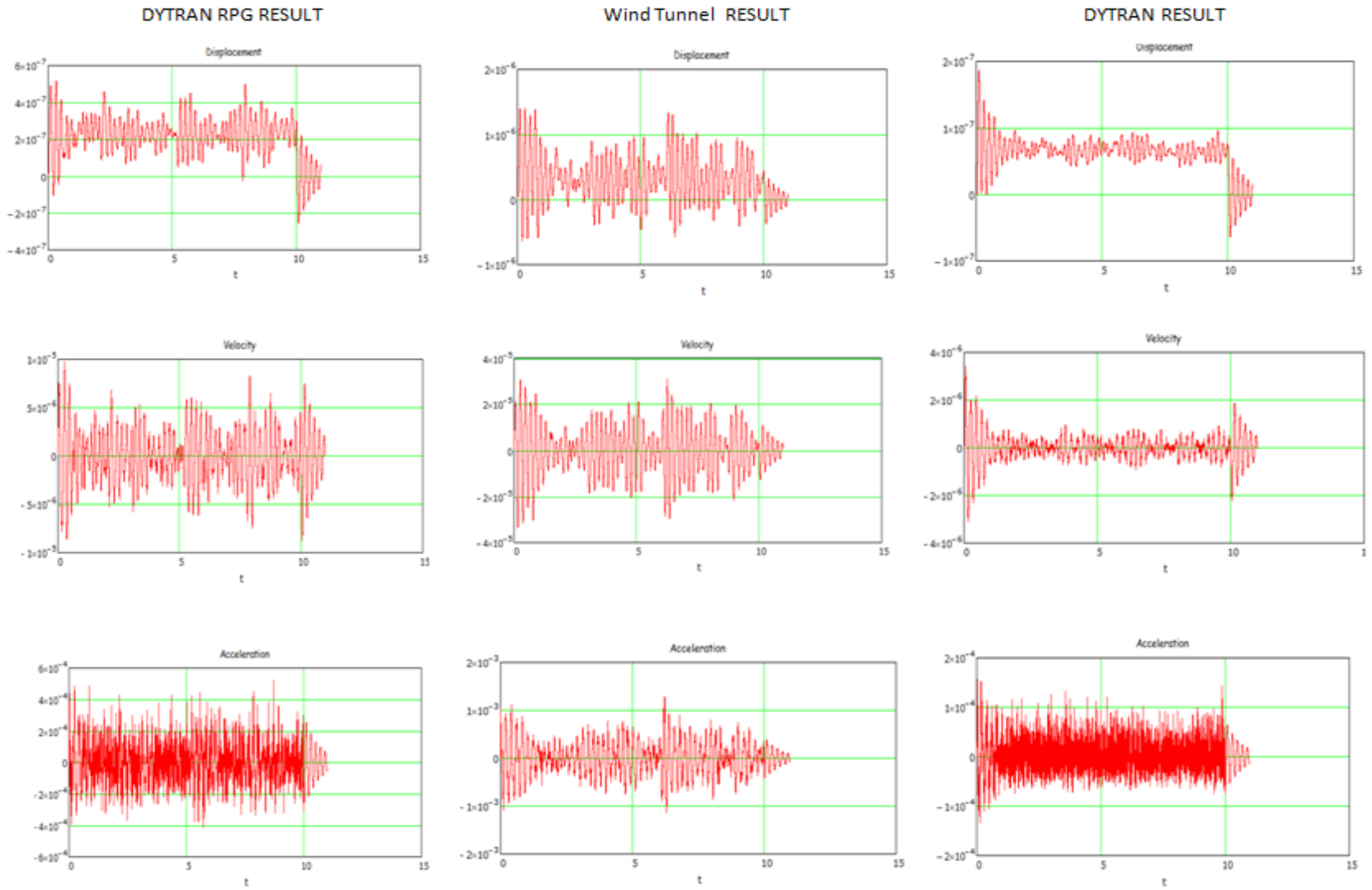

Figure 75: Leeward Wall SDOF Comparison

Wind Attack 45 Degrees

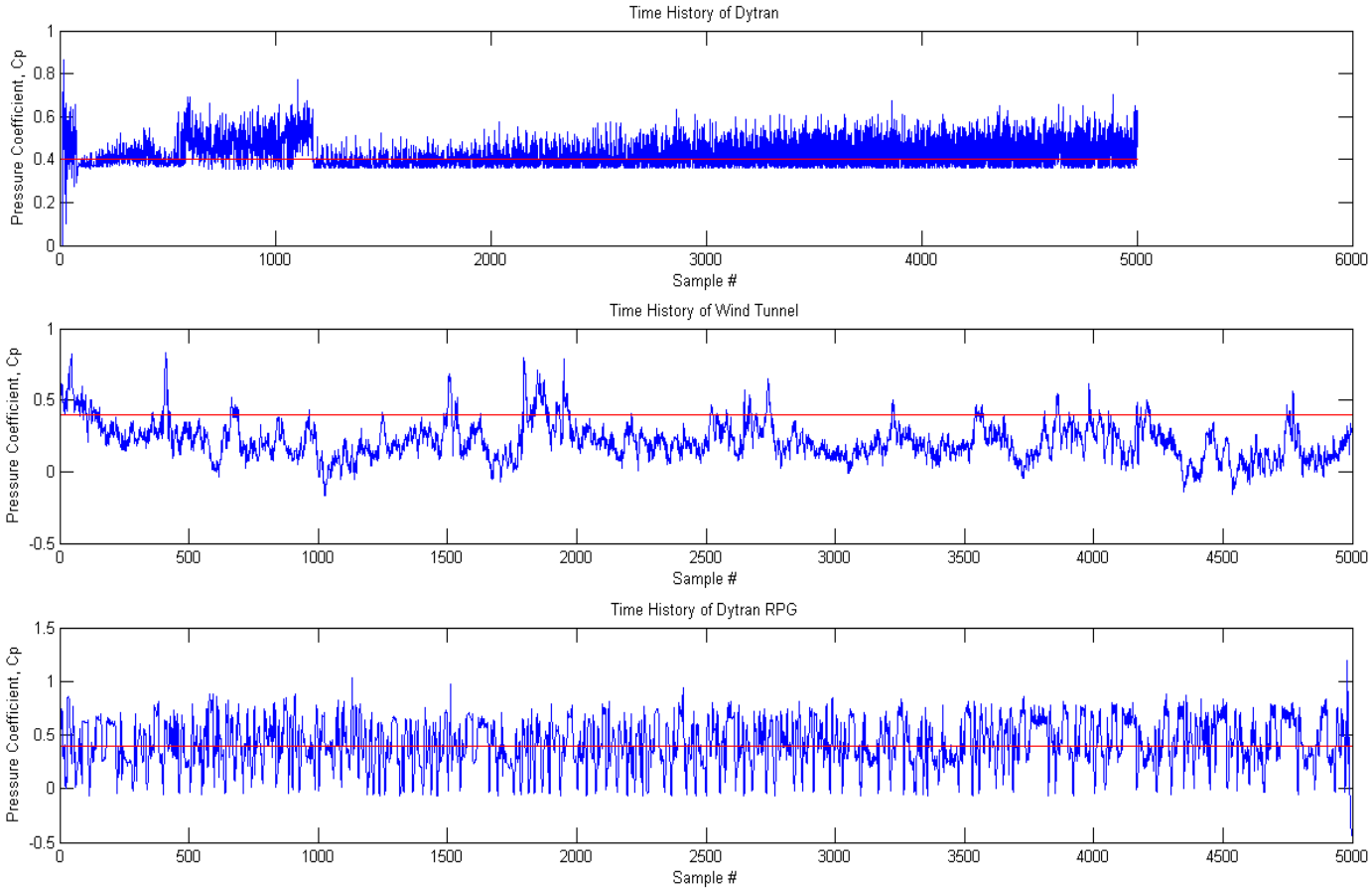

Figure 76: Windward Wall Pressure Coefficient Comparison

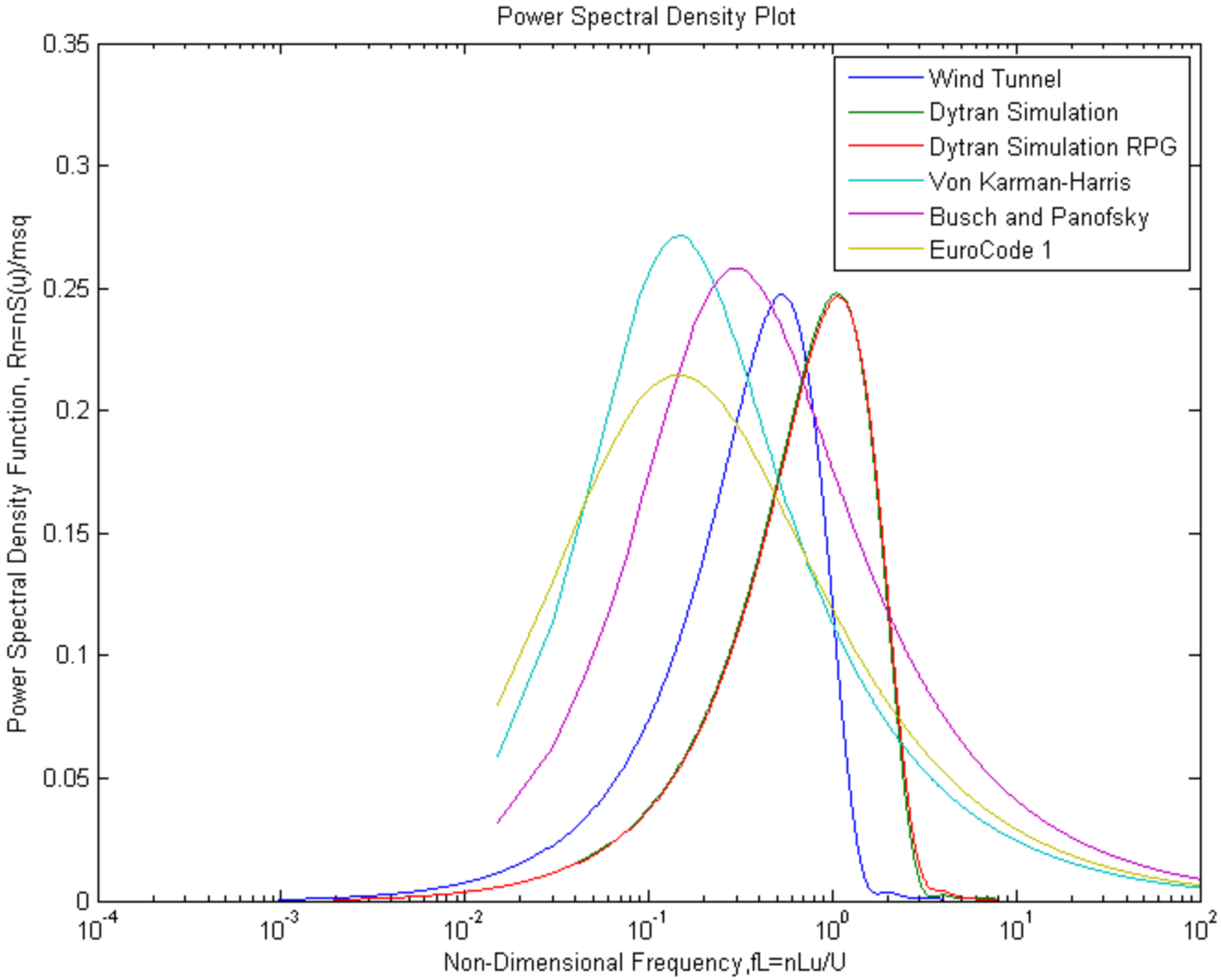

Figure 77: Windward Wall PSD Comparison

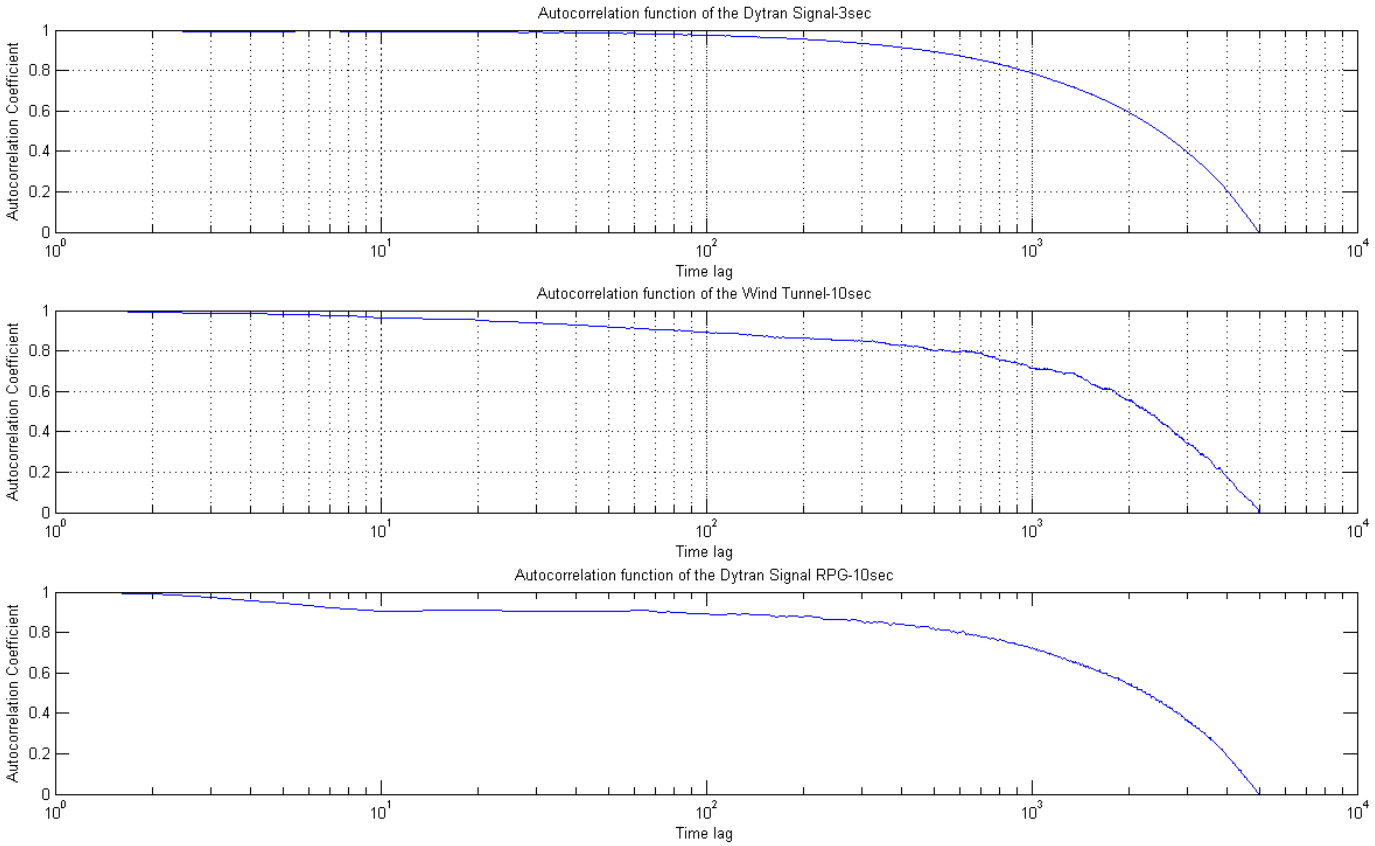

Figure 78: Windward Wall Autocorrelation Comparison

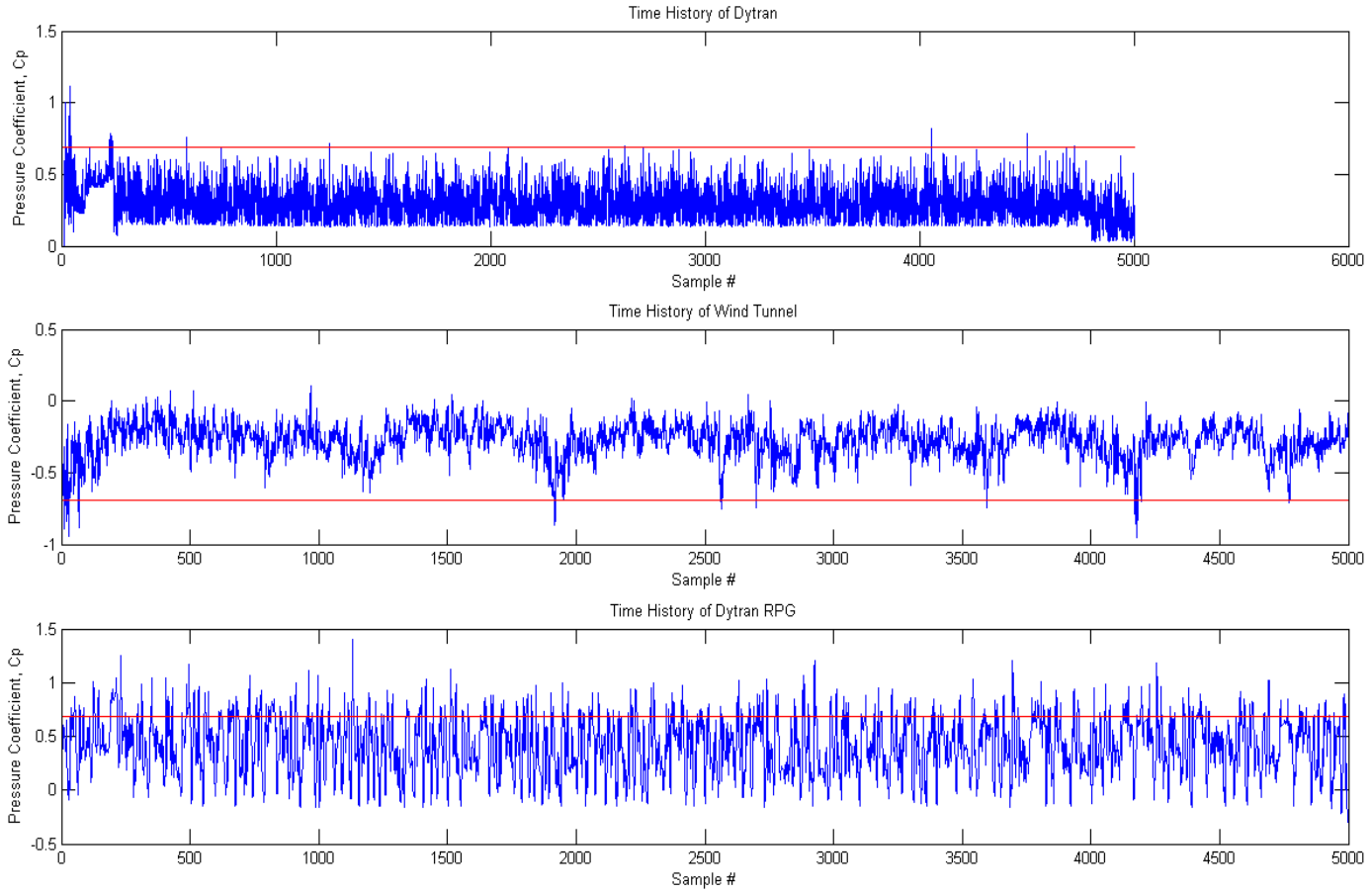

Figure 79: Windward Roof Pressure Coefficient Comparison

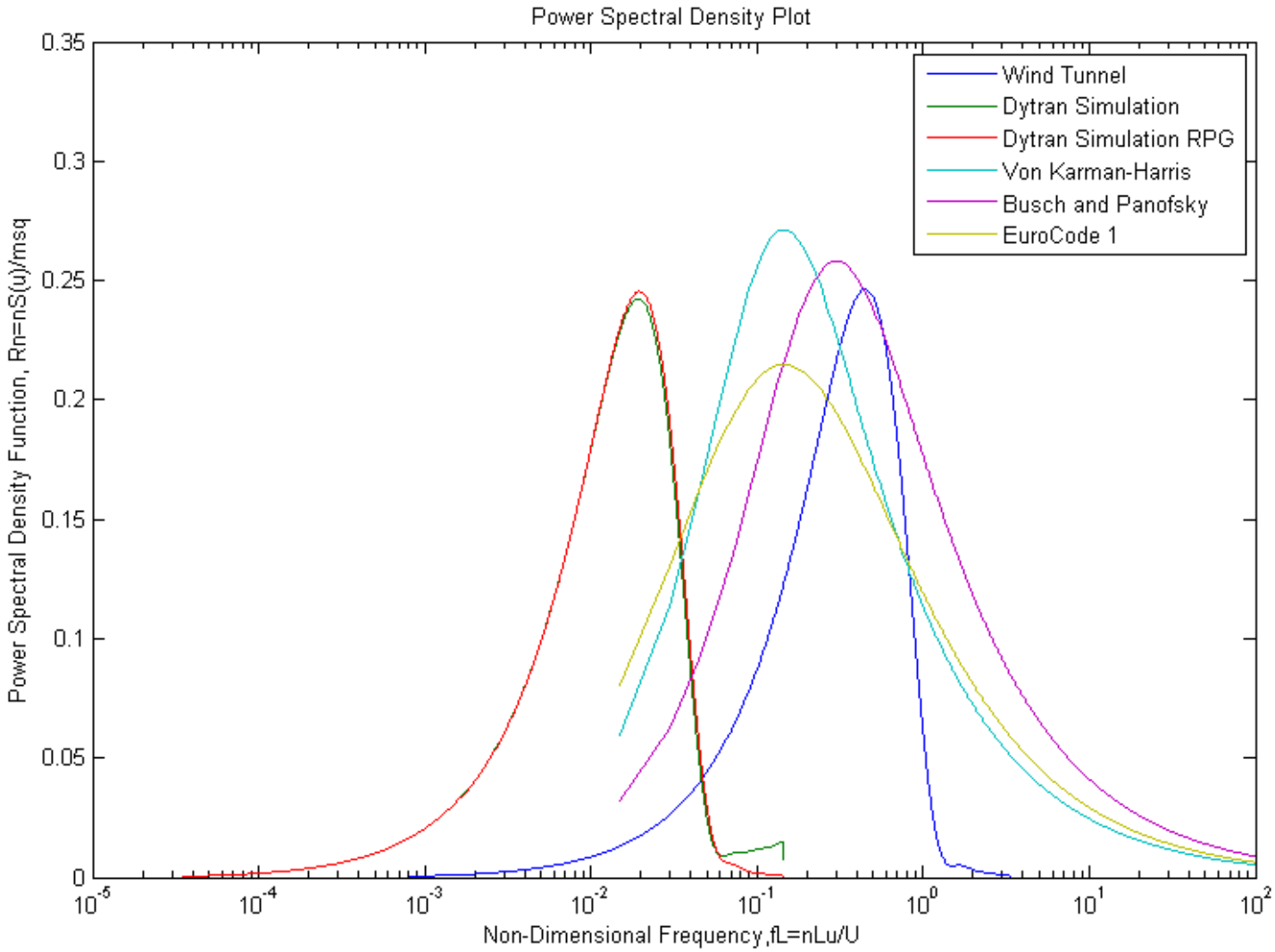

Figure 80: Windward Roof PSD Comparison

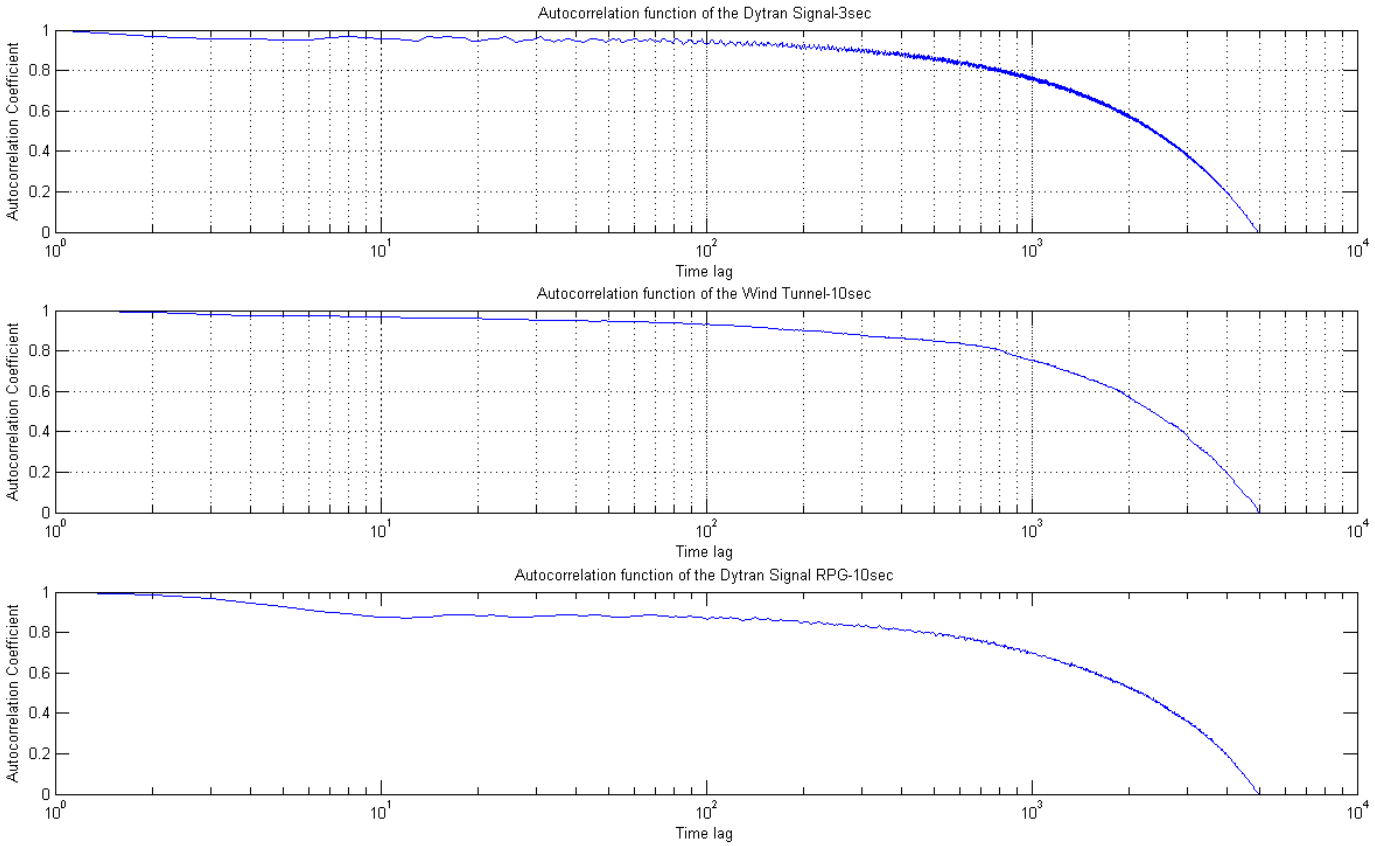

Figure 81: Windward Roof Autocorrelation Comparison

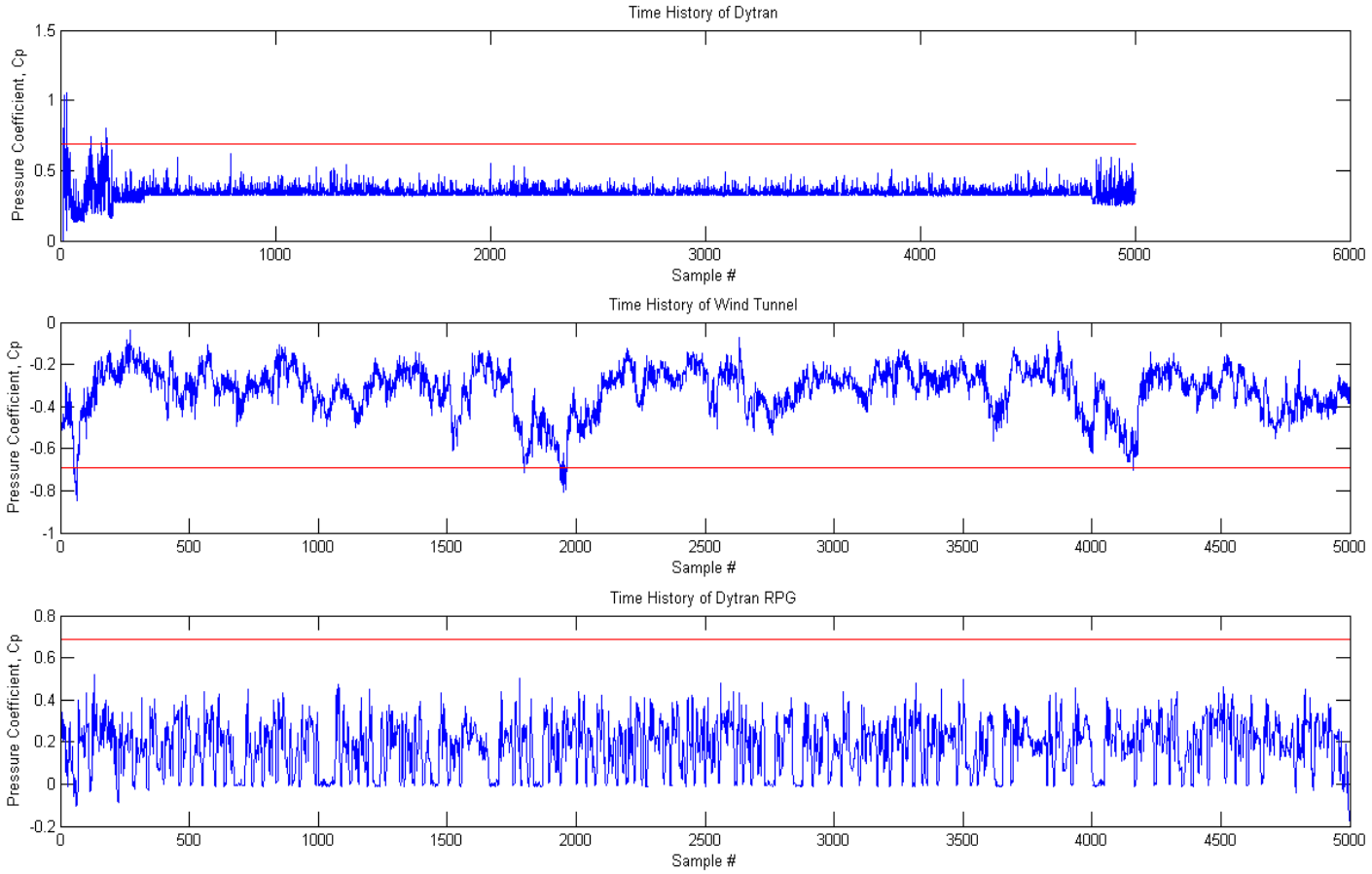

Figure 82: Roof Peak Pressure Coefficient Comparison

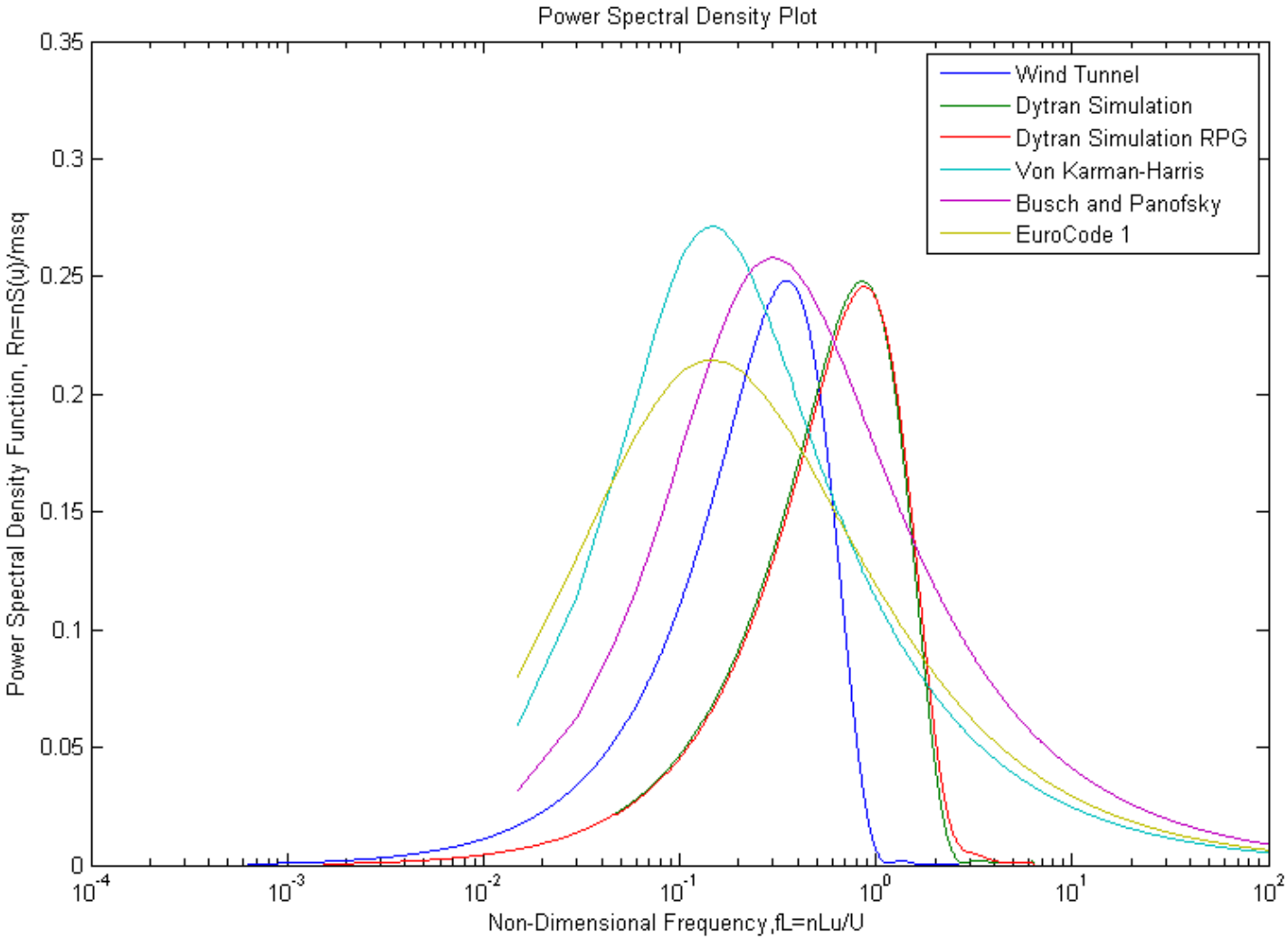

Figure 83: Roof Peak PSD Comparison

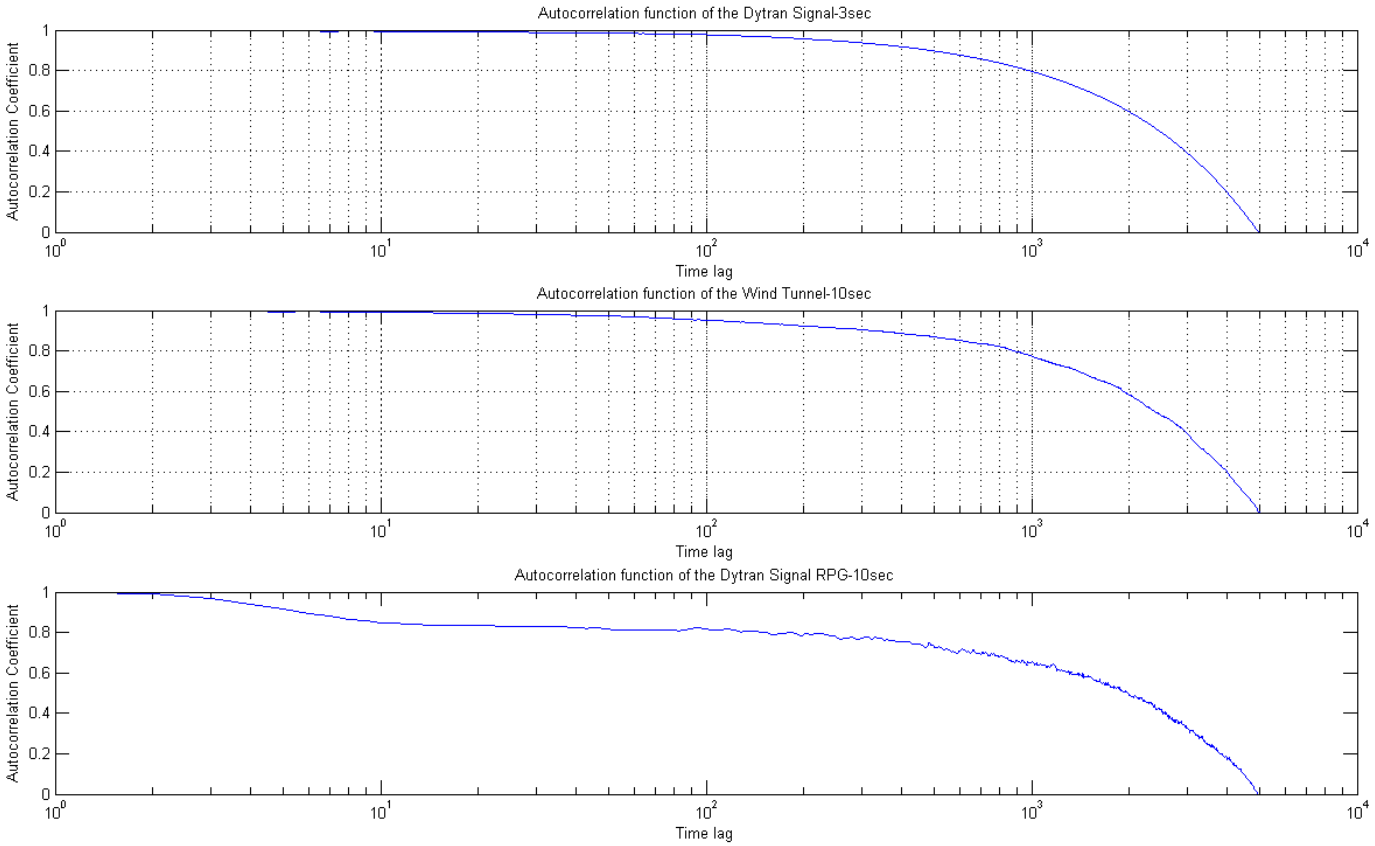

Figure 84: Roof Peak Autocorrelation Comparison

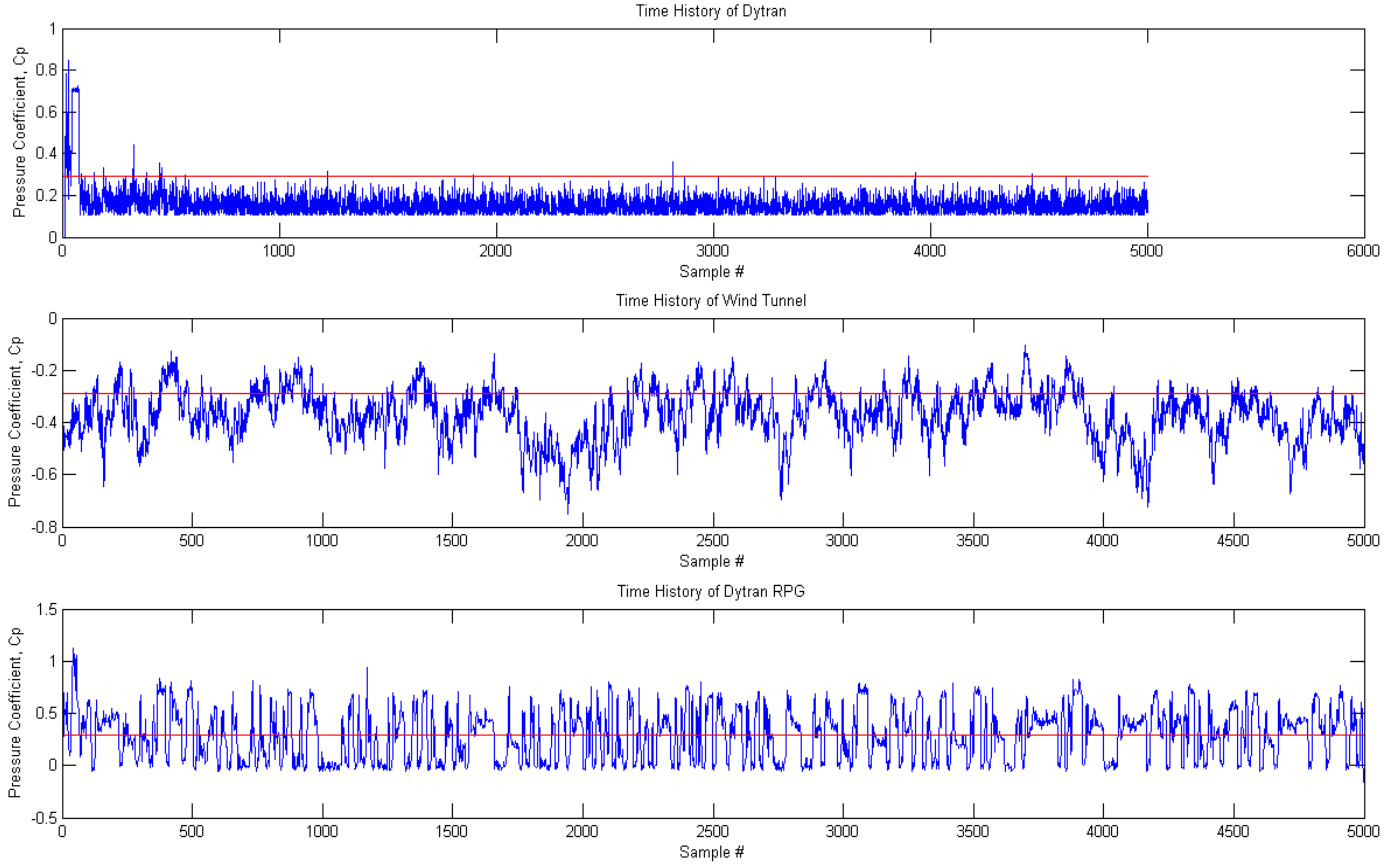

Figure 85: Leeward Wall Pressure Coefficient Comparison

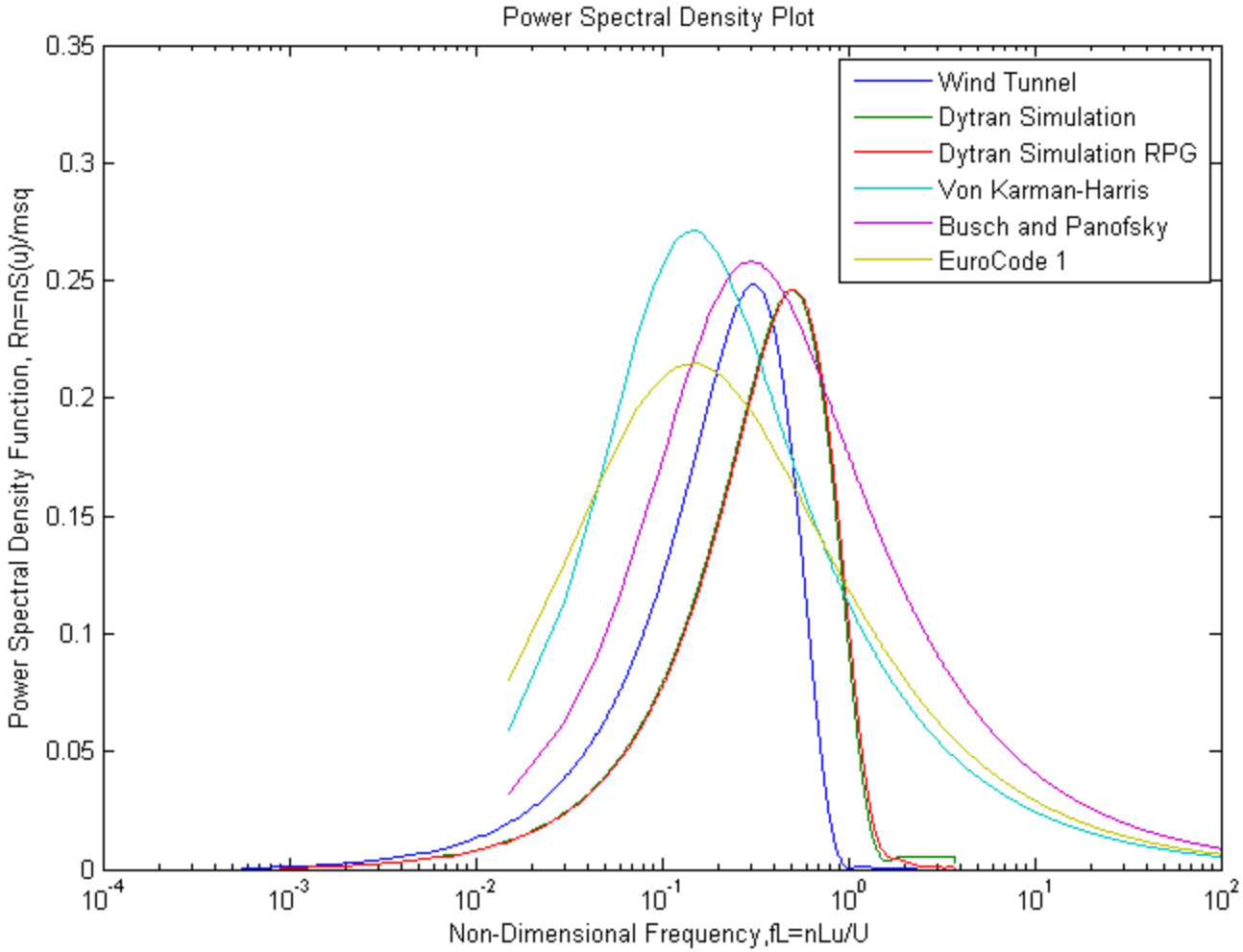

Figure 86: Leeward Wall PSD Comparison

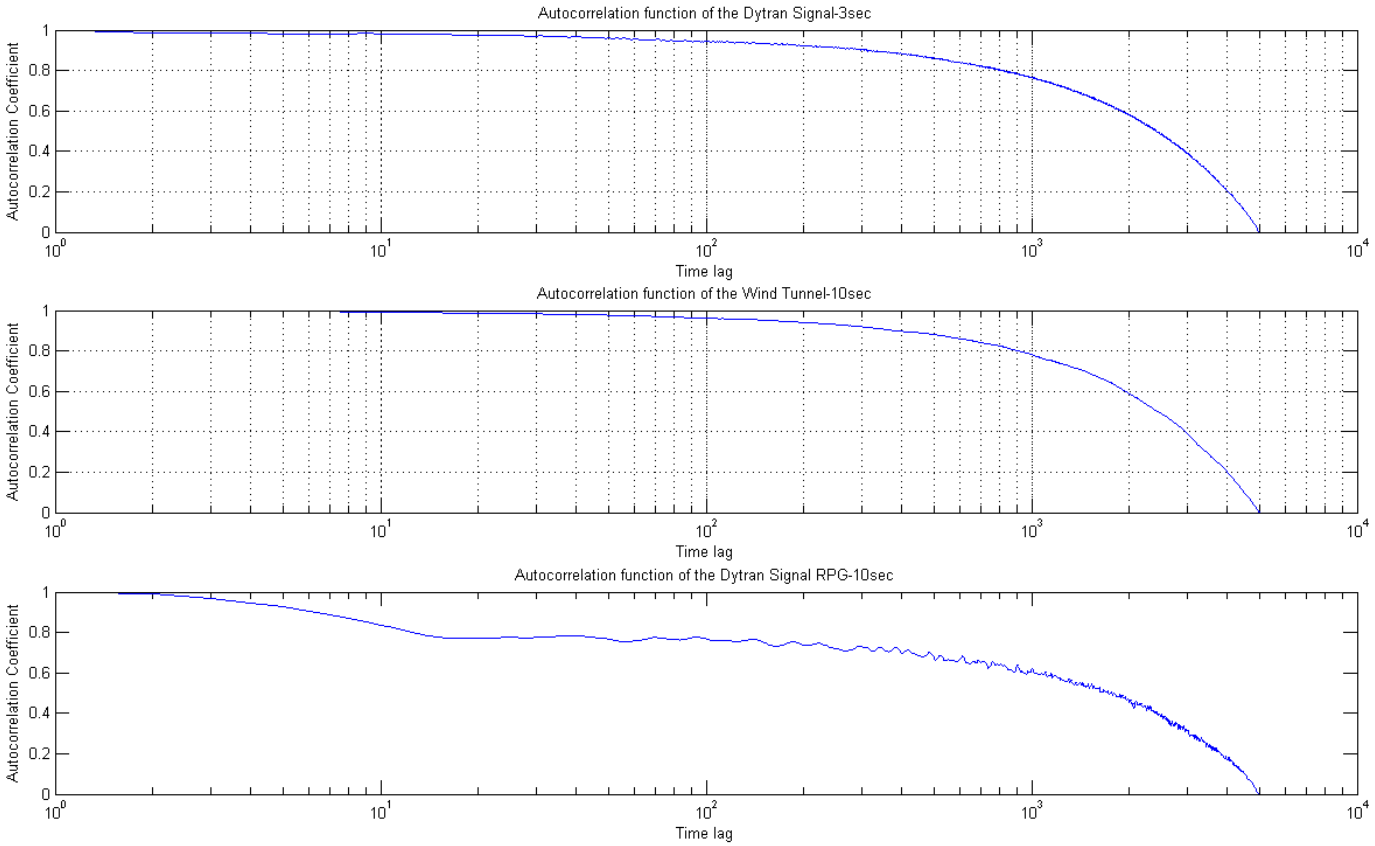

Figure 87: Leeward Wall Autocorrelation Comparison

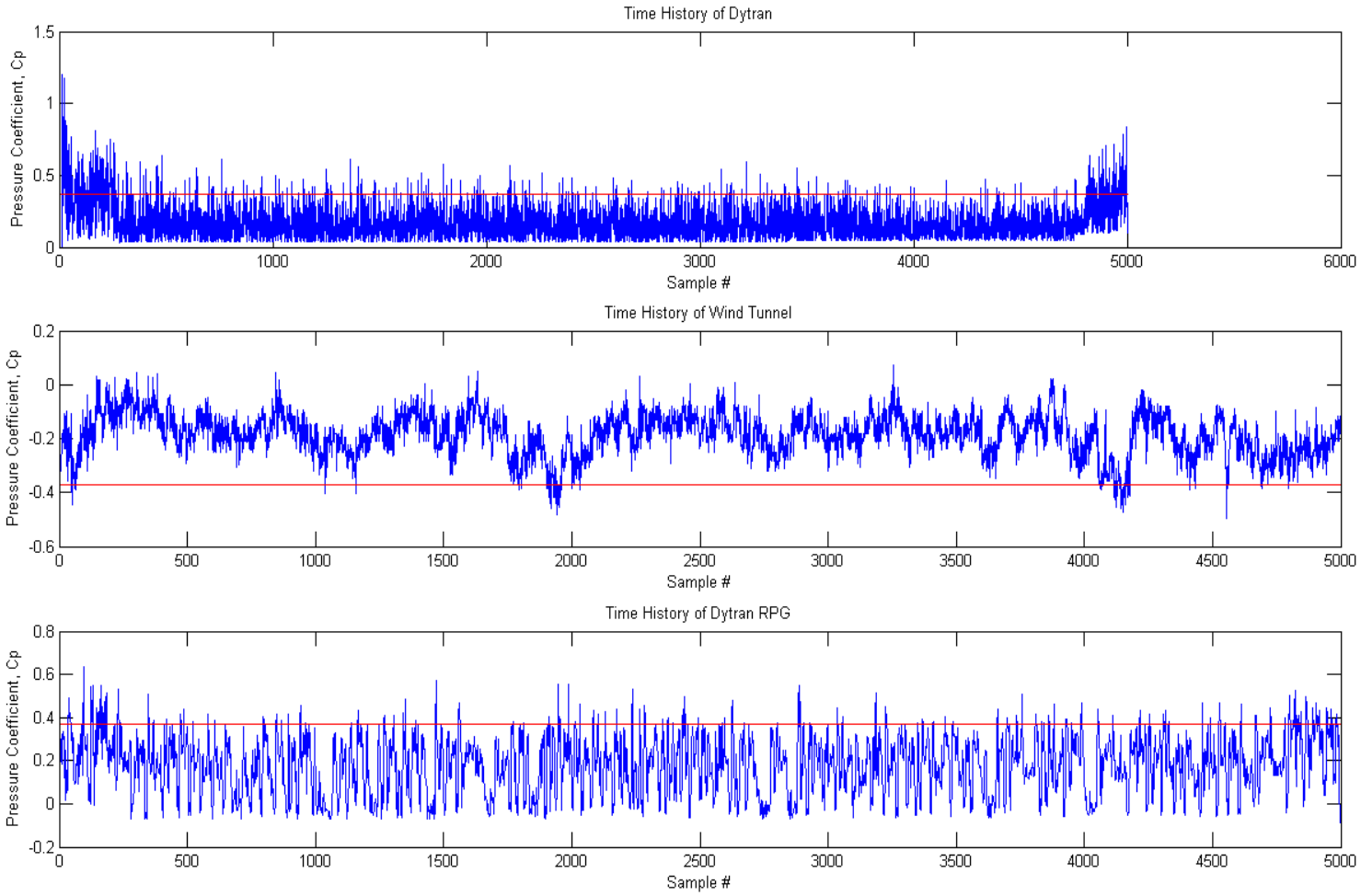

Figure 88: Leeward Roof Pressure Coefficient Comparison

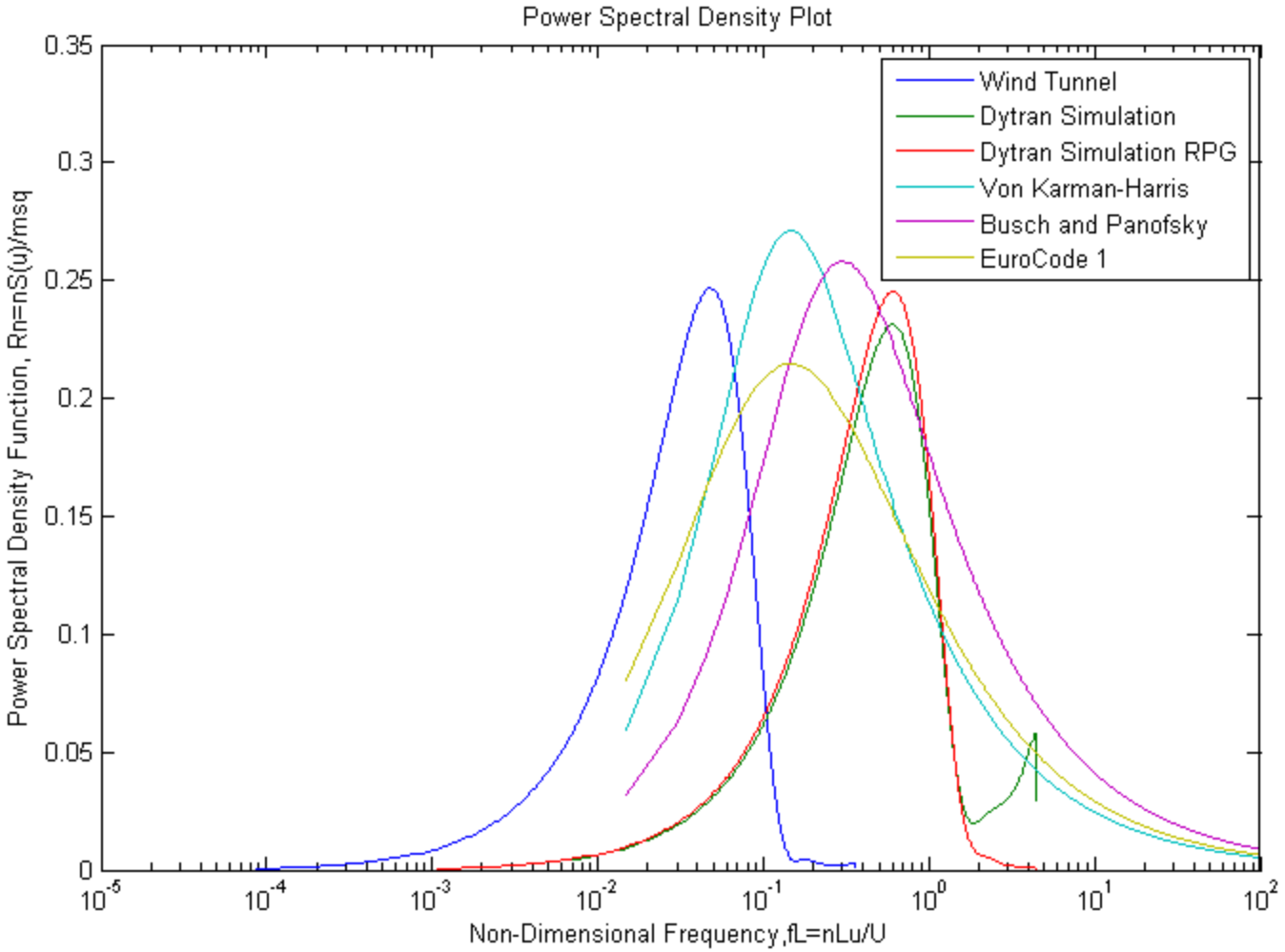

Figure 89: Leeward Roof PSD Comparison

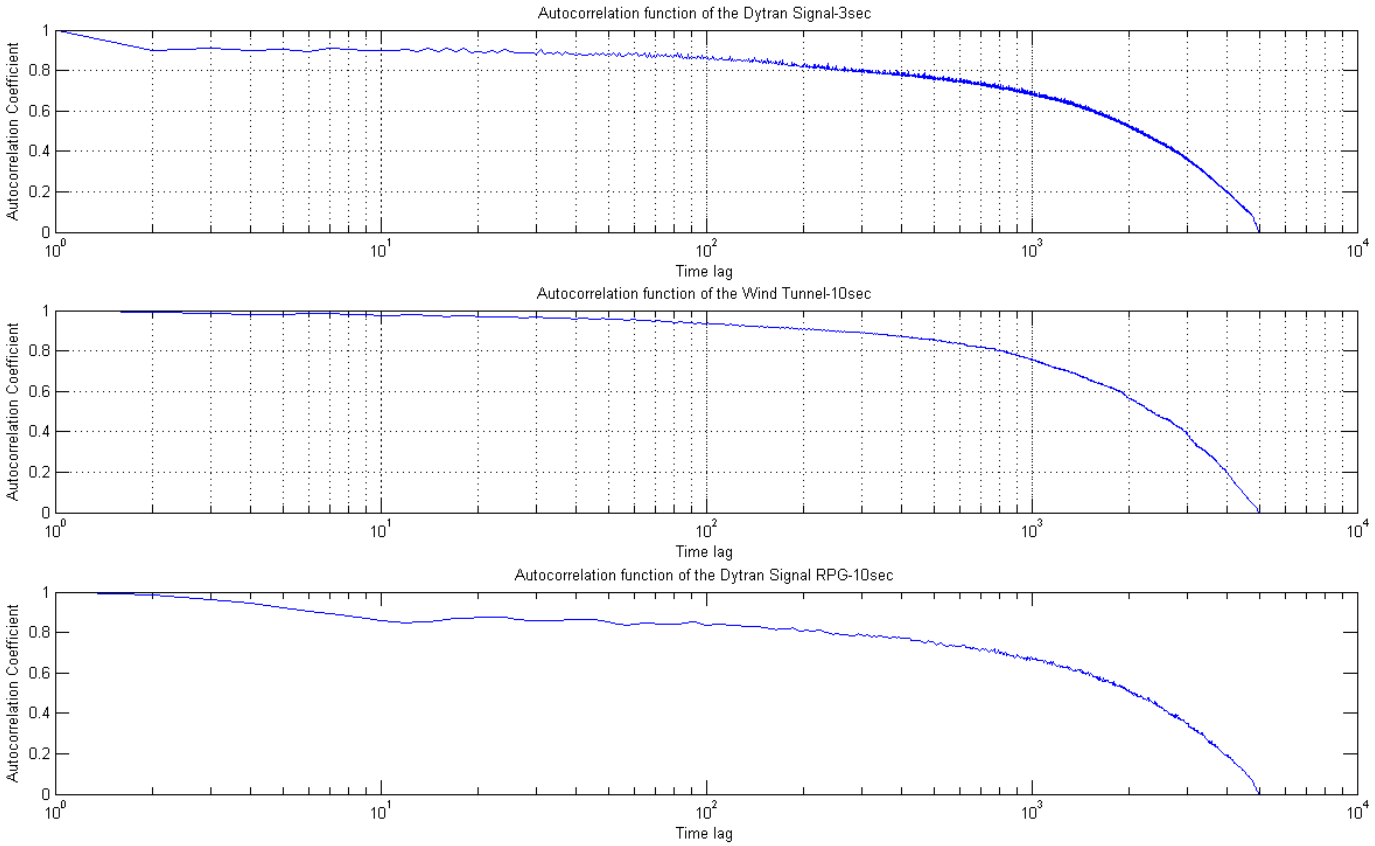

Figure 90: Leeward Roof Autocorrelation Comparison

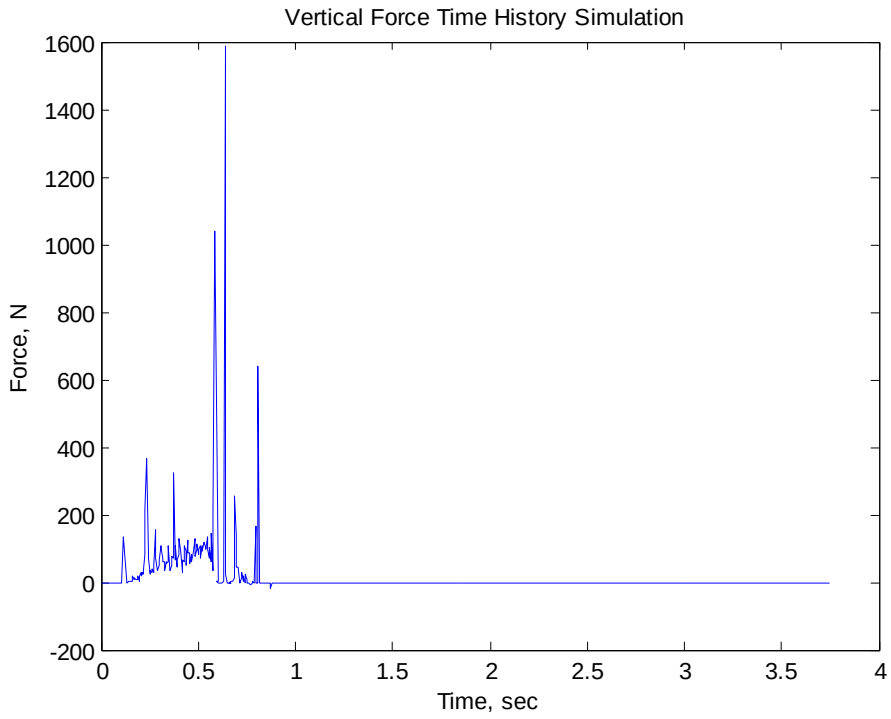

Figure 91: Test Number 47 Vertical Time History Unfiltered

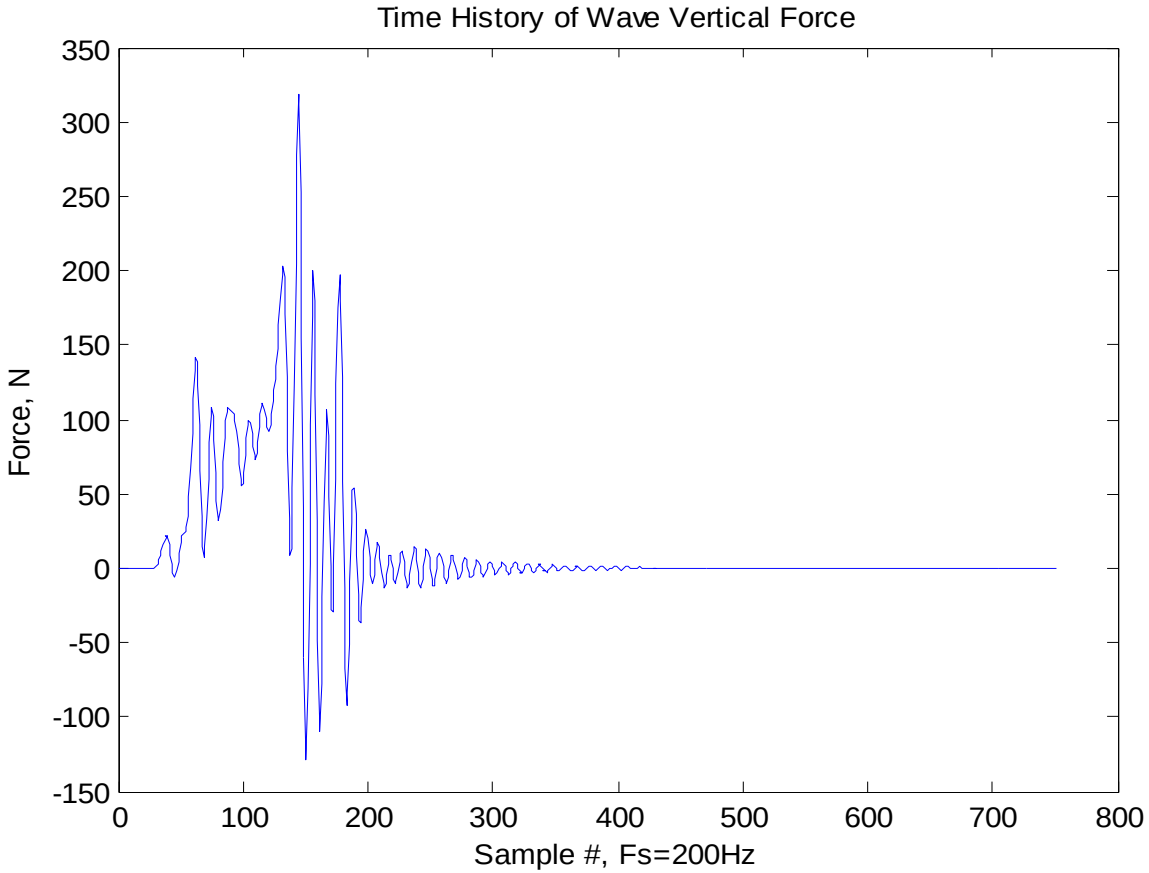

Figure 92: Test Number 47 Filtered

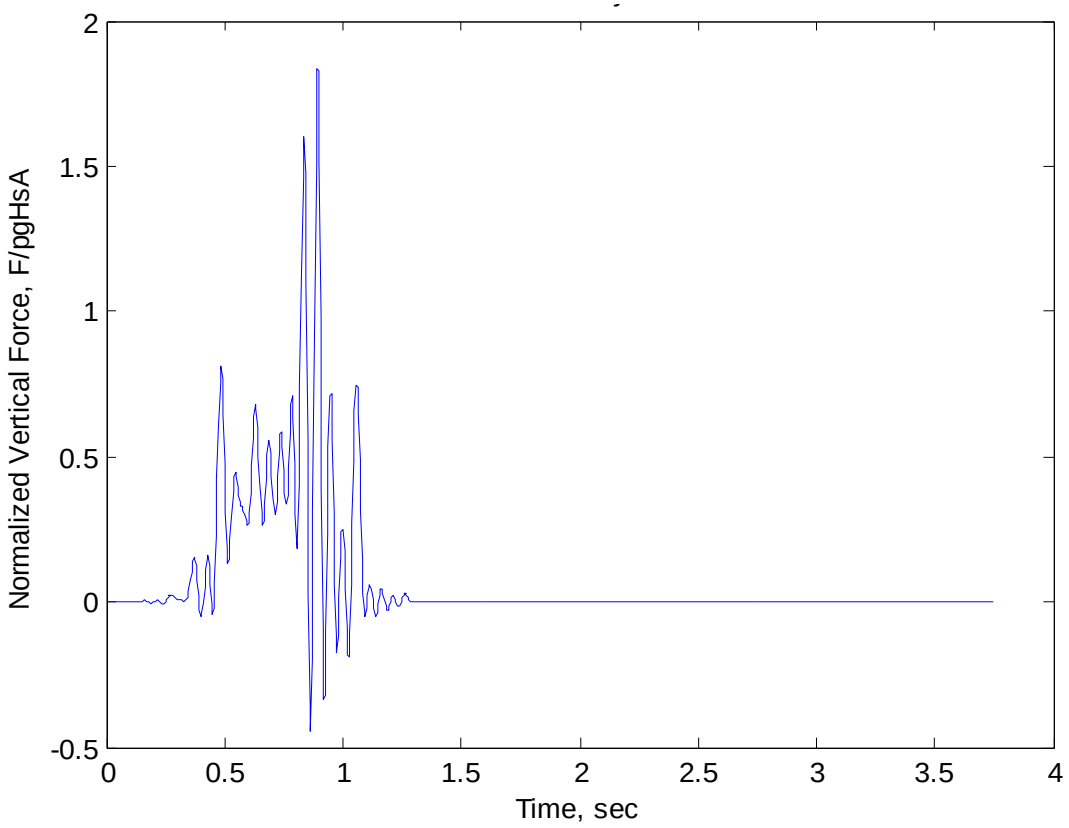

Figure 93: Vertical Time History From Test Number 47 Normalized

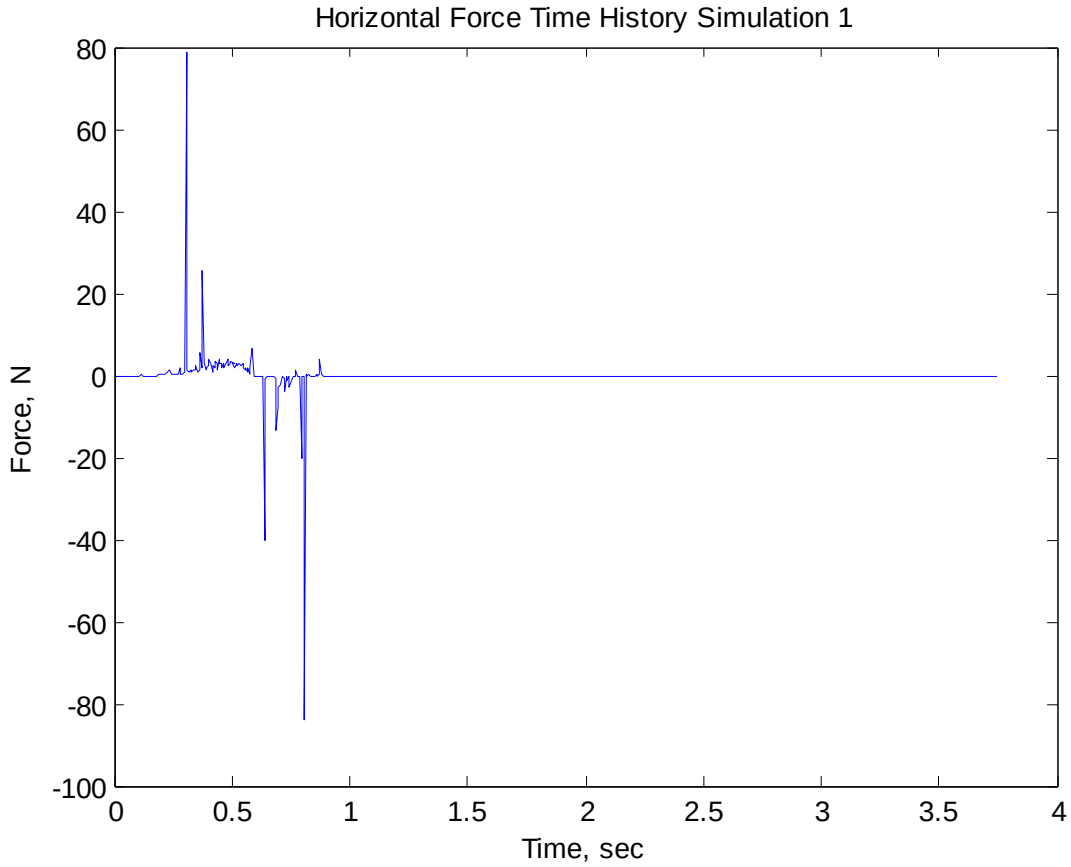

Figure 94: Test Number 47 Horizontal Time History Unfiltered

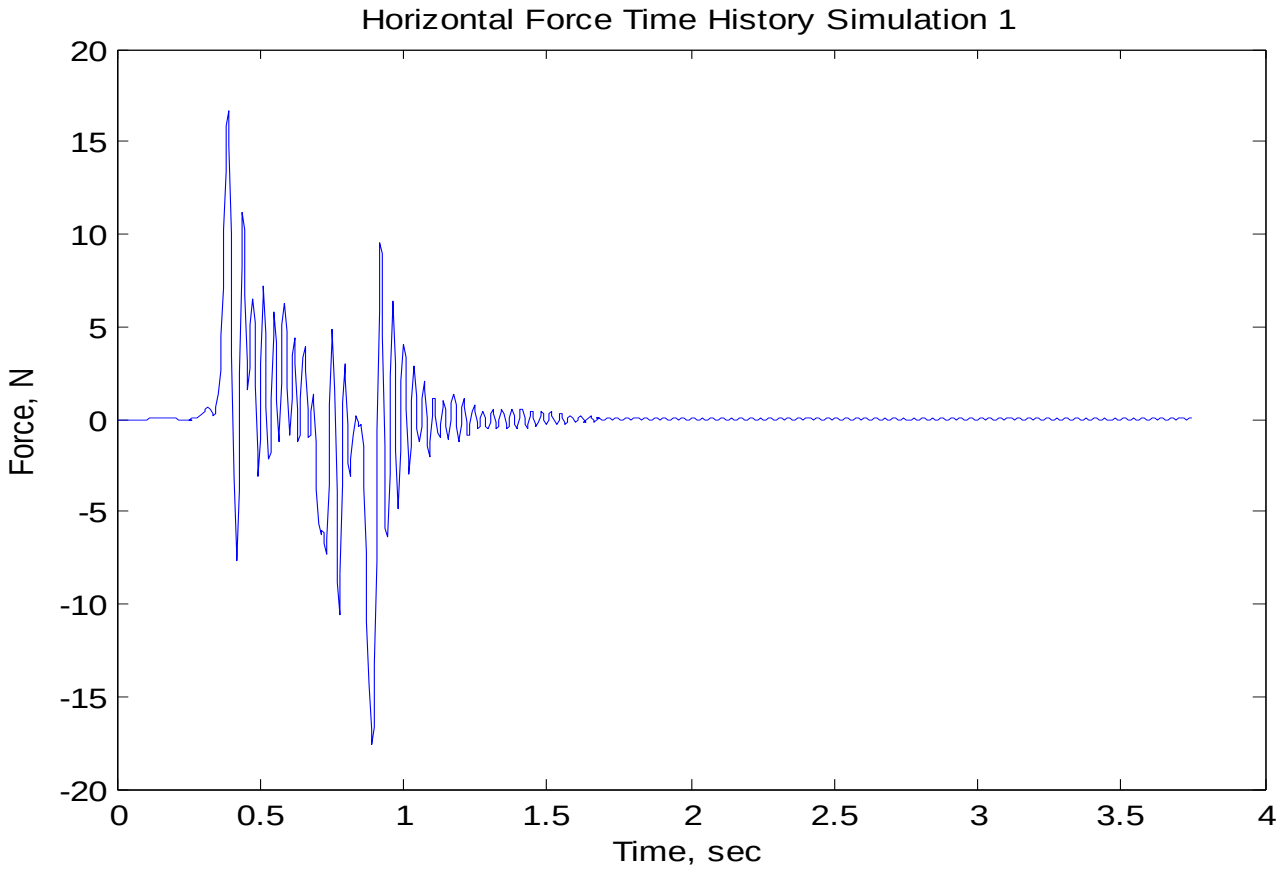

Figure 95: Test Number 47 Filtered

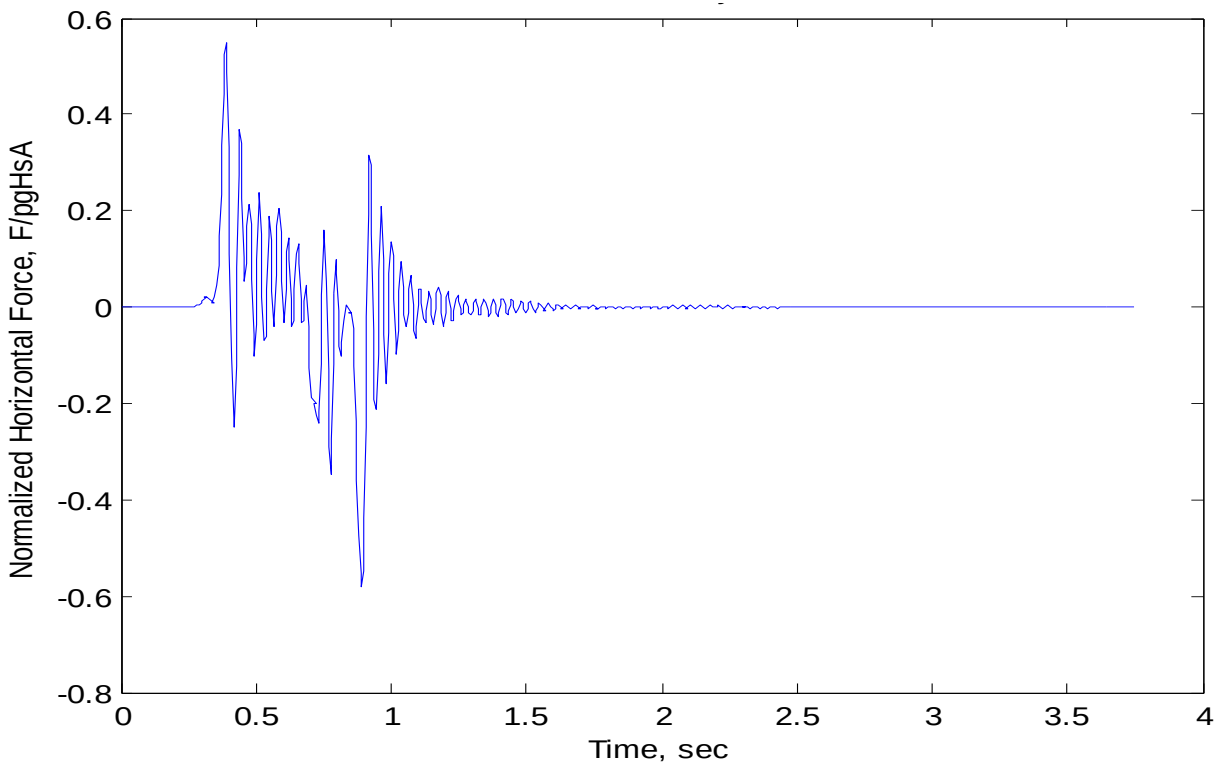

Figure 96: Horizontal Time History From Test Number 47 Normalized

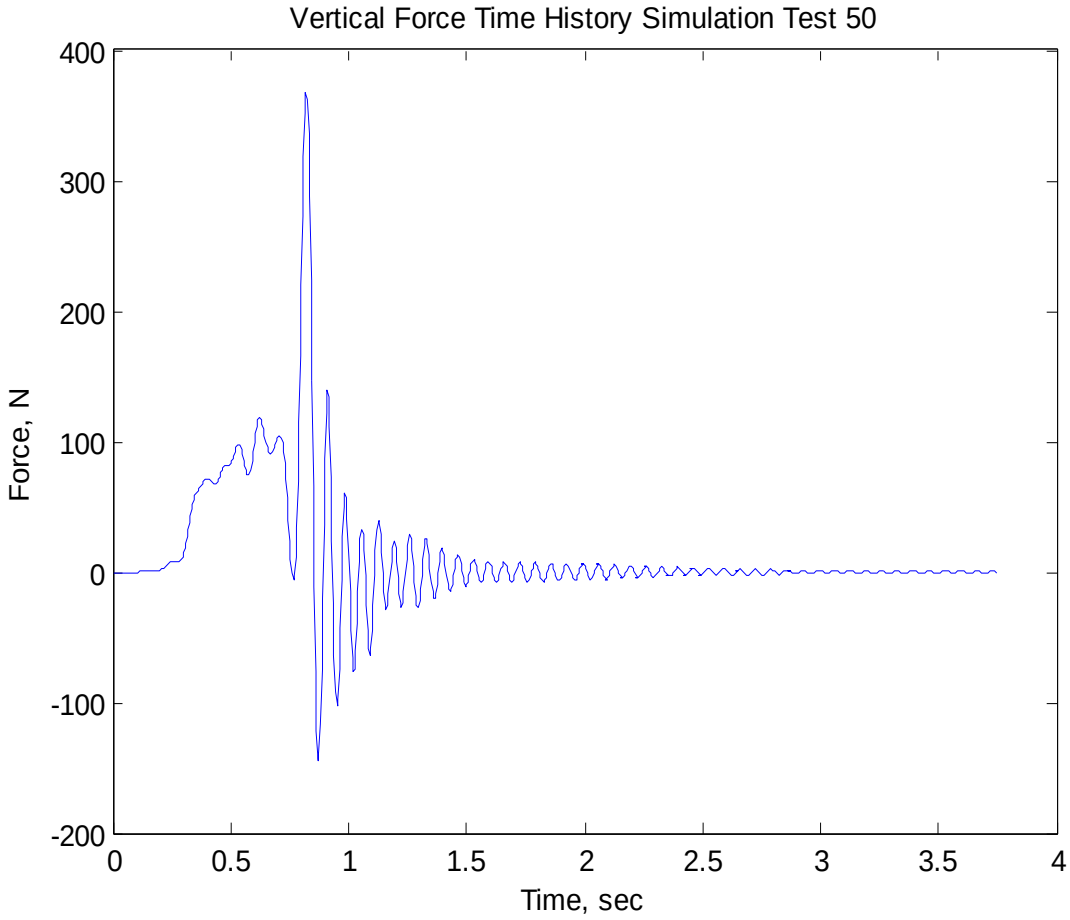

Figure 97: Vertical Force Time History Test Number 50 Filtered

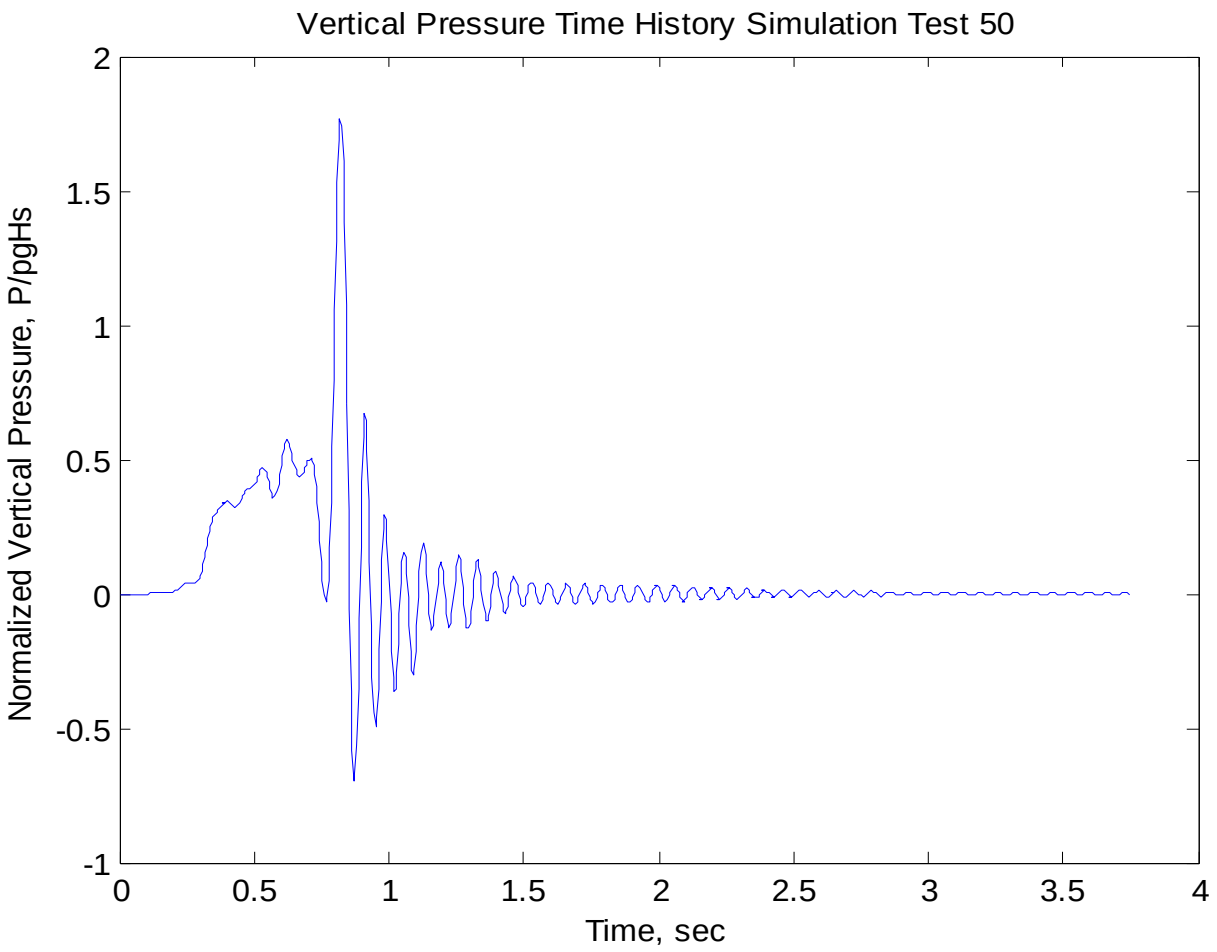

Figure 98: Normalized Vertical Force Time History

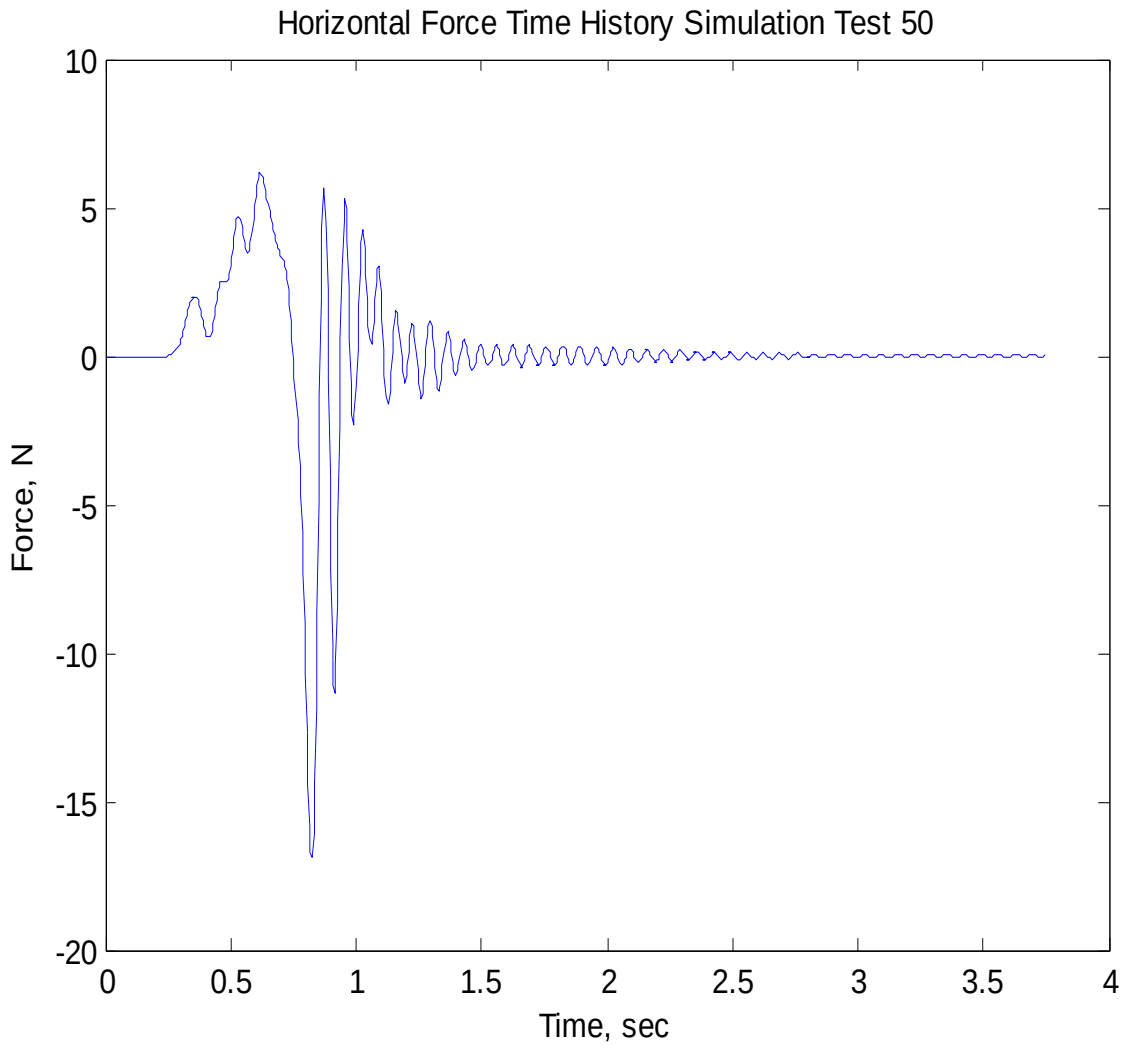

Figure 99: Horizontal Force Time History Test Number 50 Filtered

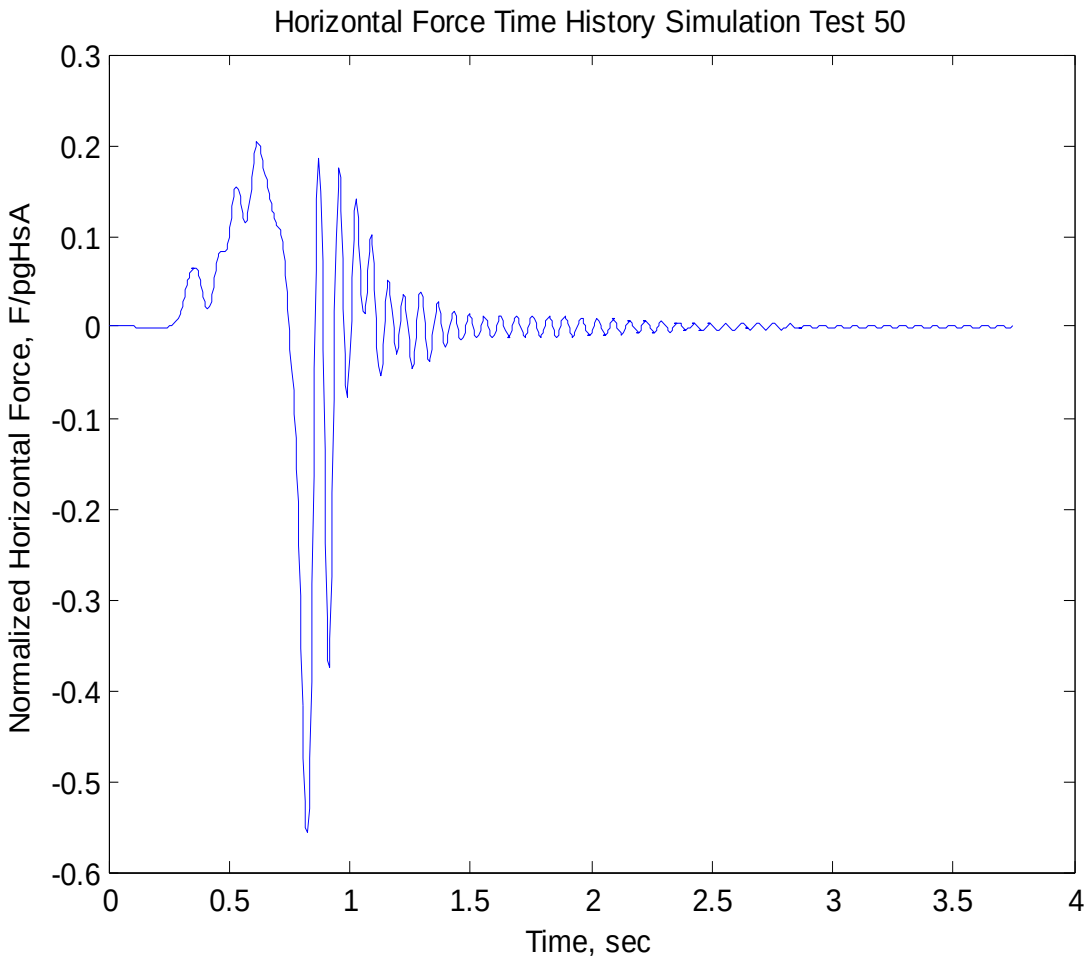

Figure 100: Normalized Horizontal Force Time History

Building Prototype Results

Wind Loads

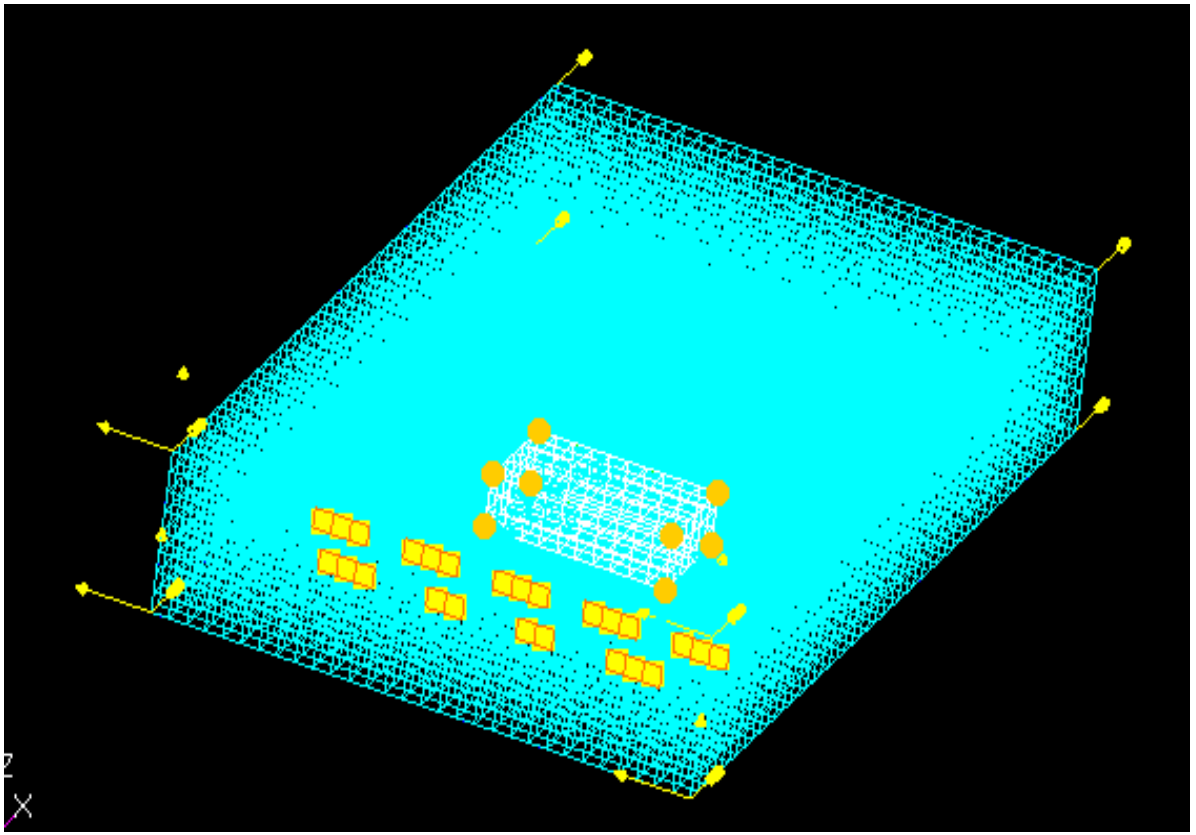

Figure 101: Building Model In CFD Wind Simulation

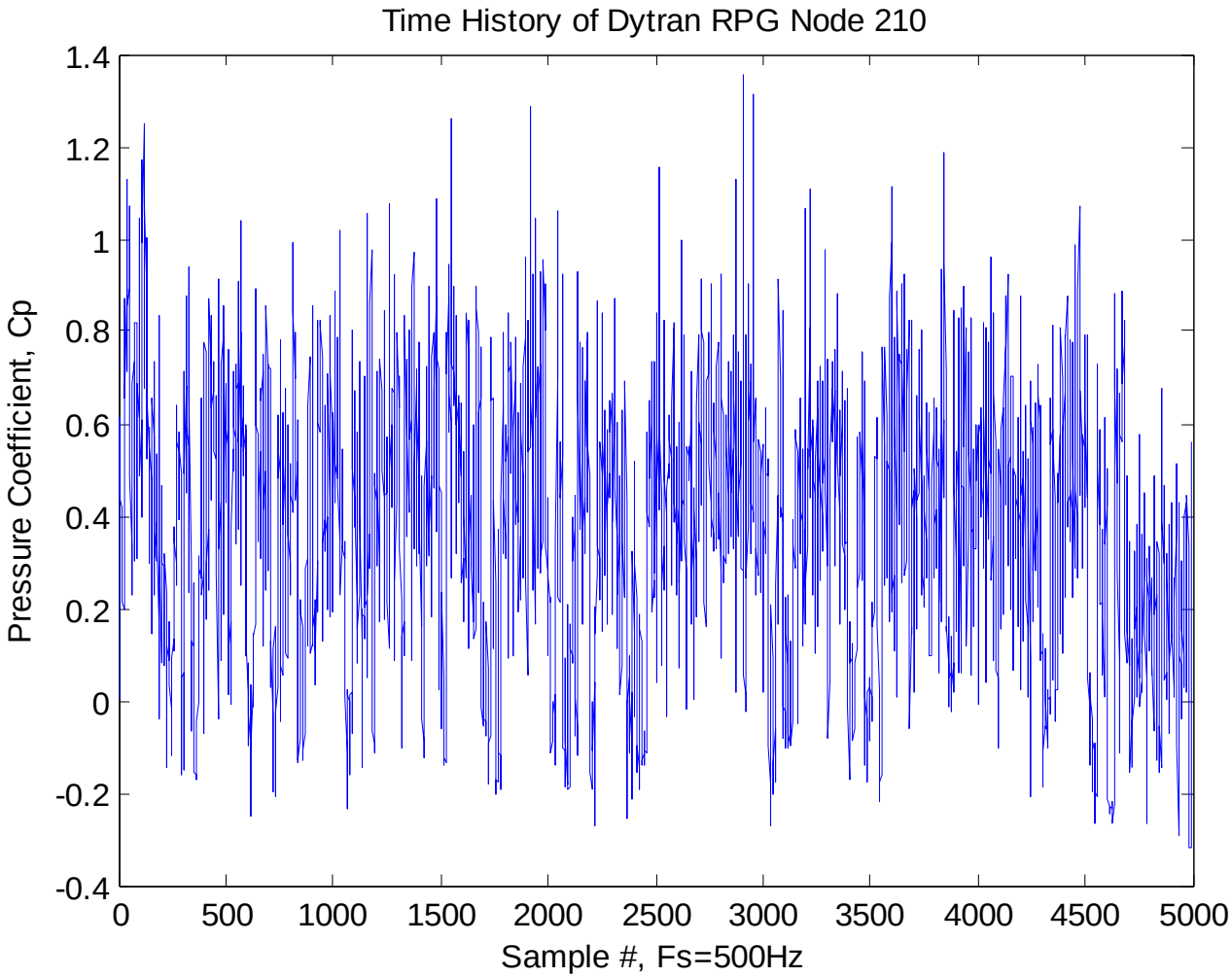

Figure 102: Third Floor Leeward Wall Nodal Time History

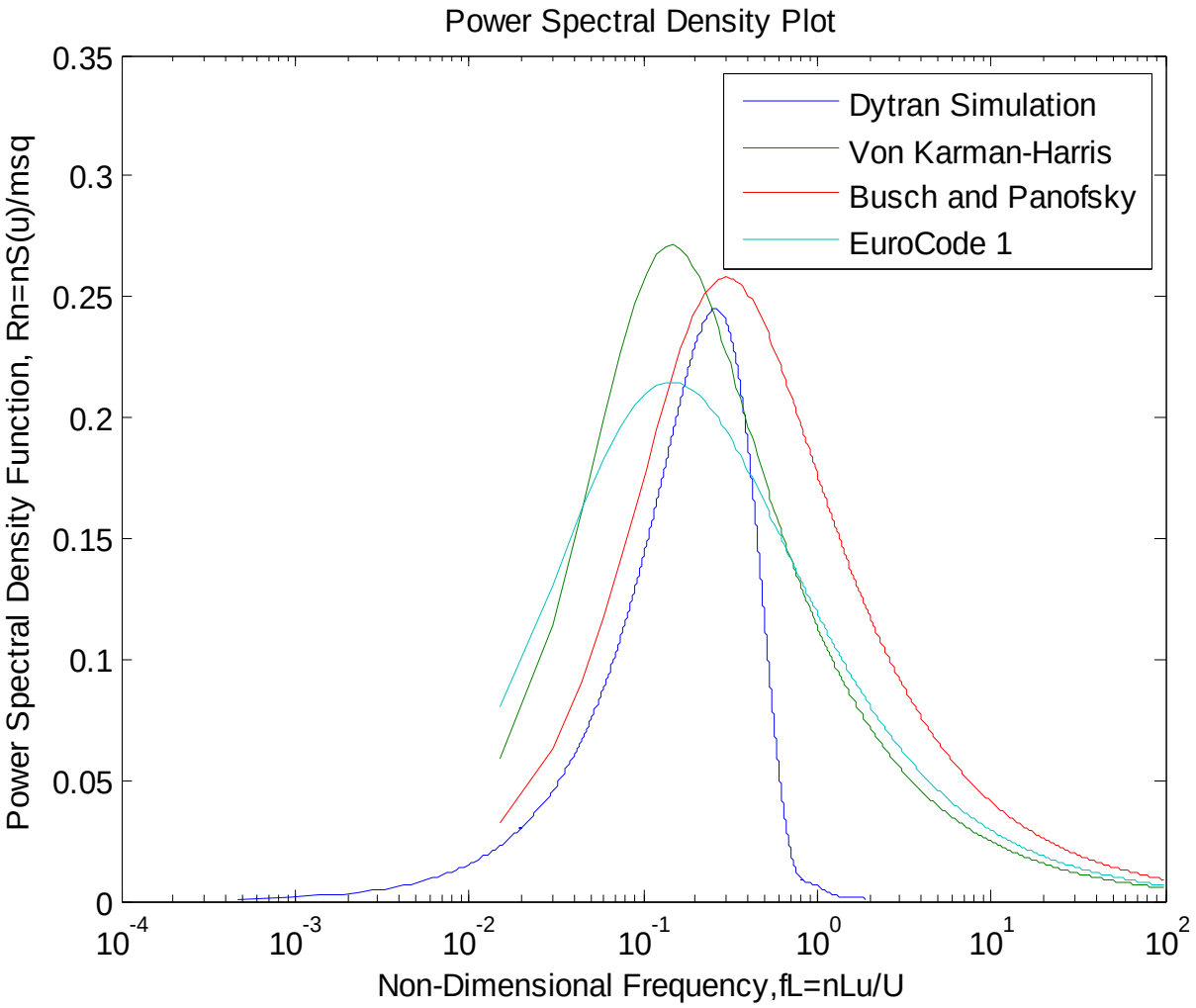

Figure 103: Third Floor Leeward Wall PSD

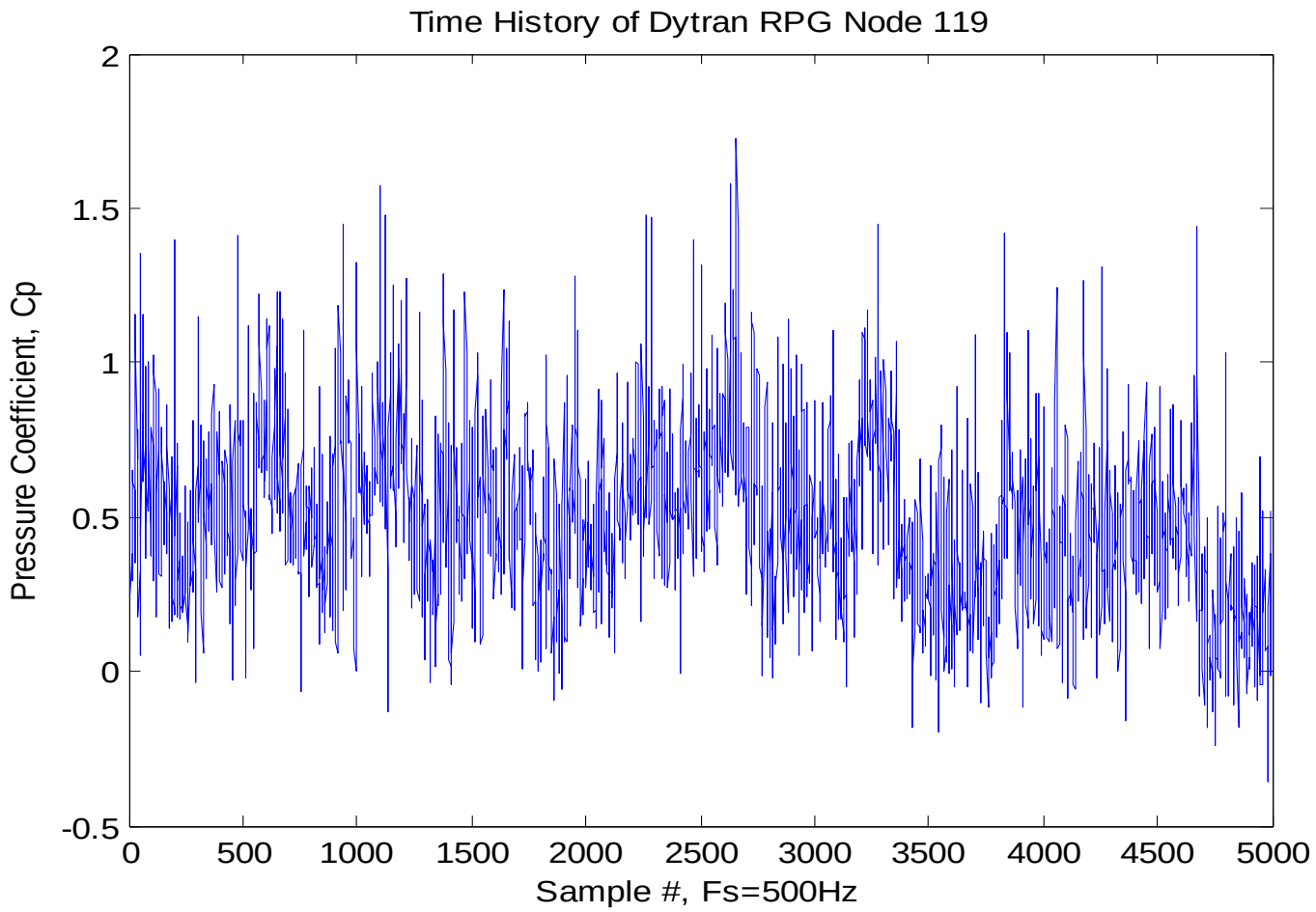

Figure 104: First Floor Windward Wall Nodal Time History

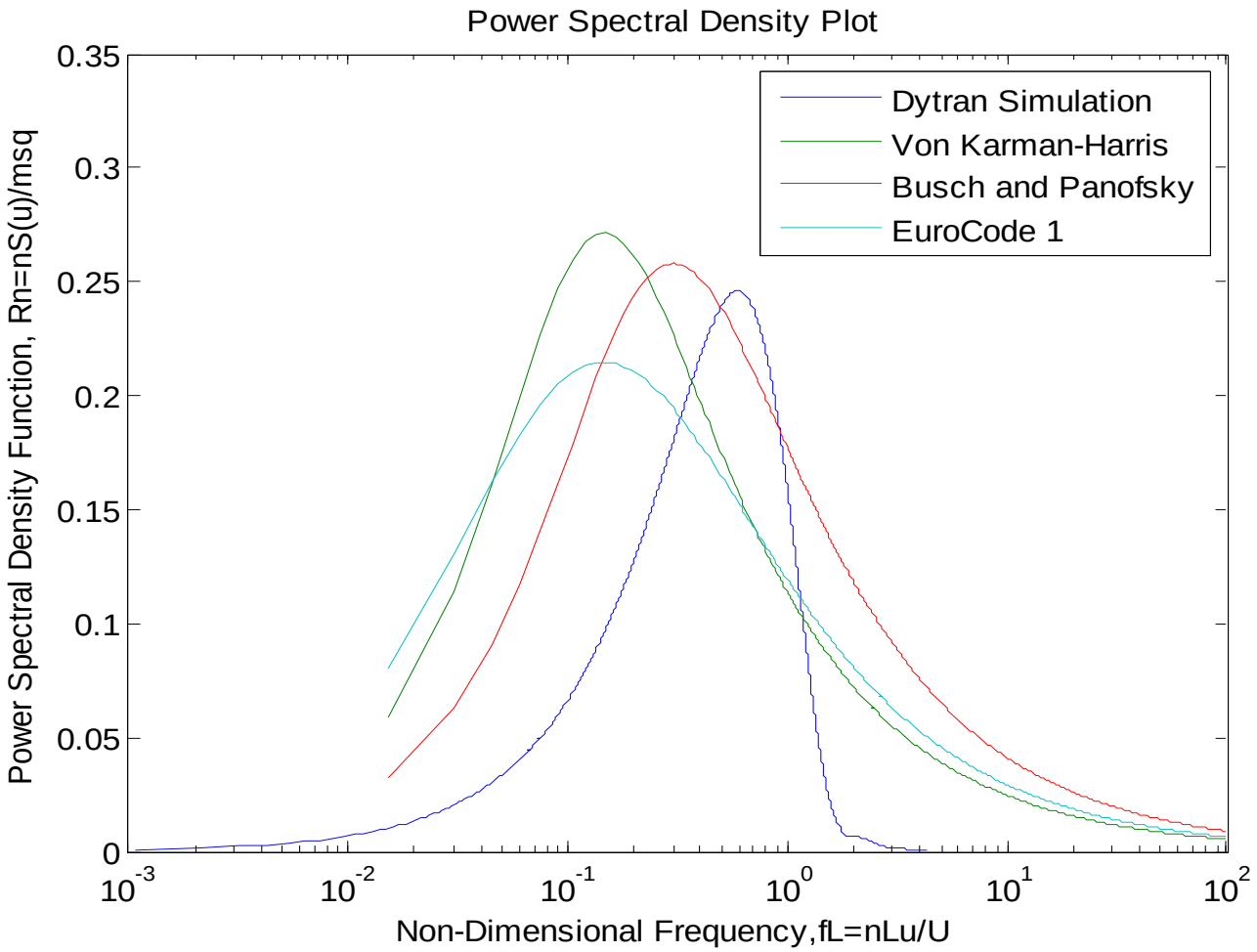

Figure 105: First Floor Windward Wall PSD

Wave Loads .

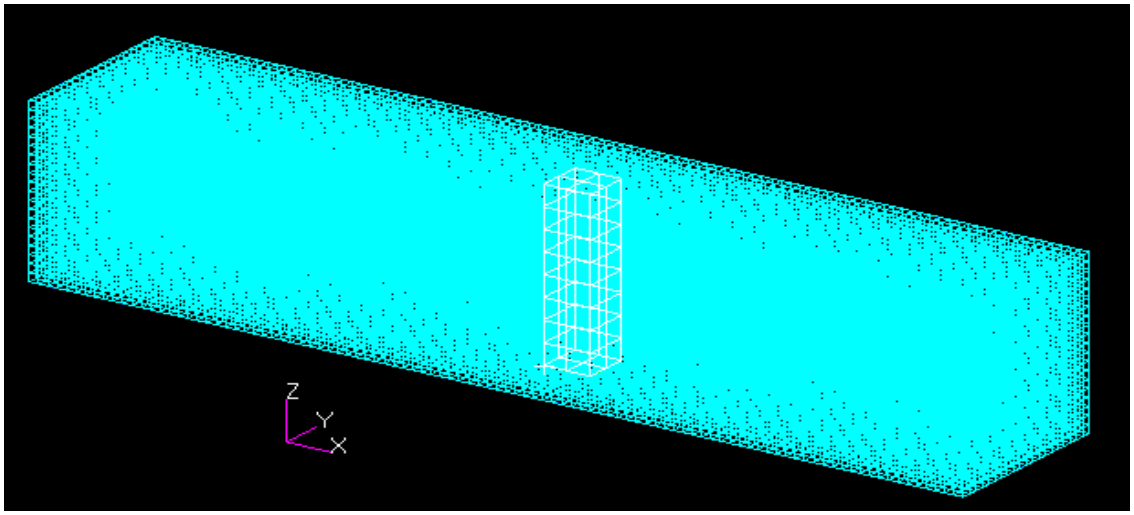

Figure 106: Column Model In CFD Wave Simulation

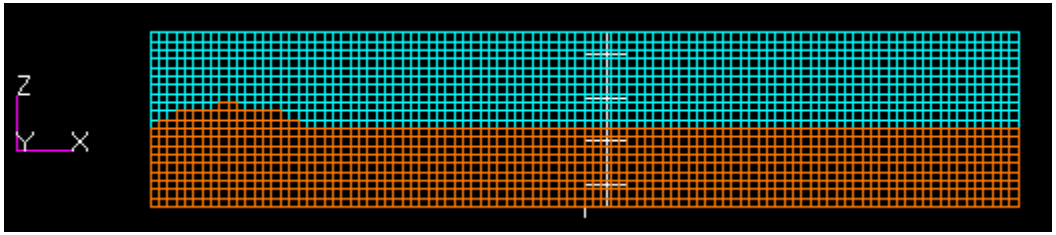

Figure 107: Input shape of Setup Wave for Column Wave Simulations.

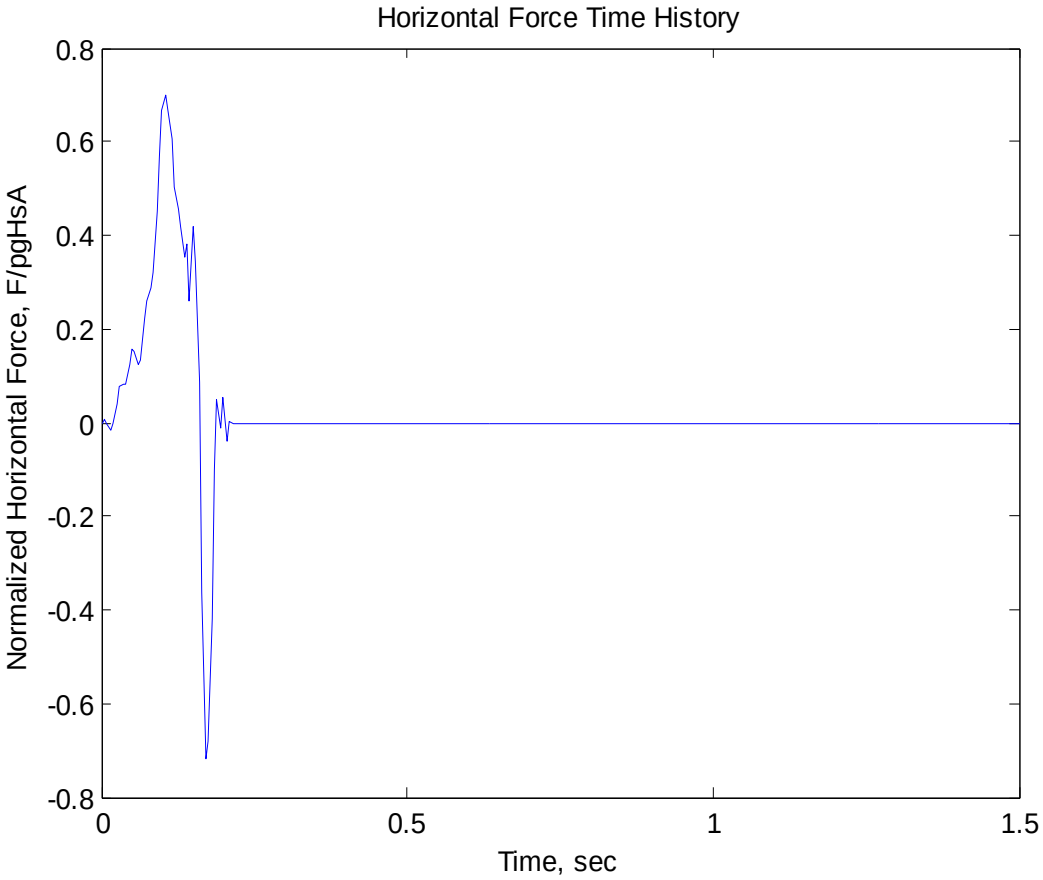

Figure 108: Normalized Horizontal Force from Column Simulations

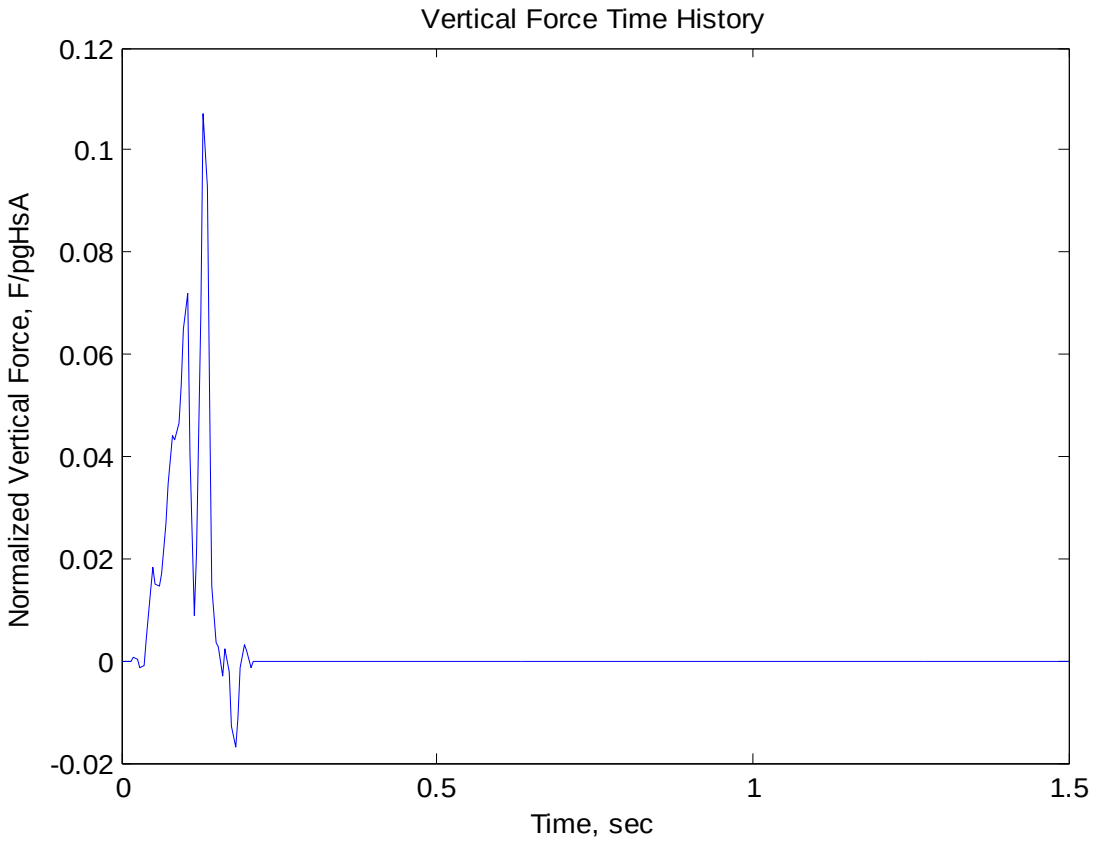

Figure 109: Normalized Vertical Force from Column Simulations

Bridge Prototype Results

Wind Loads

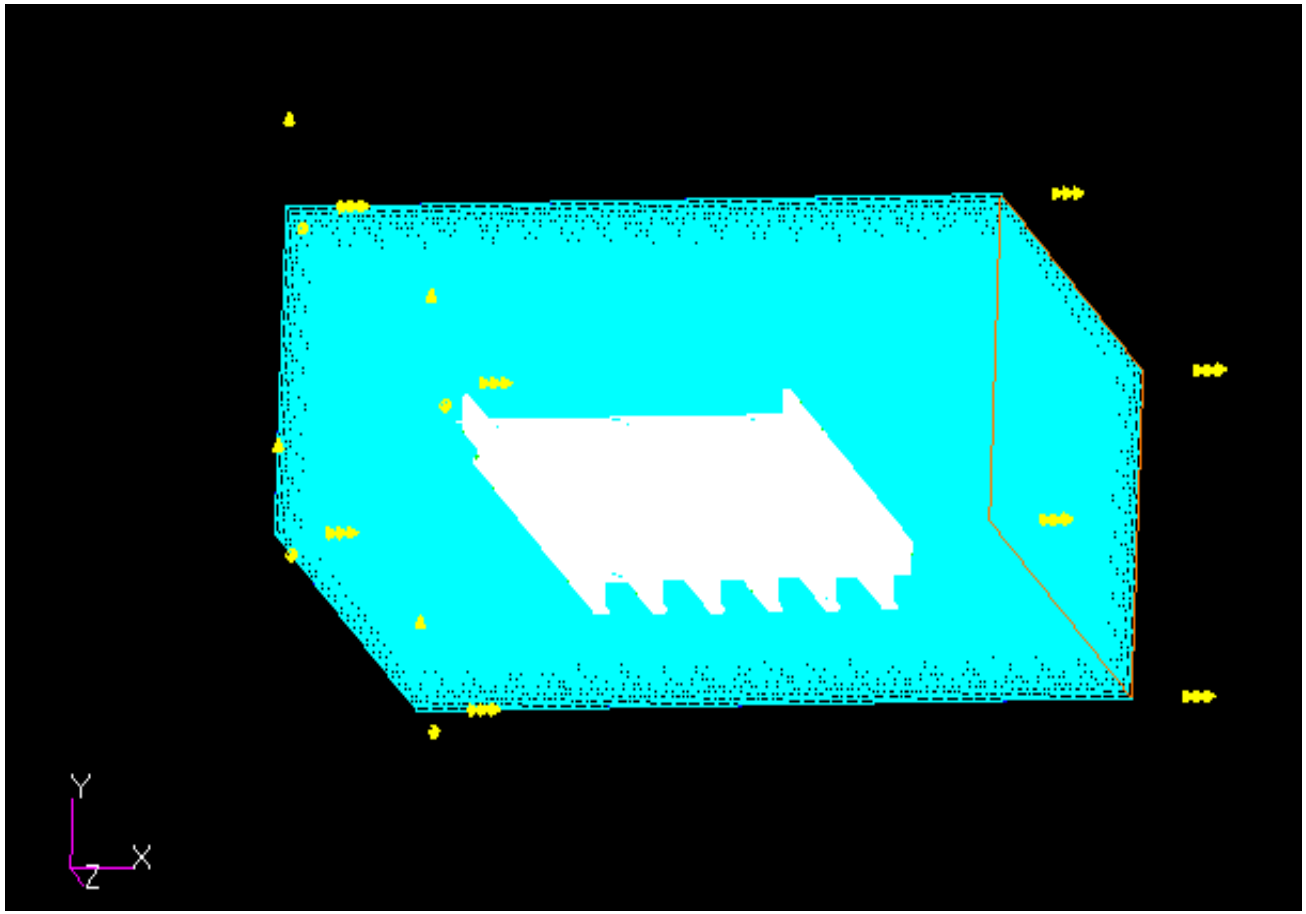

Figure 110: Model of Bridge in Wind Tunnel Simulation

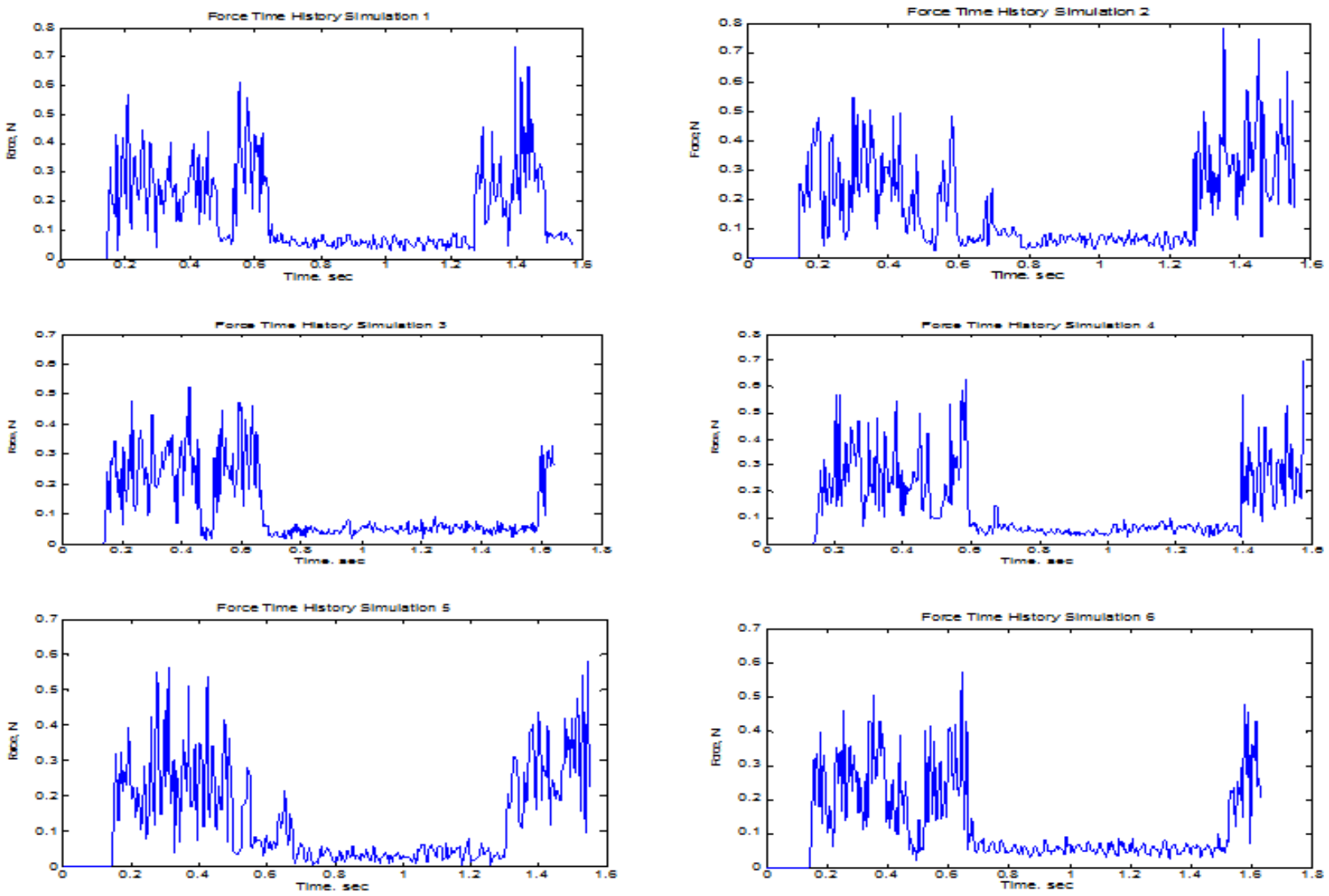

Figure 111: Windward Barrier Force/Pressure Records

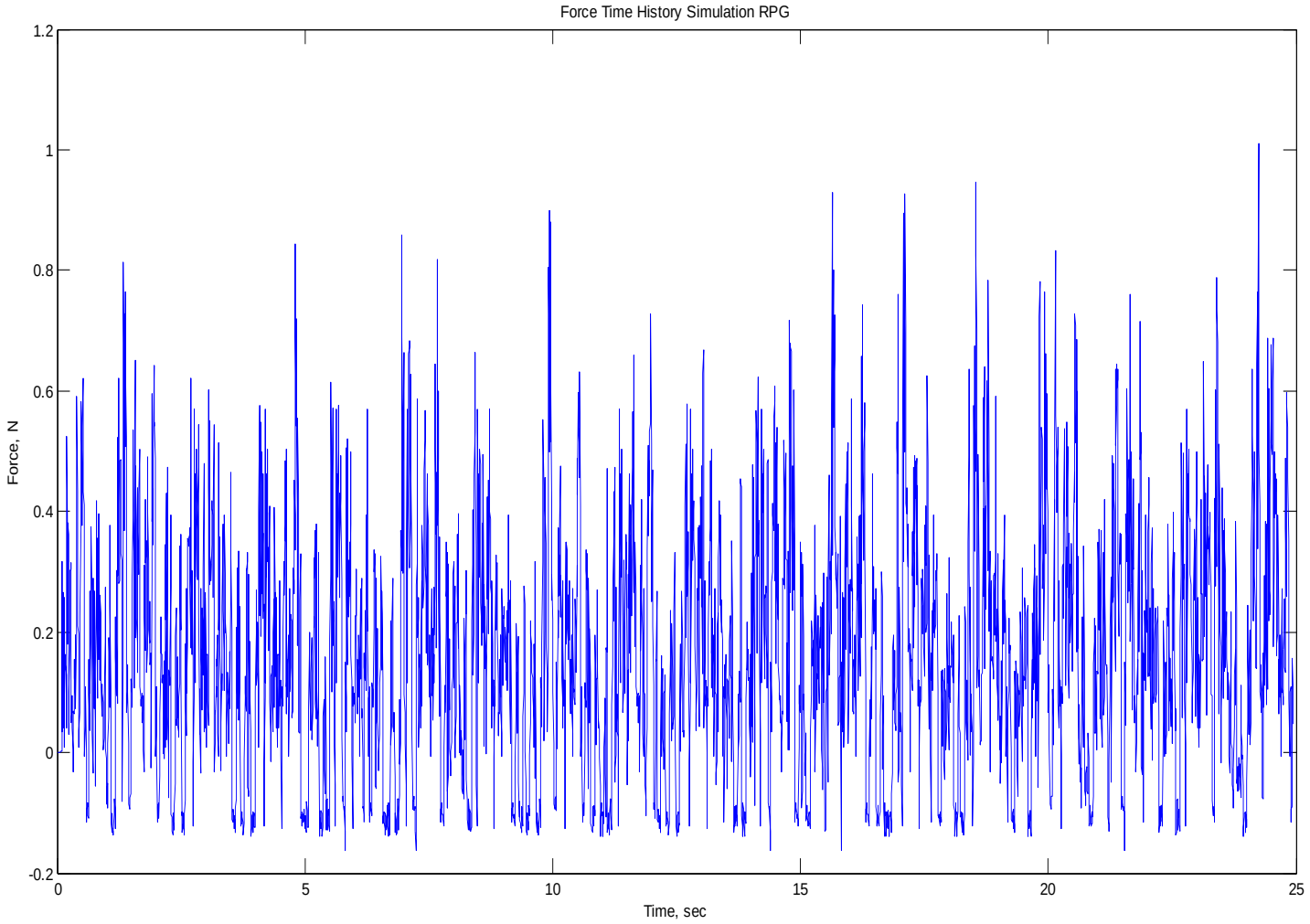

Figure 112: Windward Barrier Force/Pressure RPG Record

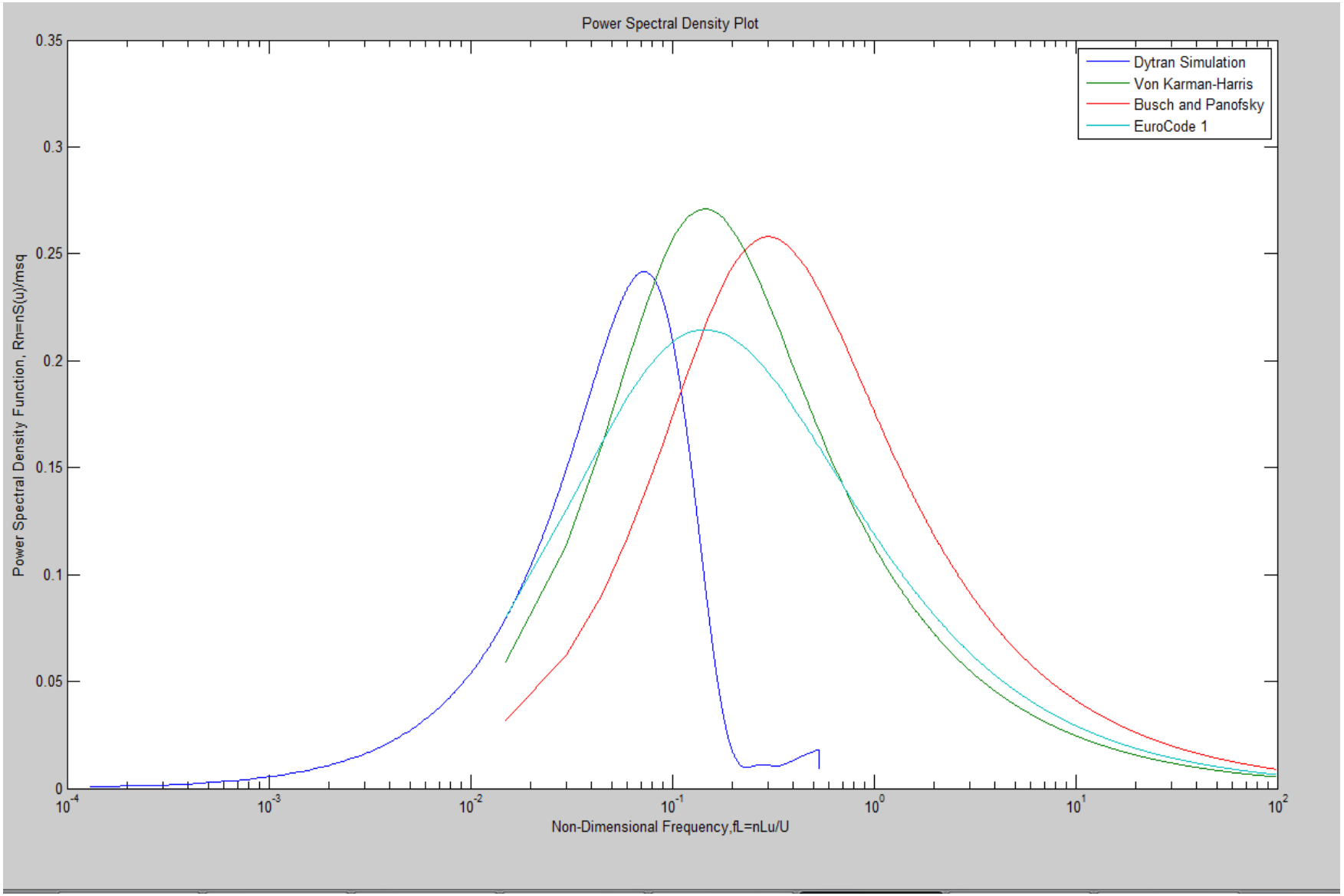

Figure 113: Windward Barrier Force/Pressure RPG Record PSD Comparison

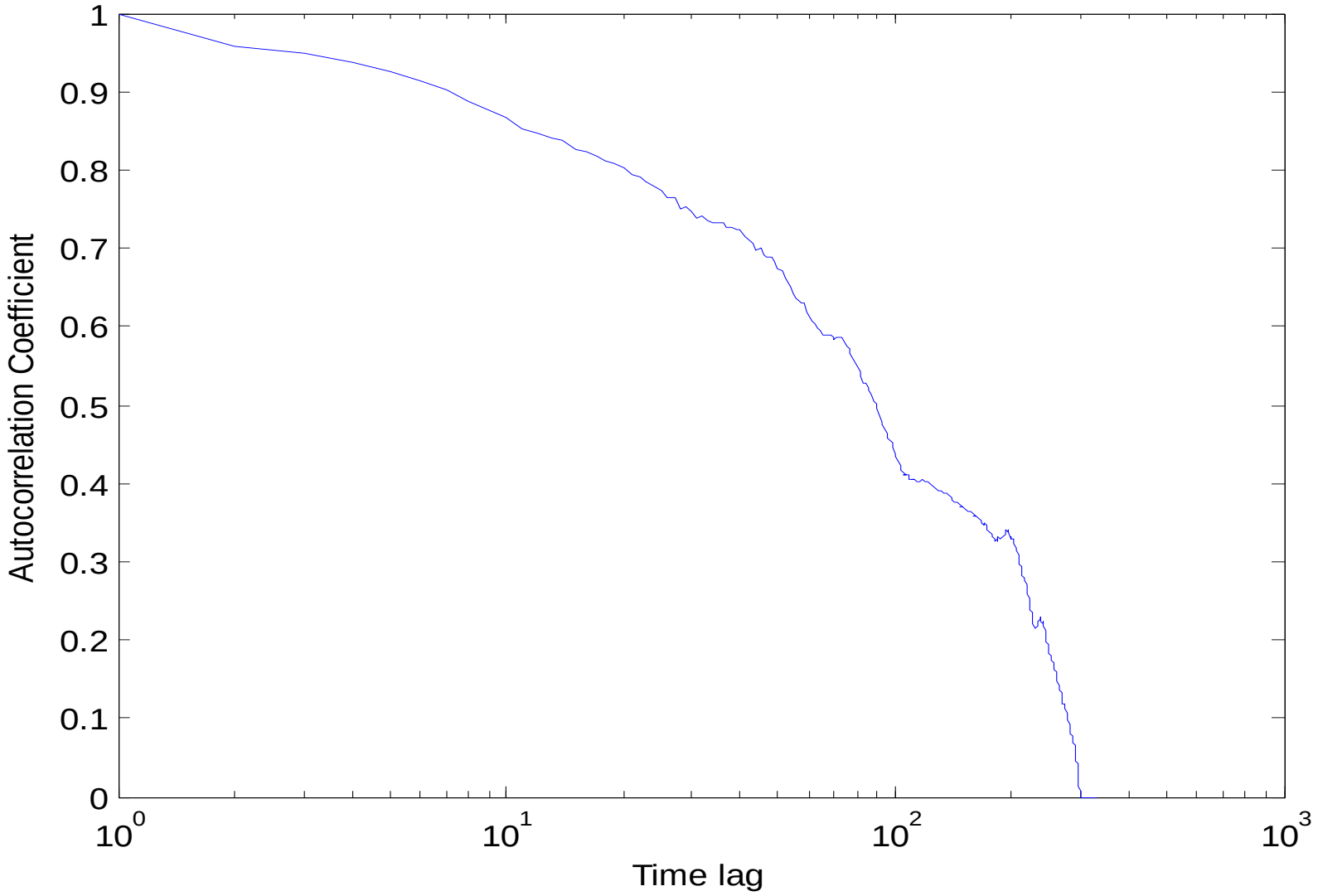

Figure 114: Windward Barrier Force/Pressure RPG Record Autocorrelation Coefficient

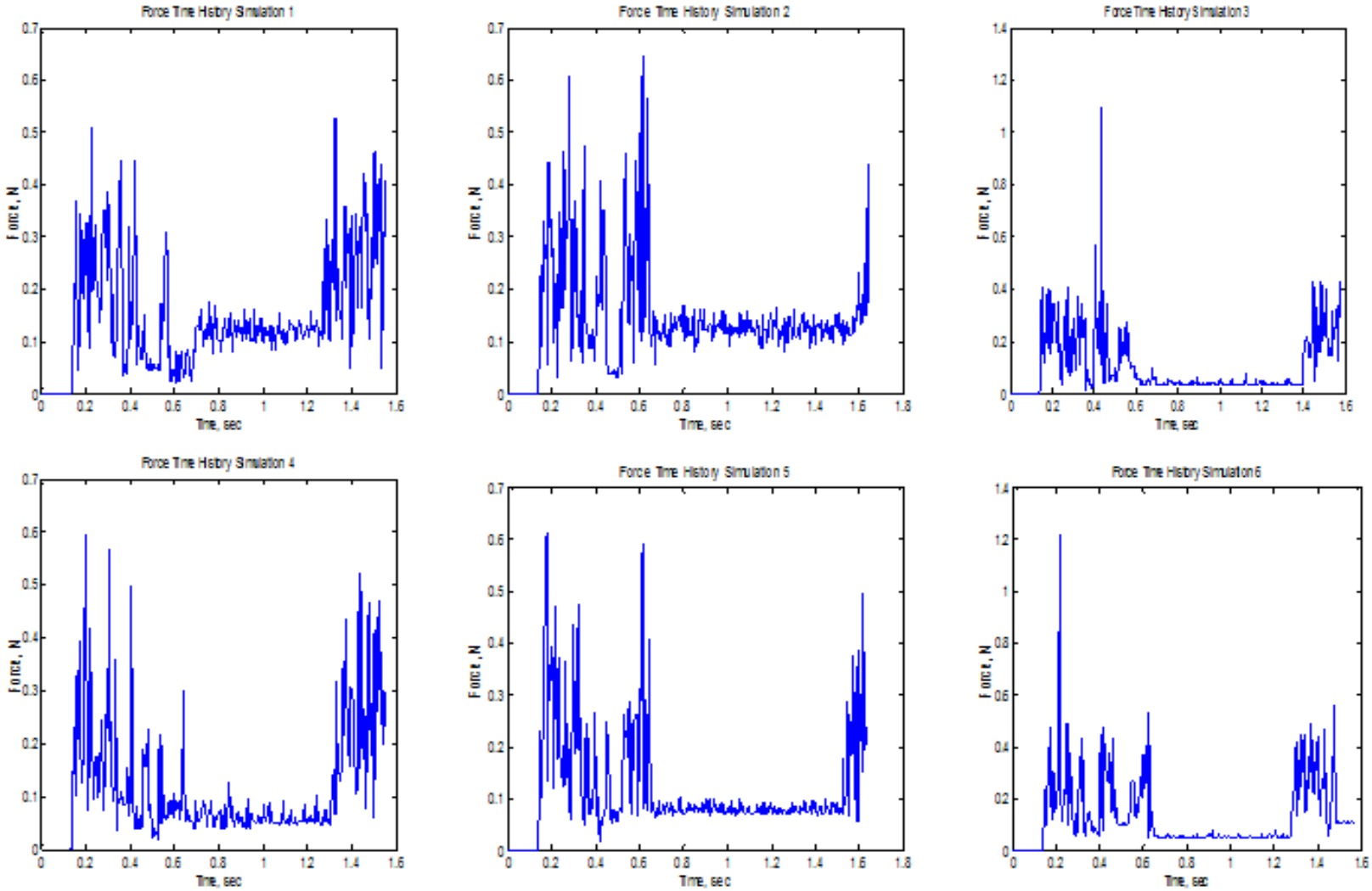

Figure 115: Top Deck Force/Pressure Records

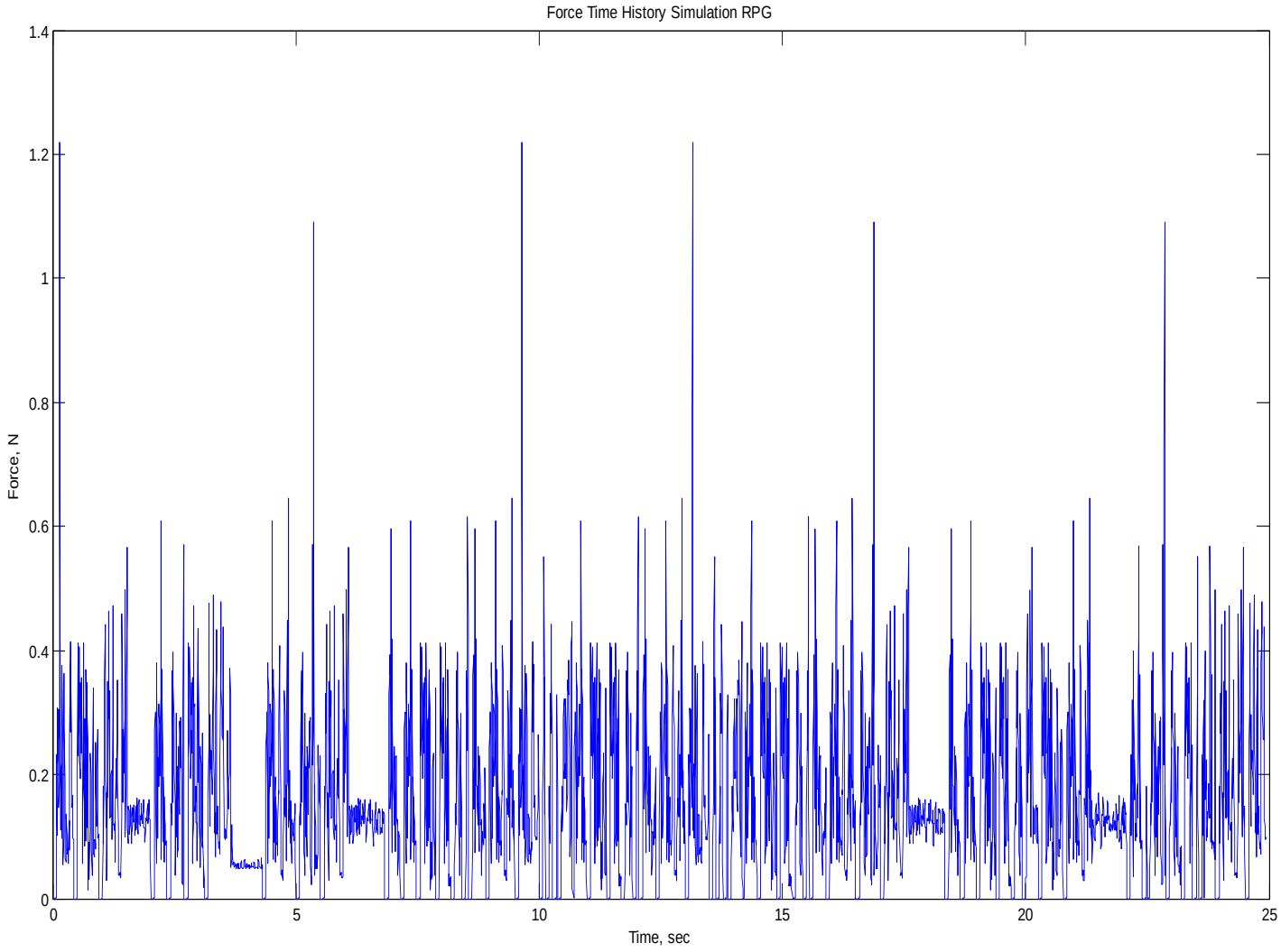

Figure 116: Top Deck Force/Pressure RPG Record

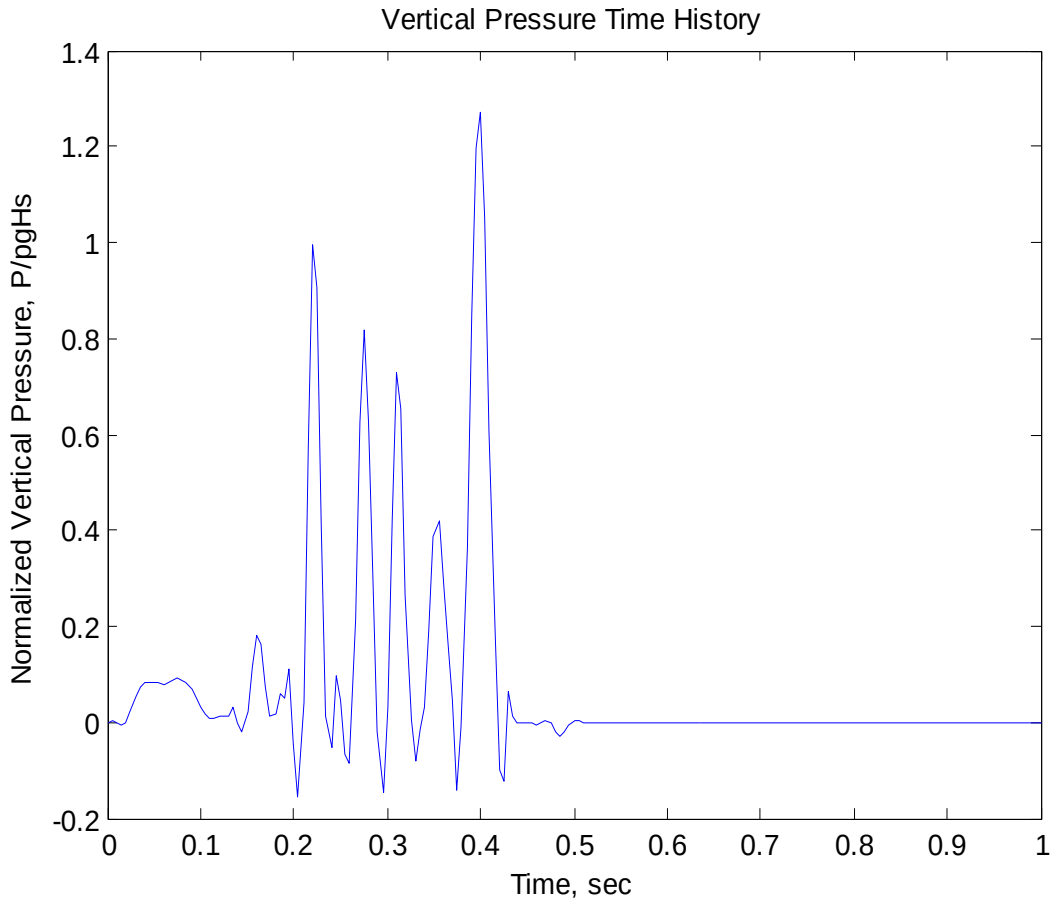

Figure 117: Vertical Wave Time History of Bridge

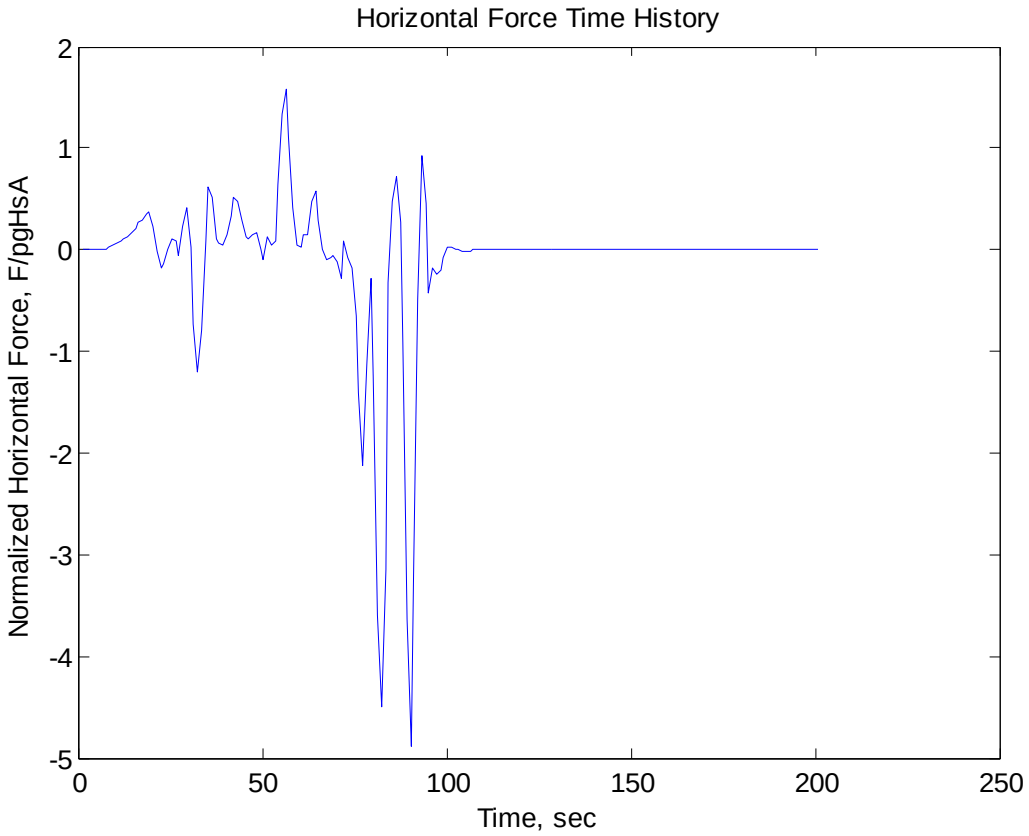

Figure 118: Horizontal Wave Time History of Bridge

REFERENCES

Batts, M.E., Cordes, M.R., Russell, L.R., Shaver, J.R., Simiu, E. (1980). Hurricane wind speeds in the United States. National Bureau of Standards, Report Number BSS-124, US Department of Commerce, 50pp.

Cuomo, G,, Allsop, W. and Takahashi, S. (2010), Scaling Wave Impact Pressures on vertical walls, Coastal Engineering, Volume (57), 604-609

Cuomo, G,, Allsop, W. and Trindelli, M. (2007), Wave-in-Deck Loads on Exposed Jetties, Coastal Engineering, Volume (54), Issue 9, 657-679

Chopra, Anil (1995), Dynamics of Structures Theory and Applications to Earthquake Engineering, Prentice Hall, ISBN 0-13-855214-2, 729 pages

Daniels, Richard (1974), Approximation Methods for Electronic Filter Design, New York: McGraw—Hill. ISBN 0-07-015308-6, p. 896

David W. Wang,* Douglas A. Mitchell, William J. Teague, Ewa Jarosz, Mark S. Hulbert (2005), Extreme Waves Under Hurricane Ivan, *Science* 5 August 2005: Vol. 309. no. 5736, p. 896

Dagnew, Agerneh, Bitsuamalk, Girma and Merricak, Ryan, (2009), Computational Evaluation of wind pressures on tall buildings, 11th Americas Conference on Wind Engineering-San Juan Puerto Rico, June 22-26, 2009

Donea, J. and Huerta, A. (2003), Finite Element Methods for Flow Problems, John Wiley and Sons, ISBN 3-2103-01184-3020 , 350 pages

Dyrbye, Claës and Hansen, Svend (1997), Wind Loads on Structures, John Wiley and Sons, ISBN 0-471-95651, 229 pages

Dytran Theory Manual r1 (2008), MSC Software Corporation, www.mscsoftware.com

Franke, J., Hirsch, C., Jensen, A.G., Krüs, H.W., Schatzmann, M., Westbury, P.S., Miles, S.D., Wisse, J.A., Wright, N.G., (2004). Recommendations on the use of CFD in wind engineering. Proceedings of the International Conference on Urban Wind Engineering and Building Aerodynamics, in: van Beeck JPAJ (Ed.), COST Action C14, Impact of Wind and Storm on City Life Built Environment, von Karman Institute, Sint-Genesius-Rode, Belgium, 5 - 7 May 2004.

Holmes, John D. (2001), Wind Loading of Structures, Spoon Press, ISBN 0-419-24610 , 356 pages

Kinsman, Blair (1984), Wind waves: their generation and propagation on the ocean surface, Dover Publications, ISBN 0-486-49511-6 , 704 pages

Kiureghian, D. and Ditlevesen, O. (2009), “Aleatory or epistemic? Does it matter?”, Structural Safety, 31, 105-112

Kiureghan, Armen and Liu, Pei-Ling (1986), Multivariate distribution models with prescribed marginals and covariances, Probability Engineering Mechanics, Vol. 1 (2), 105-112

Jelesnianski, C. P., J. Chen, and W. A. Shaffer, (1992): SLOSH: Sea, lake, and overland surges from hurricanes. NOAA Technical Report NWS 48, National Oceanic and Atmospheric Administration, U. S. Department of Commerce, 71 pp. (Scanning courtesy of NOAA's NOS's Coastal Service's Center

Lin, Y.K. and Cai G.Q. (1995), Probabilistic Structural Dynamics, McGraw-Hill, ISBN 0-07-038038-4, 476 pages

Main J. A. and Fritz W. A. (2006). "Database-Assisted Design for Wind: Concepts, Software, and Examples for Rigid and Flexible Buildings," NIST Building Science Series 180.

Mara, T.G. and King, J.P.C. (2008). "A Study of Wind Effects for Anna Marie Bridge Design Alternatives Anna Marie Island, Florida". BLWT-SS74-2008. December 2008.

Masters, F.J., Gurler, K.R., Biggerstaff, M., Knupp, K. and Coulbourne, W.L. (2010). "The Digital Hurricane Consortium: An Adaptive Mesonet to Monitor Wind, Surge, Wave and

Rainfall Intensities and Damage at Landfall". 2010 Structures Congress. Orlando, Fl 2010.

Masters, F.J., Gurler, K.R. and Prevatt, D.O. (2010). "Advancing Performance Based Design through Full-Scale Simulation of Wind Water and Structural Interaction". 2010 Structures Congress. Orlando, Fl 2010.

Petrini, F, Ciampoli, M and Augusti, G. (2009), A probabilistic framework for Performance Based Wind Engineering: EACWE 5 Florence, Italy, July 19-23 2009

Phan, Long and Simiu, Emil (2007), Methodology for Development of Design Criteria for Joint Hurricane Wind Speed and Storm Surge Events: NIST Technical Note 1482, April 2007

Prevatt, David, Datin, Peter (2009), Performance Based Wind Engineering: Interaction of Hurricanes with Residential Structures, Proceedings of 2009 NSF Engineering Research and Innovation Conference, Honolulu, Hawaii

Robertson, A. P., & Glass, A. G., (1988). The Silsoe structures building - its design, instrumentation and research facilities. AFRC Inst. Engng. Res., Silsoe, Div. Note DN 1482.

Robertson, Ian, Riggs, H., Yim, Solomon and Young, Yin. (2007) Lessons from Hurricane Katrina Storm Surge on Bridges and Buildings. Journal of Waterway, Port, Coastal and Ocean Engineering, ASCE, Vol. (133), No. 6, 463-479.

Sheppard, Max and Marin, Justin (2009) Wave Loading On Bridge Decks: Final report. FDOT Report BD 545-58. UF Number 00056675. 177 pages.

Simiu, Emil and Scanlan, Robert (1986), Wind Effects on Structures 2nd Edition, John Wiley and Sons, ISBN 0-471-86613 , 589 pages

Simiu E, Sadek F, Whalen TM, Jang S, Lu L-W, Diniz SMC, Grazini A, Riley MA., (2008) Achieving safer and more economical buildings through database-assisted, reliability-based design for wind., Journal of Wind Engineering and Industrial Aerodynamics. 2003;91(12-15):1587-1611.

Tschanz, T. and Davenport, A.G. (1983) The base balance technique for the determination of dynamic wind loads, Journal of Wind Engineering and Industrial Aerodynamics. 1983; volume 10 (1-3):429-439.

Vickery, P. J., Skerlj, P. F., Steckley, A. C., and Twisdale, L. A. (2000). ‘‘Simulation of Hurricane Risk Using Empirical track model.’’, Journal of Structural Engineering, ASCE, 126(10), 1203–1222.

Whittaker, Andrew (2005), Performance-Based Engineering of Buildings and Infrastructure for Extreme Loadings, Dover Publications, ISBN 0-486-49511-6 , 8 pages

Wu C. S., Taylor A.T., Chen J,, Shaffer W., (2003), “Tropical Cyclone Forcing of Ocean Waves”, Conference on Coastal Atmospheric and Oceanic Predication and Processes, Seattle, Washington, 62-64

Yim, S.C., Cox, D.T. and Park M.M. (2009), Experimental and Computational Activities at the Oregon State University NEES Tsunami Research Facility, Science of Tsunami Hazards, Vol 28, No. 1, 14 pages

Yu, Bo, Chowdhurry, Arindam and Masters, Forrest (2008), Hurricane Wind Power Spectra, Cospectra, and Integral Length Scales, Boundary Layer Meteorology, Vol 129, pg 411-430